Development of Zinc Slurry Air Flow Battery

zur Erlangung des akademischen Grades eines

DOKTORS DER INGENIEURWISSENSCHAFTEN

von der KIT-Fakultät für Chemieingenieurwesen und Verfahrenstechnik des

Karlsruher Instituts für Technologie (KIT)

genehmigte

DISSERTATION

von

M. Sc. Nak Heon Choi

aus Karlsruhe

Tag der mündlichen Prüfung: 01.10.2021

Erstgutachter: Prof. Dr. Jens Tübke

Zweitgutachter: Prof. Dr. rer. nat Helmut Ehrenberg

DECLARATION

I declare that this dissertation is the product of my own work and it has not been submitted before for any degree elsewhere. All the sources and contributions to this work have been indicated or acknowledged particularly.

Nak Heon Choi

ABSTRACT

Batteries have gained large interest in past few decades as energy storage systems because their merits such as relatively high efficiency, good durability of battery and unique power and energy output design. There are many types of batteries which can be used as reversible, or secondary, energy storage systems like redox flow batteries or metal-air batteries. The hybrid of those two types of batteries which is the Zinc slurry air flow battery uses zinc particles suspended in highly alkaline solution as the electrolyte and electrode for the negative compartment, whereas air is flowing in and out of the positive compartment for the oxygen reaction. As this is a relatively new concept of battery, there are two important factors which needs to be investigated. First, the discharge performance of the battery is the primary problem to be solved and the second challenge is the rechargeability of the battery to make it a secondary battery. In order to achieve those two goals, the bipolar plates are one of the key components to be studied in redox flow batteries as they require not only a good electrical conductivity, but also good mechanical durability with high corrosion resistance. Furthermore, this component is also important as the electrolyte flow can be improved by carving a flow field on the bipolar plate.

Hence, this study aims first to improve the discharge performance of the Zinc Slurry Air Flow Battery. To do this, several types of flow field designs and material compositions have been tested as they play an important role in the performance of the redox flow battery, especially when using highly viscous liquids. To enhance the discharge power density of zinc slurry air flow batteries, an optimum slurry distribution in the cell is key. Hence, several types of flow fields (serpentine, parallel, plastic flow frames) were tested in this study to improve the discharge power density of the battery. The serpentine flow field delivered a power density of 55 $mW \cdot cm^{-2}$, while parallel and flow frame resulted in 30 $mW \cdot cm^{-2}$ and 10 $mW \cdot cm^{-2}$, respectively. Moreover, when the anode bipolar plate material was changed from graphite to copper, the power density of the flow frame increased to 65 $mW \cdot cm^{-2}$, and further improvement was attained when the bipolar plate material was further changed to copper–nickel. These results show the potential to increase the power density of slurry-based flow batteries by flow field optimization and design of bipolar plate materials.

The second aim of this work is to improve the rechargeability of the battery. In the last section of this study, carbon additives were introduced to achieve a rechargeable zinc slurry flow battery by minimizing the zinc plating on the bipolar plate that occurs during charging. When

no carbon additive was present in the zinc slurry, the discharge current density was 24mA·cm^{-2} at 0.6 V, while the use of carbon additives increased it to up to 38 mA·cm^{-2}. The maximum power density was also increased from 16 mW·cm^{-2} to 23 mW·cm^{-2}. Moreover, the amount of zinc plated on the bipolar plate during charging decreased with increasing carbon content in the slurry. A rheological investigation revealed that the elastic modulus and yield stress are directly proportional to the carbon content in the slurry, which is beneficial for redox flow battery applications, but comes at the expense of an increase in viscosity (two-fold increase at 100s^{-1}). These results show how the use of conductive additives can enhance the energy density of slurry-based flow batteries.

Zusammenfassung

Batterien erlangten in den letzten Jahrzehnten große Aufmerksamkeit als Energiespeichersysteme, aufgrund mehrerer Vorteile wie einem relativ hohen Wirkungsgrad, einer guten Haltbarkeit und einer modularen Skalierbarkeit von Leistung und Energie. Es gibt viele Arten von Batterien, die als reversible oder sekundäre Energiespeichersysteme verwendet werden können, wie Redox-Flow-Batterien oder Metall-Luft-Batterien. Die Mischform dieser beiden Batterietypen, die Zink-Slurry-Luft-Flussbatterie („Flow Battery“), verwendet Zinkpartikel, die in einer hochalkalischen Lösung als Elektrolyt und Elektrode für das negative Kompartiment suspendiert sind, während im positiven Kompartiment Luft für die Sauerstoffreaktion ein- und ausströmt. Da es sich hierbei um ein vergleichsweise neues Batteriekonzept handelt, gibt es vorrangig zwei wichtige Faktoren, die untersucht werden müssen. Erstens muss die Entladeperformance der Batterie verbessert werden. Die zweite Herausforderung ist die Wiederaufladbarkeit der Batterie, welche diese erst zu einer Sekundärbatterie macht. Um diese beiden Ziele zu erreichen, sind die Bipolarplatten eine der Schlüsselkomponenten, die in den Redox-Flow-Batterien untersucht werden müssen, da sie nicht nur eine gute elektrische Leitfähigkeit, sondern auch eine gute mechanische Haltbarkeit mit hoher Korrosionsbeständigkeit erfordern. Darüber hinaus ist diese Komponente auch wichtig, da der Elektrolytfluss durch das Einlassen eines Strömungsfelds („Flow-Field“) auf der Bipolarplatte verbessert werden kann.

Daher zielt diese Arbeit zunächst darauf ab, die Entladeleistung der Zink-Slurry-LuftFlow-Batterie zu verbessern. Zu diesem Zweck wurden verschiedene Arten von Flow-Field-Designs und Materialzusammensetzungen getestet, da sie eine wichtige Rolle für die Leistung der Redox Flow-Batterie spielen, insbesondere bei der Verwendung von hochviskosen Flüssigkeiten. Um die Entladeleistungsdichte von Zink-Slurry-Luft- Flussbatterien zu erhöhen, ist eine optimale Slurry-Verteilung in der Zelle entscheidend. Daher wurden in dieser Studie verschiedene Arten von Flow Fields (Serpentinen-, Parallel-, Kunststoffflussrahmen) getestet, um die Entladeleistungsdichte der Batterie zu verbessern. Das serpentinenförmige Fow Feld lieferte eine Leistungsdichte von 55 mW cm^{-2}, während parallele und Kunststoffrahmen Werte von 30 mW cm^{-2} bzw. 10 mW cm^{-2} ergaben. Wurde das Material der Anoden-Bipolarplatte von Graphit auf Kupfer geändert, stieg die Leistungsdichte des Flussrahmens auf 65 mW cm^{-2}, und eine weitere Verbesserung wurde erreicht, wenn das Material der Bipolarplatte weiter auf Kupfer-Nickel geändert wurde. Diese Ergebnisse zeigen das Potenzial, die Leistungsdichte von

Slurry-basierten Flow-Batterien durch Flow-Field-Optimierung und Design von Bipolarplattenmaterialien zu erhöhen.

Das zweite Ziel dieser Arbeit war die Verbesserung der Wiederaufladbarkeit der Batterie. Im letzten Abschnitt dieser Studie wurden Kohlenstoff-Additive eingeführt, um eine wiederaufladbare Zink-Slurry-Flow-Batterie zu erreichen, indem die Zinkabscheidung auf der Bipolarplatte, die während des Ladens auftritt, minimiert wird. Wenn kein Kohlenstoffzusatz in der Zinkaufschlämmung vorhanden war, betrug die Entladestromdichte 24 mA cm^{-2} bei 0,6 V, während die Verwendung von Kohlenstoffzusätzen sie auf bis zu 38 mA cm^{-2} erhöhte. Auch die maximale Leistungsdichte wurde von 16 mW cm^{-2} auf 23 mW cm^{-2} erhöht. Darüber hinaus nahm die Menge an Zink, die während des Ladens auf der Bipolarplatte abgeschieden wurde, mit zunehmendem Kohlenstoffgehalt in der Aufschlämmung ab. Eine rheologische Untersuchung ergab, dass der Elastizitätsmodul und die Fließspannung direkt proportional zum Kohlenstoffgehalt in der Aufschlämmung sind, was für Redox-Flow-Batterieanwendungen vorteilhaft ist, aber auf Kosten einer Erhöhung der Viskosität geht (zweifacher Anstieg bei 100 s^{-1}). Diese Ergebnisse zeigen, wie die Verwendung von leitfähigen Additiven die Energiedichte von Slurry-basierten Flow-Batterien erhöhen kann.

TABLE OF CONTENTS

LIST OF ABBREVIATIONS

A	Amps
AORFBs	Aqueous Organic Redox Flow Batteries
ATT	Attagel
CAES	Compressed Air Energy Storage
CCE	Catalyst Coated Electrode
CCM	Catalyst Coated Membrane
CE	Coulombic Efficiency
CER	Chlorine Evolution Reaction
CFD	Computation Fluid Dynamics
CMC	Carboxymethyl cellulose
EE	Energy Efficiency
EIS	Electrochemical Impedance Spectroscopy
EPDM	Ethylene Propylene Diene Monomer
ESS	Energy Storage System
FF	Flow Frame
GDL	Gas Diffusion Layer
GPEs	Gel polymer electrolytes
HBr	Hydrobromic Acid
HER	Hydrogen Evolution Reaction
LVR	Linear Viscoelastic Region
MEA	Membrane Electrode Assembly
OCV	Open Circuit Voltage
OER	Oxygen Evolution Reaction
ORFB	Organic Redox Flow Battery

ORR	Oxygen Reduction Reaction
PAA	Polyacrylic Acid (Carbopol 940)
PEM	Proton Exchange Membrane
P&ID	Piping and Instrument Diagram
PP	Polypropylene
PTFE	Polytetrafluoroethylene
RAOMs	Redox Active Organic Molecules
REDOX	Reduction-Oxidation
RFB	Redox Flow Battery
RPM	Rotation per minute
SOC	State of Charge
UPS	Uninterruptible Power Supply
V	Voltage
VE	Voltage Efficiency
VRFB	Vanadium Redox Flow Battery
XG	Xanthan Gum

LIST OF TABLES

LIST OF FIGURES

Chapter 1: Introduction

1.1 Overview

Energy storage systems (ESS) are a promising technology which can serve as a long-term solution for empowering the sustainability of electricity generation. Currently, around 67% of electricity generation comes from the combustion of fossil fuels, which causes a high CO_2 production [1] and is one of the main contributions to global warming. Alternative electricity production could be achieved by using thermal energy, but this has a lower efficiency than other methods [1-2]. The increasing concern over global warming inspires new electricity production technologies with clean, high-efficiency, renewable energy resources [2]. Renewable energies, such as solar or wind energies, offer clean and highly efficient electricity, yet they still have some limitations in terms of accessibility and climate dependency [3]. This can be an issue as electricity production needs to match its consumption to maintain a stable grid. Consequently, it is important for future that research and investigating on renewable energies which are independent of time and temperature to provide electricity in any circumstances [3-4]. Therefore, ESSs can be a solution to unravel the concern and deliver continuous and protected energy to the grid [4].

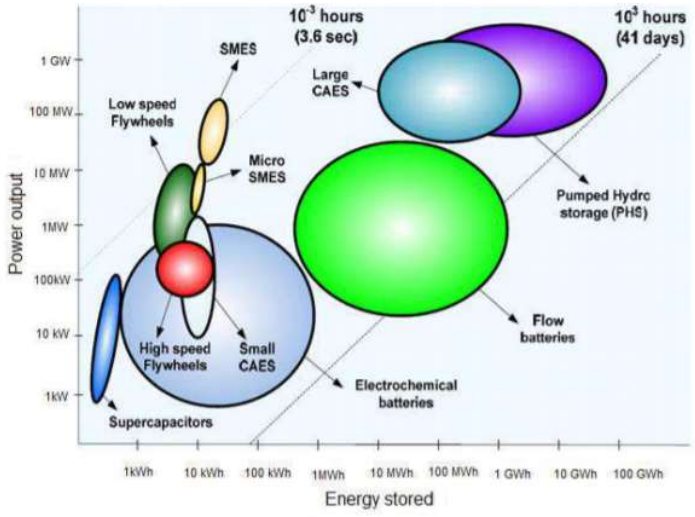

Figure 1. Energy against power output of different technologies [5]

Figure 1 displays ESS that are being researched and investigated. It can be noted that the main ESS for large scale are flow batteries, pumped hydro and compressed air energy storage (CAES). Furthermore, at the low energy stored and power output region, electrochemical batteries are the most dominant devices for ESS. Electrochemical batteries consist of

lithium-ion batteries, metal air batteries and others. Hence, in order to provide power from ESS, it has been shown that both electrochemical batteries and flow batteries have a good potential for future application.

1.2 Redox Flow Battery (RFB)

Redox flow batteries are one of the most favorable battery types compared with the other existing technologies [6]. A redox flow battery produces electrical energy from chemical energy by reversible reduction-oxidation (redox) reaction with electrolyte flowing into the device. Consequently, one of the necessary components of RFB is an electrolyte tank (electrolyte reservoirs) which provides a flow of electrolyte pumping into the battery [7]. The battery, also known as a single cell or stack, consists of a negative and a positive compartment. An ion exchange membrane is used to separate the two compartments preventing the cross-mixing of the electrolyte solutions. The size of the battery controls the power of a RFB, whilst the size of the tank establishes the energy capacity of the battery, which makes it easier to scale up the system in real life application [6-8]. There are already many different types of RFB which have been commercialized in recent years, such as zinc-bromine (e.g. Redflow), organic RFB (e.g. JENABatteries) and hydrogen bromine RFB (Elestor) [9-11]. Chief among those, the all-vanadium redox flow battery (VRFB) is yet the most successful RFB presented and commercialized by several companies (e.g. Largo clean energy., H_2, UniEnergy Technologies) with grid installations [12-14].

1.2.1 Vanadium Redox Flow Battery (VRFB)

Amongst the many types of flow batteries, VRFB is the most established technology as it has many advantages including its flexibility of electrolyte. As it uses the same parent species in the positive and negative electrolytes (vanadium sulfate), the crossover in the system does not degrade the cell performance. In the VRFB, the positive electrolyte consists of a vanadium ion in the +4 and +5 ionization state, which is oxidized to +5 when charging and reduced to +4 when discharging. The chemical formula of the +4 ionized state is VO^{2+} while the +5 ionized state is VO_2^+. The negative electrolyte consists of a vanadium ion of the +2 and +3 ionization states, which is reduced to +2 for charging and oxidized to +3 ionized stated when discharging and the basic schematic diagram of VRFB is shown in figure 2. The chemical reactions of the VRFB are shown below [15-17] :

Negative electrode : $V^{3+} + e^- \rightleftharpoons V^{2+}$ (Equation 1)

Positive electrode : $VO^{2+} + H_2O \rightleftharpoons VO_2^+ + 2H^+ + e^-$ (Equation 2)

Overall : $VO^{2+} + V^{3+} + H_2O \rightleftharpoons VO_2^+ + V^{2+} + 2H^+$ (Equation 3)

As the equations 3 show, when battery is charging, water molecules break up at the positive electrode. Hydrogen ions and electrons are freed when V^{4+} ions are oxidized into V^{5+} ions. As VRFBs use a proton exchange membrane (PEM), this membrane allows the hydrogen ions to migrate to the negative electrode while the electrons are also transferred to the negative current collector through an external circuit. Simultaneously, V^{3+} ions at the negative electrode reduce to V^{2+} ions with electrons from positive electrode. When battery is discharging, V^{2+} is oxidized to V^{3+} at the negative electrode, and the electrons then flow to the positive electrode via the external circuit. At the same time in the positive electrode, charged V^{5+} ions react with hydrogen ions and an electron to produce a V^{4+} ion and a water molecule. [16-17]

The application of VRFBs is very broad. For example, it can be utilized in electrical peak shaving, Uninterruptible Power Supply (UPS), hybrid with wind turbine and solar power, emergency back-up power, and some electric vehicles. This is possible as this battery has a range of 80-90% energy efficiency in large commercial applications combined with a cost attractive battery maintenance. Furthermore, another advantage of this system is that it can be relatively easy to check the status of the system and its state of charge (SOC) during charge and discharge. [18-20]

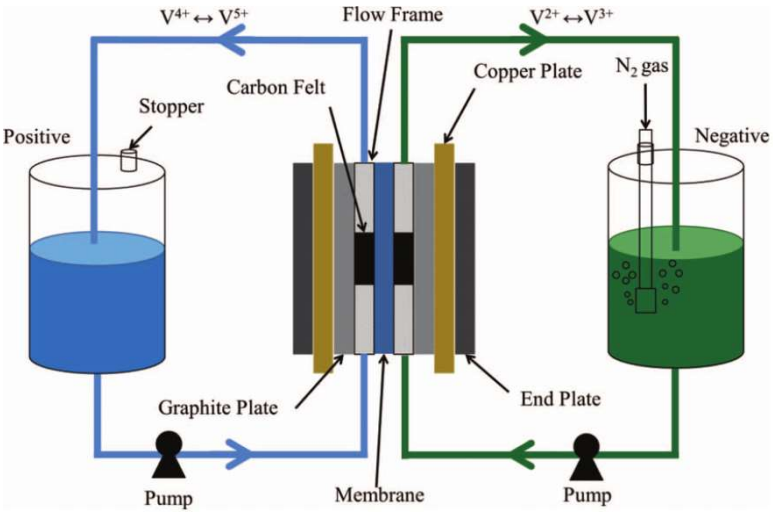

Figure 2. Schematic diagram of Vanadium Redox Battery single-cell [21].

However, there are also drawbacks of this battery. For instance, it has a relatively lower specific energy density (25- 35 Wh/kg) compared to other secondary batteries. In fact, lead

acid or lithium ion, batteries show approximately 30-40 Wh/kg and 100-265 Wh/kg respectively which is higher than the VRFB. Moreover, there is also a limitation of concentration of vanadium ions in the electrolyte which is 2M and the operating temperature of the battery is restricted from 5℃ to 40℃, as V^{5+} precipitates above 40℃ in the sulfuric acid electrolyte. As these restrictions limit the VRFB performance there is a lot of active research undertaken to overcome them [22-23].

1.2.2 Hydrogen Bromine Redox Flow Battery (HBr RFB)

The hydrogen bromine redox flow battery is another appealing ESS system, especially for large scale, as it exhibits high power density, high efficiencies with low cost materials. As shown in figure 3, hydrobromic acid (HBr) is flowing into the battery and it breaks up into hydrogen and bromine during charging. In other words, hydrogen and bromine are supplied from outside of the system and flowing into the battery whenever it is required. When the battery is discharging, the flow is reversed, hence a bromine in HBr solution is delivered to the positive compartment of the battery, and simultaneously hydrogen flows into the negative compartment of the battery. When they react, hydrogen bromide is formed and its open circuit voltage is 1.098 V. [24-25].

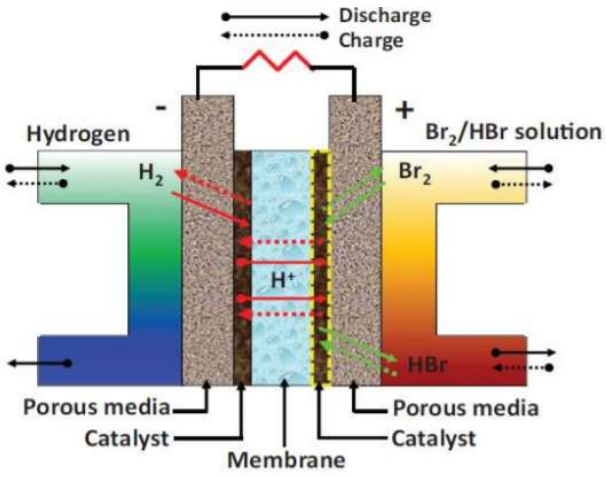

Figure 3 Schematic view of Hydrogen bromine redox flow battery [24]

Hydrogen Bromine Redox Flow batteries are ideal for applications for long term ESS which needs to be discharged daily maximum half a day for 10 to 20 years. Examples could be integration of renewables, deferral of infrastructure investment, peak management and micro grids. However, this battery has lower energy densities than existing commercial batteries like lithium-ion batteries and the system configuration is rather complicated to setup. These limitations avert from application of this battery to transportation. Furthermore, use of bromine

can also be hazardous to both users and the environment which requires additional sealing technique requires than other batteries [24-26].

1.2.3 Organic Redox Flow Battery (ORFB)

The Organic Redox Flow Battery (ORFB) is also a promising redox flow battery technology as it uses a relatively environmentally friendly organic electrolyte in the system. This advantage allows it to be used in grid-scale renewable energy applications, with lower cost restrictions. Comparing this battery to VRFBs, it shows better financial advantages as VRFBs require large amounts of vanadium which is highly expensive. Although the some of the limitations of existing RFB systems are diverted, the mission of reducing the lifecycle cost of the ESS still remains. To overcome this cost issue along with environmental problems, one possible suggestion that has been lately investigated is utilize the carbon-based redox-active aqueous-soluble electrolytes. In last decade, electrolytes of different species of ORFB have been tested including the development of aqueous organic redox flow batteries (AORFBs) through a chemistry pairing 9,10-anthraquinone-2,7-disulfonic acid (H_2AQDS /AQDS). This brings a new opportunity for ESS to avoid using expensive active electrolytes, like vanadium. Moreover, the flexibility of redox active organic molecules (RAOMs) has been researched by many teams to enable the wide chemical space of RAOMs for RFBs. As a subsequent, research in RAOMs is still undergoing aiming to develop low and high potential species which can be dissolved in aqueous and non-aqueous solutions [27-28].

As mentioned above, one of the major advantages of this battery is safety. However, safety may come as a challenge when an organic solvent is used as it must be treated with protections. This is because that organic solvent may have flammability issues which can be a drawback towards commercialization of this battery. Hence, as the lithium-ion battery went through similar issue, the ORFB may learn from them to improve their safety and achieve a market-ready system. Another concern about this RFB is the power density, like other existing RFBs. As they have relatively low voltage, this led the battery to discharge and charge at lower power densities [29].

1.3 Metal-Air Battery

Not only redox flow batteries are attractive for ESS but also metal-air batteries are very promising as they use air from atmosphere, which is an almost limitless resource, to generate electricity. The metal-air system utilizes a metal to carry electrons as the oxygen reduction reaction (ORR) takes place with the help of an oxygen catalyst. For a rechargeable secondary battery, not only the ORR has to take place in the system but also oxygen evolution reaction (OER) occurs during charging. The schematic diagram of a metal air battery is shown in figure 4 below [30].

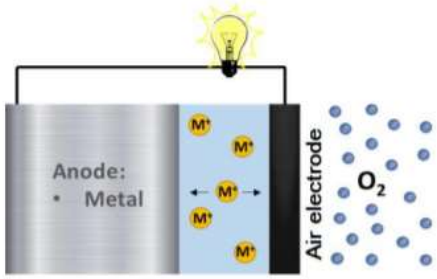

Figure 4 Schematic diagram of metal-air battery [30]

There are number of researched/commercialized metal air batteries using different metal species and its corresponding reaction mechanisms. Primarily, metal-air batteries can be divided into two types based on the electrolyte. First type are batteries using an aqueous-based electrolyte, whereas the other type are water sensitive systems with electrolytes based on aprotic solvents or/and ionic liquid. Furthermore, there are two different types of secondary metal air batteries depending on whether they are electrochemically rechargeable or mechanically rechargeable. A mechanically rechargeable battery consists of a primary battery that, when fully discharged, the active materials can be replaced with fresh ones. Figure 5 below shows a diagram of the most commonly used metal-air batteries divided by the electrolyte and state of the battery [31-32].

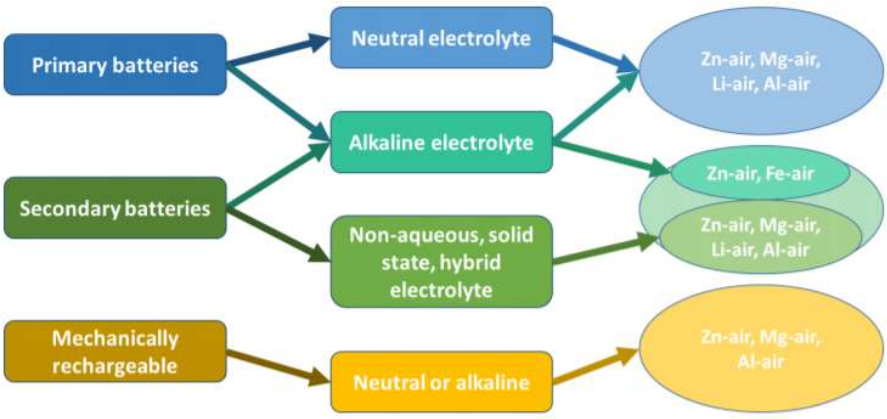

Figure 5 Listing of metal air batteries divided by its characteristics and classification [32]

Hence, the basic reaction mechanisms of the metal air batteries are presented below:

$$\text{Anode} : M^{\circ} \rightleftharpoons M^{x} + xe^{-} \qquad \text{(Equation 4)}$$

$$\text{Cathode} : \frac{1}{2} O2 + H_2O + 2e^{-} \rightleftharpoons 2OH^{-} \qquad \text{(Equation 5)}$$

$$\text{Overall} : M^{\circ} + nO_2 + yH_2O \rightleftharpoons M(OH)_x \qquad \text{(Equation 6)}$$

In particular instances, further process may happen in the electrolyte when the pH is different, or metal anode is used. In such cases, the overall reaction may end differently as further electrolyte reaction can take place.

$$\text{Electrolyte} : M(OH)_x \rightleftharpoons MO_z + yH_2O \qquad \text{(Equation 7)}$$

$$\text{Overall} : M^{\circ} + nO_2 \rightleftharpoons MO_z \qquad \text{(Equation 8)}$$

The last overall reaction is the reason why there is number of research undertaken in this type of battery. When the oxygen is used from the unlimited atmosphere, the metal is reacting accordingly. Which means that when a metal with a high theoretical specific energy is used, the battery will also have a high specific energy as it will be just limited by the amount of metal on the anode. However, in practice, this is very challenging as positive electrode must contain a bi-functional catalyst of both ORR and OER, also must take account that electroplating during charging may have to be prevented to protect battery. These challenges are yet to be fully solved which makes these systems still challenging and there are limited successful products [33-34].

1.3.1 Lithium-Air Battery

The lithium air battery is a non-aqueous based battery that has been proposed by Abraham et al. in 1996. It has been frequently compared with a lithium-ion battery as they have both an active lithium metal for operation. The lithium-air battery consumes oxygen from the atmosphere which dissolves in the electrolyte while the ORR occurs forming lithium peroxide during discharge. The merit of this battery is that using lighter elements like carbon reduces the weight of a battery by avoiding heavy transition metals. As shown in figure 6 below, the theoretical energy density of this battery is approximately 3.8-11.7 kWh/kg [35-37].

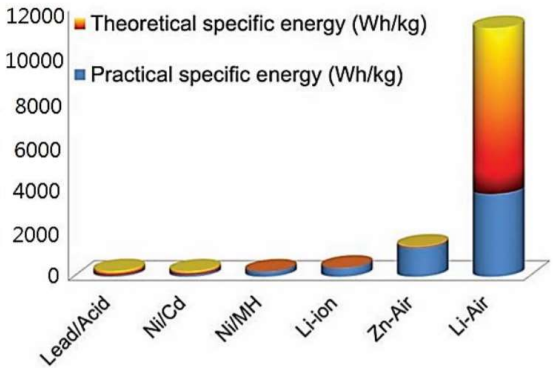

Figure 6 Theoretical and practical specific energy of different metal-air batteries [34]

In the first stage of its investigation, the lithium-air battery had low interest until researchers were able to show it rechargeability. Because of this rechargeability performance, it got further attention in the scientific community and these results led IBM to begin the Battery 500 project. This project is aimed to develop a lithium-air battery for electrical vehicles which is able to drive up to 800km [37].

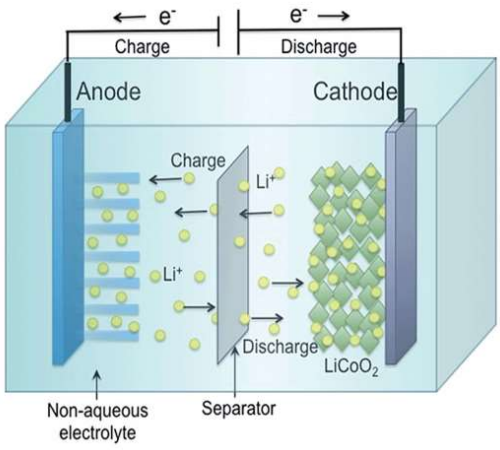

Figure 7 Schematic diagram of lithium-based battery [38]

As Figure 7 shows a basic schematic diagram of how lithium-based batteries operates, and it can be seen that Li^+ ions are transferred via the electrolyte from the negative compartment to the positive compartment during discharge and reverse reaction during charge. The function of both positive and negative compartments is to store and release Li^+ ions at different potentials, and the cell open circuit voltage (OCV) is controlled by the difference between the two potentials [39-40].

The discharge of the battery occurs by electrically connecting the two materials via an external circuit. Electrons can be move to positive compartment from negative compartment via this connection and this can be used to calculate the energy by multiplying voltage difference by the current. The energy produced when discharging can be a good application as the electrons transferring via an external circuit can be used to power electrical devices like laptop, mobile phones or etc. The charging of this battery is happening when a potential difference of two electrodes is bigger than the equilibrium potential. When charging, electrons are forcing back to anode from cathode. For instance, in the case of Li-ion batteries, the crystalline intercalation materials are used for the two electrodes, and the lithium is stored in the crystal. Whereas, for lithium air batteries, both electrodes are both growing and shrinking during charging and discharging as the electrodes are different [40-41].

As mentioned above, the basic mechanism of the lithium air battery relies on the selection of electrolyte. Electrolytes can be aqueous, aprotic (water-free) or solid. The aprotic configuration has attained most interest in scientific society as the limitations of ohmic resistances, rechargeability of the battery and concerns about low energy density have already been found in the other systems [39,42].

1.3.2 Zinc-Air Battery

Another good example of metal-air battery is the zinc-air battery, which is also a very promising technology in terms of both power and energy density. There are also commercial zinc-air batteries in the market with a coin-cell configuration but these cannot yet be fully stably recharged. Like other metal-air batteries, there are three main components in a zinc-air battery, which are the positive electrode, the negative electrolyte and the electrolyte. Figure 8 shows the basic schematic diagram of a zinc-air cell with an alkaline electrolyte. The open circuit voltage of this battery is 1.65 V which is the potential difference between the air electrode and the zinc electrode. When the battery is discharging, zinc oxidizes into zincate molecules providing two electrons to air side. Like other batteries, electrons are moving via

the external circuit to the air electrode where these travelled electrons are occupied for ORR from the air. This whole reaction can be classified as a three-phase reaction, consisting on a solid electrolyte reaction in air catalyst, liquid reaction in the electrolyte, and gas reaction using oxygen from the atmosphere. The consumption of atmospheric oxygen produces hydroxyl ions in the electrolyte as well as production of water and oxygen gas as by-products. This hydroxyl ions further react with zincate which oxidizes to zinc oxide (ZnO) [43-45].

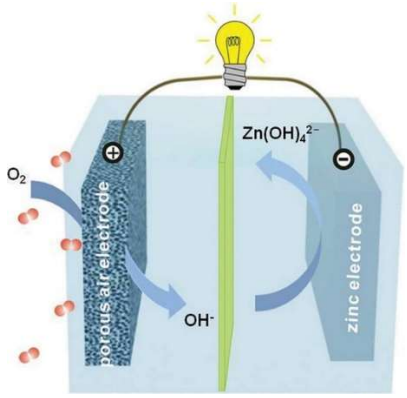

Figure 8 Basic schematic diagram of zinc-air battery [45]

In this battery, the metal anode is pure zinc metal for the reaction. Consequently, performances of battery can be improved when a bigger zinc plate is used as an electrode. In order to make better performances, not only making bigger is the solution but also controlling the morphology of zinc particles in the metal is important [46].

As oxygen from atmosphere is not a limiting factor of most of metal-air batteries, the research is focused on the zinc negative electrode rather than any other components of this battery. Additionally, the zinc morphology is currently investigated by coating the electrode with other metals like mercury to improve the electrical conductivity between the zinc electrode and the current collector. Likewise, in order to suppress the hydrogen evolution reaction (HER), other metal alloys along with zinc are under study, like using nickel, indium, palladium and cadmium. These metal alloys not only suppress HER but also help limit the undesired corrosion of the electrode [46-47].

In zinc-air batteries, the most commonly used alkaline electrolytes are potassium hydroxide (KOH), and sodium hydroxide (NaOH). Out of these two electrolytes, KOH is more popular than NaOH or other electrolytes as it provides the desirable ionic conductivity for this battery. Furthermore, like other types of batteries, the concentration of salt in the electrolyte is also very critical to enhance the battery performance. Increasing the concentration of electrolyte will enhance the electrochemical performance of the battery by reducing the internal resistance,

but at the same time, a high concentration may cause the formation of ZnO leading to a highly viscous electrolyte. When a low concentration of KOH is used, it may lead to unwanted HER. Therefore, it is important to use an optimal concentration of salt in the electrolyte to maintain the durability of the battery [46-48].

Moreover, membrane selection of this battery is also important as it operates in highly alkaline media. Hence, a porous membrane (separator) is widely used in this system because it allows the hydroxyl ions in the electrolyte to travel to the electrodes via pores in the separator. In order to select an ideal separator, requirements are stability in highly alkaline solution, right pore size and porosity, high ionic conductivity and insulating to electron transport. Among those requirements, the porosity of the separator is the most important during operation as it should be adequate to suppress the migration of zincate ions between electrodes. Lastly, to make this battery rechargeable, electrolyte selection, separator, and anode metal selection is required. Moreover, the use of a bi-functional oxygen catalyst is critical as battery will undergo ORR during discharge and OER during charge [49].

1.4 Literature review of Zinc Slurry Air Flow Battery

Back in 1970's there were a few groups that investigated the zinc slurry air flow battery system. A. J. Appleby, J. Jacquelin and J. P. Pompon from Laboratoires de Marcoussis (France) have published a paper entitle "Charge-Discharge Behavior of the C.G.E. Circulating Zinc-Air Vehicle Battery". They were able to reach up to 300mA cm^{-2} by using 12 M KOH with zinc powder in the electrolyte with an operating temperature 55℃ [50]. Moreover, they performed two separate experiments for charging and discharging to achieve high efficiencies of the system. By separating charge and discharge of the battery, each electrode was individually performance-optimized. However, even when they separated two reactions apart, still it was inevitable to form zinc dendrites when charging which caused a high ohmic drop and performance degradation. They used tubular cell for charging as shown in figure 9 below.

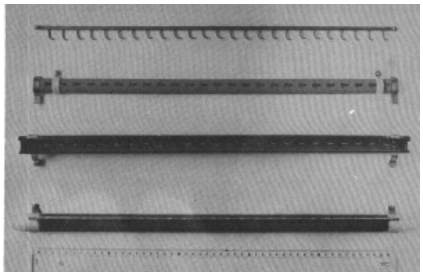

Figure 9. Picture of charging tube [50]

Moreover, there was another group from England who studied the discharge behavior of the zinc slurry air flow battery in 1975 [51]. Marshall, A., Hampson, N. A., & Drury, J. S. from Loughborough university and Shell have showed that different types of additive may increase the discharge capacity of the zinc slurry air flow battery. Without any additive, discharge capacity showed as good as normal static zinc air battery, and when additives like silicate or lithium ions were introduced the discharge capacity was enhanced.

In 2007, Zinc air fuel cell have been proposed by Stuart I. Smedley and X. Gregory Zhang from New Zealand and Canada respectively [52]. They used zinc pellets in the KOH and circulate into the 12-cell stack providing 1.8kW of the battery. They also had a separate system for discharging and charging of the system to perform stackable zinc air fuel cell as shown in figure 10 below.

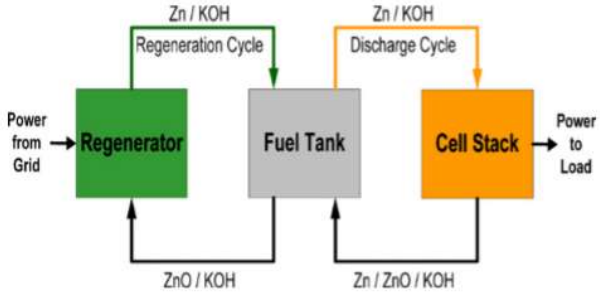

Figure 10 : Zinc regenerative fuel cell configuration [52]

1.5 Thesis Overview

As shown from chapter 1.4, there were some research about zinc slurry air flow battery back in 1970's but then it was not continued. Hence, this thesis brings a relatively new concept of battery by combining a redox flow battery and a metal-air battery. As the zinc air battery showed potential for future ESS, application of zinc air battery was tested by suspending zinc metals in a highly alkaline solution to make a zinc slurry. While the positive electrode will consist of air flowing from atmosphere for oxygen reactions, the negative electrode will consist of a zinc slurry flowing into the battery. Hence, instead of static a zinc-air battery, a zinc slurry air flow battery has been performed. As static zinc-air battery performance is limited by the size of active zinc metal, this battery can boost the energy density by adding more zinc particles in the slurry. In other words, this battery has a potential to become a higher energy density battery than zinc-air battery. Furthermore, as zinc has a higher theoretical capacity than other types of RFB, this battery can be a good choice for future ESS. Consequently, this thesis will show how to improve discharge power density and capacity from this battery, then recharge performance of the battery in one cell, not diving cells from charging and discharging.

Chapter 2
Design of Zinc Slurry Air Flow Battery

2.1 Operation of Zinc Slurry Air Flow Battery

As mentioned in the chapter 1.5, zinc slurry air flow battery is a hybrid technology of redox flow battery and metal air battery. The main principle of zinc-air battery is air flowing in the positive electrode while zinc as an active static negative electrode material. However, different to conventional zinc air battery, the zinc slurry air flow battery comprises a negative side is formed by zinc particles suspended in a highly alkaline electrolyte forming a slurry which flows in and out of the system. During discharge, air flows in the positive electrode and the ORR takes place, while in the negative electrode zinc particles in the slurry oxidize to zincate which can further decompose to zinc oxide in highly alkaline media.

One of the main advantages of zinc slurry air flow batteries is their higher capacity compared to conventional zinc air battery. As the capacity of the battery is determined by the amount of active material in the slurry, it can be boosted by adding additional zinc to the slurry. On the other hand, the current and power densities will be determined by the flow of zinc slurry in the battery. For zinc-air RFBs, the electrolyte flow is an important factor because the lack of a static electrode to provide additional reaction surface to the electrochemical reaction. In other words, carbon felts or other porous electrodes, which are used for to increase surface area in other RFBs, will not be part of the zinc slurry air flow battery at the negative electrode. This is because the slurry consisting of zinc particles are suspended in a highly alkaline electrolyte acts as both electrode and electrolyte.

2.2 Planning of Zinc Slurry Air Flow Battery

As this battery have not yet performed by other groups, flow chart was first completed in order to make a successful battery for the thesis and flow chart is shown in figure 11 below.

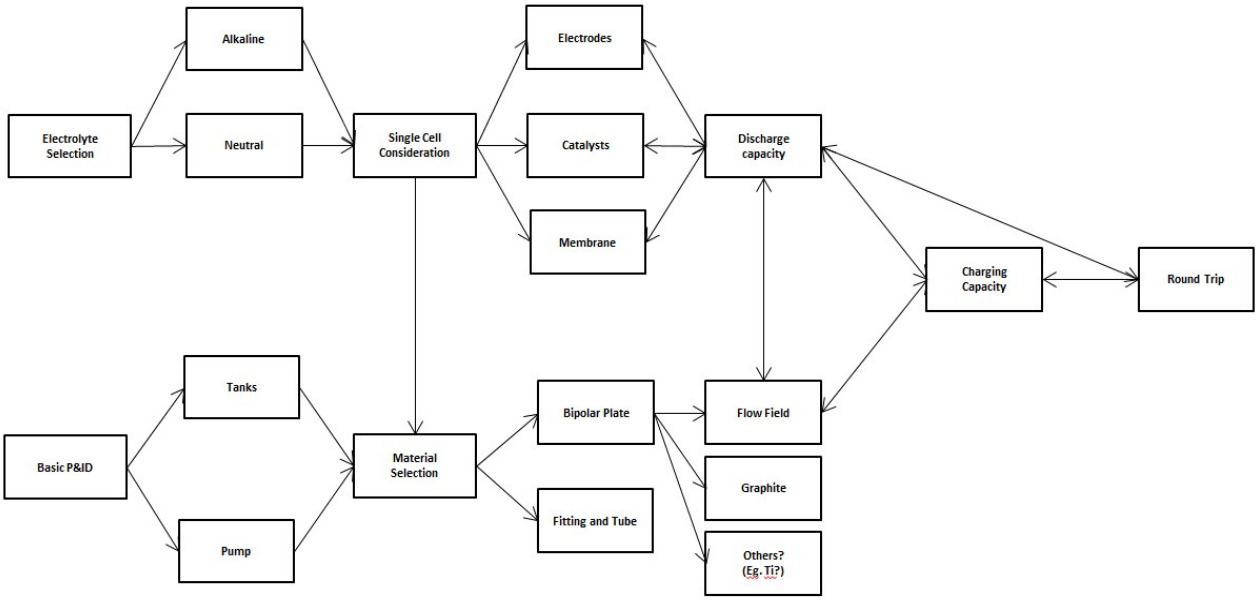

Figure 11 Flow chart of planning the experiments for Zinc Slurry Air Flow Battery

After completing the flow chart, selection of electrolyte was the next step as it was not fixed with using alkaline electrolyte. Hence, a table with advantage/disadvantage has been completed based on the literature review and shown in table 1 below. It was concluded that our battery will be starting with alkaline electrolyte as they will show better electrochemical performances as this is important for new concepts of the battery. Subsequently, materials which will be using for to construct the system and the electrochemical devices have been researched. Materials for fittings and tubes were selected to use a Teflon basis as they have strong resistivity against highly alkaline solution. Material for bipolar plates have been selected with impregnated with a cure furan resin as they have showed good performance under highly alkaline solution.

Table 1. Comparison of electrolyte between Neutral and Alkaline

	Neutral	Alkaline
Advantages	1. Avoid carbonization of electrolyte 2. Reduces dendrite formation	1. Inherent electrochemical reversiblity and fast electrochemical kinetics (low overpotential) of the zinc 2. High ionic conductivity of the electrolyte 3. Good electrochemical performances at low temperature 4. High solubility of zinc salts
Disadvantages	1. Corrosion Issue - Chlroine based electrolyte leads to the Chlorine Evolution Reaction (CER) when charging - Leads to the disfavor OER therefore decrease in charging efficiency	1. High dissolution (when charging) - Dendrite growth - Electrode shape change 2. Corrosion of zinc - HER on the surface of the zinc will decrease the efficincy

Furthermore, selecting pump was challenging as electrolyte is highly alkaline zinc slurry. Pump needs to match criteria of pumping the slurry electrolyte, and also flow rate of electrolyte. Hence, based on those requirements, Verderflex OEM pump from VERDER was selected. After selecting all materials for system and single cell, the design for the lab scale system and single cell have started. Simple piping and instrument diagram (P&ID) were completed for lab-scale system and shown in figure 17 in the following chapter.

In order to design a single cell, the key factor is designing flow fields. By designing a suitable flow field, the pressure drop of the cell can be optimized. The electrolyte will be evenly distributed, and therefore the reaction can occur uniformly on the surface of the electrode. Consequently, flow field for both anode and cathode will be designed differently as state of reactants is slurry and gas respectively. Flow field on positive plate will be normal serpentine for this single cell, as they are conventional flow type for gas reactants. Negative plate flow field however will be different. They will be designed in variety of patterns.

As a result, most of designs for system, and single cell have completed at this stage, material selections are also completed following by ordering equipment like pump, fittings, bipolar plates have been progressed.

2.3 Design of Zinc Slurry Air Flow Battery

2.3.1 Preliminary single cell design

Most of materials for single cell were ordered and received in hand on time. However, the delivery date of carbon-based graphite plate took 6 months as this graphite plate was delivered from U.S.A. As a zinc electrolyte is based on highly alkaline potassium hydroxide, this graphite plate is impregnated with cure furan resin so it can be chemically stable in highly alkaline media. Meanwhile, an additional experimental was planned to study the flow of slurry with a preliminary cell. The material used for this cell is mostly transparent PMMA, to observe fluid flow visually. As pictures are shown below, this preliminary cell is a one single horizontal line based on rectangular shape. There is no flow field on this single cell, and material for bipolar plate is just normal graphite plate as durability is not a parameter for this experiment.

The transparent end plate and flow plate are shown in fig 12. Before measuring electrochemical performance, mechanical pre-test is required to proceed for the safety reasons. Pre-test is a flowrate test with water, which will be examine the durability such as leakage for cell and system as well as determining the pump performance.

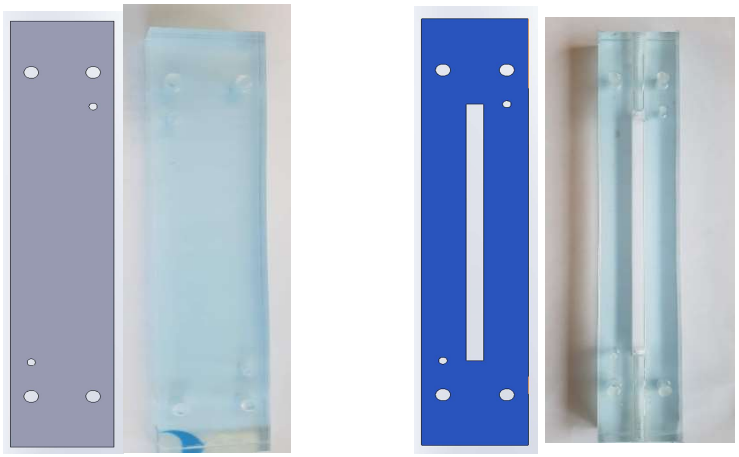

Figure 12 Transparent end plate and flow plate

Pump performance is very important step as flowrate is a parameter for mass-transfer resistance, hence after pre-test, flowrate experiment will further test not only with water but also with different types of zinc slurries before testing electrochemical performances. Fig 13 is a picture of preliminary cell.

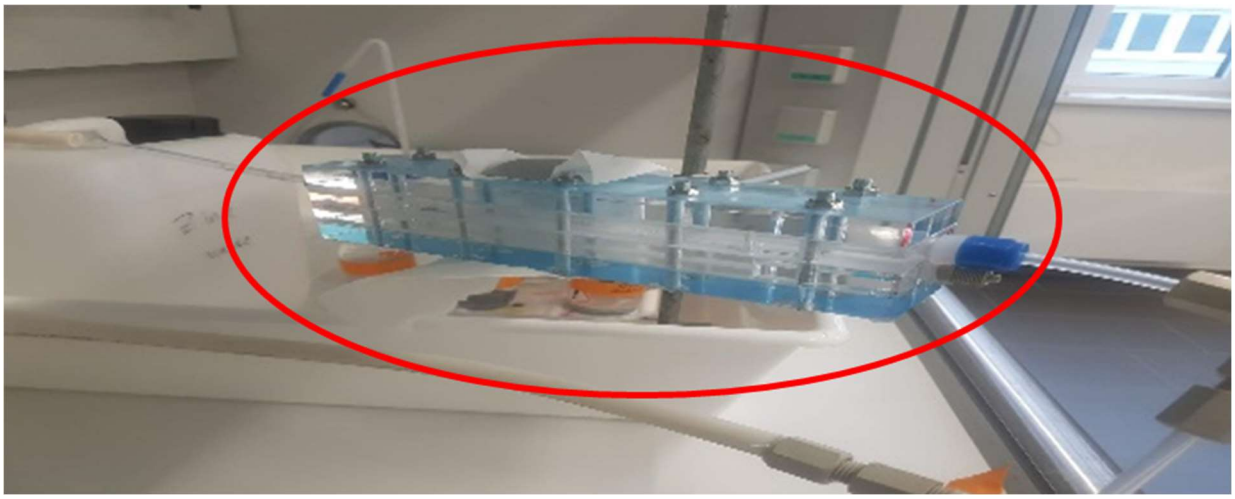

Figure 13 Transparent Single Cell

The experimental result for flowrate with water circulating is shown in fig 14 below, and it was tested over 3 times to minimize the differences of each trial. By using same technique, highly alkaline KOH and different types of zinc slurries have been tested. All the experiments were tested 3 times and most of them actually showed similar results. There are some zinc slurries (shown in fig 15) which cannot be suspended, and as a subsequent, these slurries have to be mechanically agitated to measure flowrate performances.

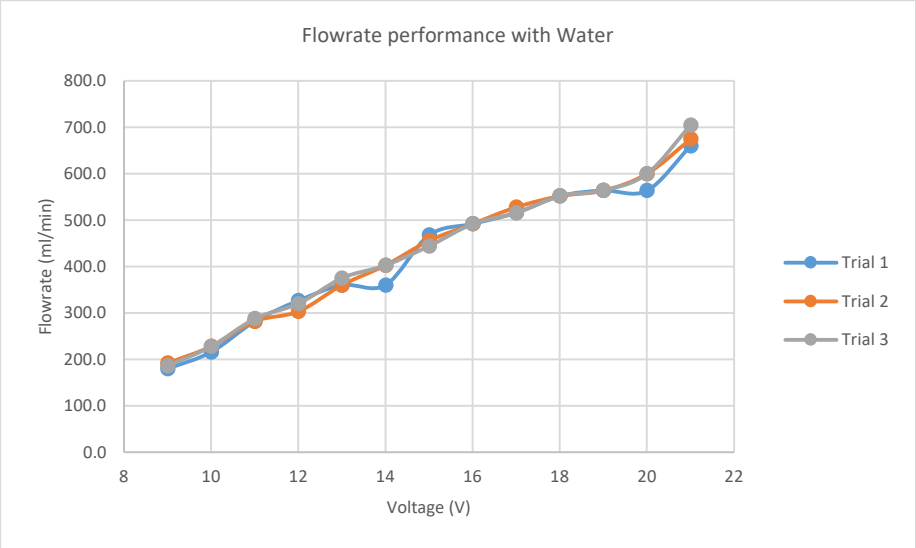

Figure 14 Flowrate performance with water

For the flow of zinc slurry test, first attempt was making slurries without adding gelling agent for economical purpose, however, they never suspended. Consequently, gelling agents were added to make zinc solution to slurry, and polyacrylic acid (PAA) was selected as a gelling agent. Standard PAA with molecular weight of 1800 and PAA with molecular volume of 1,250,000 was purchased for comparison. As shown in fig 24 below, zinc slurries

without PAA and with standard PAA have not suspended whereas zinc slurries with higher molecular volume of PAA have suspended. As a result, Zinc slurry with higher molecular volume is selected to start basic experiments for future.

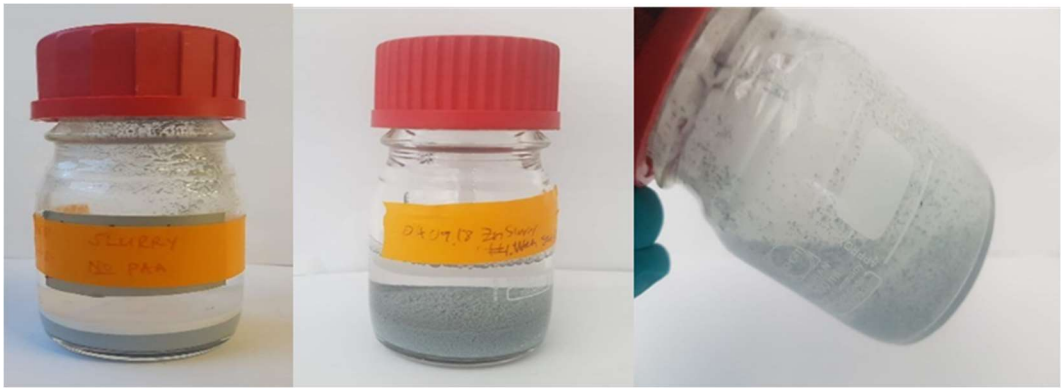

Figure 15 Zinc slurry with no PAA(left), with standard PAA (middle) and with higher Mv PAA (right)

Lastly, catalyst and spraying has been completed. For zinc slurry air flow battery, anode is circulating zinc slurry, however, cathode requires catalyst for ORR, and gas diffusion layer. Therefore, Pt/C was selected as a catalyst for oxygen reaction and as catalyst is not the main research field, the amount of catalyst loading was relatively high with a 2mg cm^{-2} to minimize the kinetic influence. Fig 16 is the first attempt to spray catalyst onto membrane, and this will be continuously working to minimize the synthesis of Membrane Electrode Assembly (MEA)

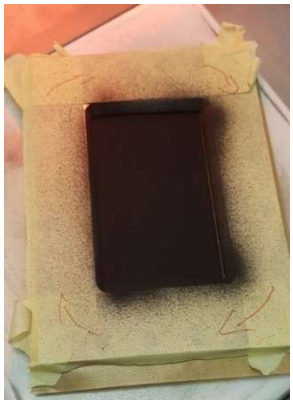

Figure 16 Pt/C catalyst sprayed onto membrane

After setting up of preliminary cell was complete, electrochemical performance test was directly tested. First, electrochemical performances were tested by using constant current mode from potentiostat. Experiments were tested from current density range from 10mA cm^{-2} and increased by 10mA cm^{-2} for each step, however, test was directly terminated with all zinc slurries. Hence, another technique was used which was constant voltage mode.

It was tested from 1.4V and decreasing by 0.1V until the battery hit the 0.3V. As a result, the maximum current output of first attempt was 1 mA cm^{-2} (15mA). There were many parameters that resulted in poor performances which will be discussed in the later part of the thesis.

2.3.2 Design of single cell and each component

While preliminary test is running, a design of single cell was also investigated so it can be manufactured directly after new graphite plate is arrived. Furthermore, as mentioned in chapter 2.1, there are some requirements to design and construct a single cell system for zinc slurry air RFB, which are single cell components, tubes and fittings and pump which must be highly alkaline resistive, and also synthetic gas cylinder or compressed air need to be prepared for oxygen reaction.

- System Design

As zinc particles are suspended in highly alkaline potassium hydroxide, tubes and fittings must be highly alkaline resistance to make system durable and reliable. Therefore, polytetrafluoroethylene (PTFE) material was chosen for both fittings and tubes as they are very stable in highly alkaline media. Materials selected are summarized in table 2.

Table 2 Material list for zinc slurry air flow battery system for single cell

Name	Material	Size	Quantity	Units	Vendor	Price/ea (EUR)
Systems (Zinc Side)						
Electrolyte Tank	PFA	100 mL	1	ea	ICT	-
Electrolyte pump	-	1/4" fitting	1	ea	Verder	217,15
Tubing	PTFE	6mm	10	m	EM Technik	2,62
Straight connector	PTFE	1/4"	8	ea		12,02
Elbow Unioin	PTFE	1/4"	4	ea		30,1
T Unioin	PTFE	1/4"	6	ea		38,71
Magnetic stirrier	-	-	1	ea	VWR	487
Systems (Air Side)						
Air Cylinder	-	-	1	ea	ICT	-
Humidifier	-	-	1	ea	Gasmet	334
Mass Flow Meter	-	-	1	ea	Vögtlin	315

Then, piping and Instrument diagram (P&ID) needs to be drawn before construct a system. P&ID is a detailed diagram in the full system which shows the piping and required equipment together. For the lab-scale zinc air RFB, P&ID is very simple as shown in figure 17.

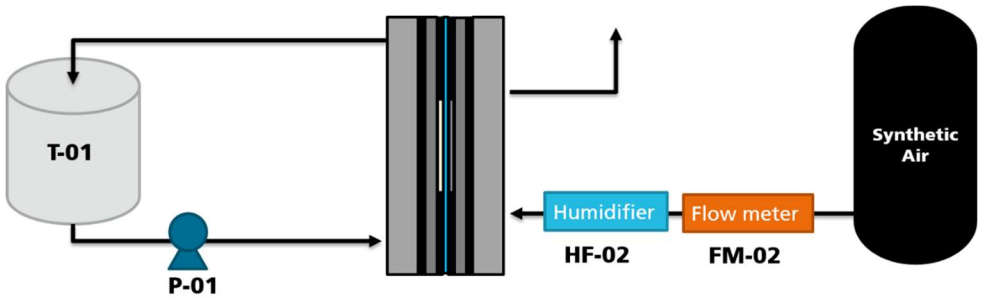

Figure 17 P&ID of zinc slurry air flow battery single cell system

As P&ID is shown in figure 17, components such as electrolyte tank, pump, gas flow meter are primary requirements for the system, but among those chief, pump is very important as pump makes electrolyte flow, which makes flow battery. Hence selection of pump is significant to have an optimized condition to operate zinc slurry air flow battery. To select an appropriate pump, it has to be chemically stable and also able to provide required flow rate of electrolyte into the system.

Tube diameter is set from the material selection, concentration of zinc slurry is gained from literatures, and also test condition can be estimated. Therefore, flow rate of zinc slurry required to operate this system can be calculated. All the conditions needed to calculate minimum flow rate is listed in table 3 below.

Table 3 List of system condition for zinc slurry air RFB

Active Area (cm2)	25	cm^2
Number of Cell	1	
Voltage (V)	0,7	V
Amps (A)	0,5	A
Current Density (mA/cm^2)	20	mA/cm^2
Volume of Electrolyte (mL)	70	mL
Tube inner diameter (mm)	6	mm
Tube Area	28,26	mm^2
Concentration of zinc (Cw)	30	%
Specific Gravity of zinc (Ss)	7,14	g/cc
Density of zinc	7,14	t/m^3
Density of KOH	2120	Kg/m^3
	2,12	t/m^3
density of slurry (ρP)	2,68	t/m^3

Hence, minimum volumetric flow rate of zinc slurry required could be calculated. From the electrolyte preparation, mass flow rate of solid was calculated to 46g s^{-1}, which is 0.164t h^{-1}. As mass flow rate of slurry can be determined by dividing mass flow rate of solid by concentration of solid, mass flow rate of slurry is 0.00549t h^{-1}. Then, volumetric flow rate can be determined by dividing mass flow rate of slurry by density of slurry. Density of slurry can be calculated from table 3 and it is calculated to 2.68t m^{-3}. Hence, minimum volumetric flow rate of slurry required to operate this system is 0.034L min^{-1}, which is 34mL min^{-1}. To satisfy this value and chemical resistance, a Verderflex M1500 OEM peristaltic pump from VERDER was selected. After purchasing M1500 pump, flow rate test has been performed without any electrochemical devices like single cell and as it is shown in figure 18 below, zinc slurry flow rate can be performed up to 200mL min^{-1}.

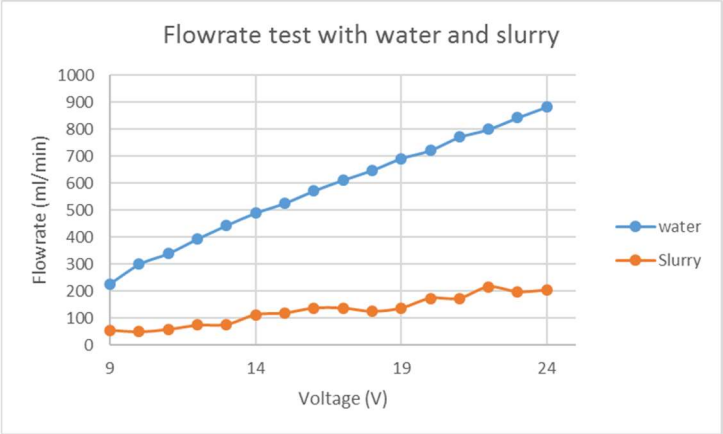

Figure 18 Flow rate test with water and slurry

- Flow Field design for single cell

As one of the key factors for single cell is a flow field as written in previous section, a single serpentine flow field was designed for air side a), and serpentine b), parallel c), and flow frame d) was designed for zinc side as shown in figure 19 below. The air side was fixed to single serpentine flow field as it is one of the most common flow field for the gas reactant. However, for the zinc side, as the reactant is not a gas nor a liquid, it is a slurry and not many studies have been taken for this topic. Hence three different types were designed to observe the performances. First, serpentine but with wider width was designed and this was to force the reactant to one direction so minimize the dead zones. Second flow field was a parallel type and this was chosen as it is one of the most commonly used flow field for the liquid reactant devices like electrolyzer. Lastly, flow frame was designed as most of the RFB is using flow frame type flow field but with diffuser (carbon felt) in the active area. In this

experiment, there was a no diffuser as zinc slurry is behaving as both an electrolyte and an electrode

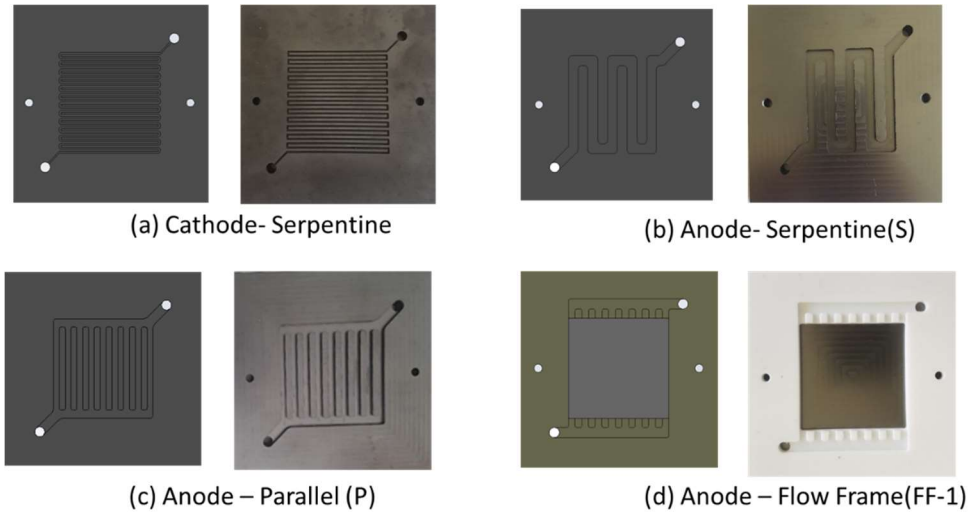

Figure 19 Flow Field designed and manufactured – a) Air side Serpentine, b) Zinc side serpentine, c) Zinc side Parallel, d) Zinc side Flow Frame

- Zinc Slurry

In the beginning of the experiment, zinc slurry was prepared by using 8.5M of KOH with a polymeric gelling agent PAA. Moreover, zinc oxide is also added to prevent self-discharge as well as hydrogen formation. Hence, the composition of zinc slurry is shown below in table 4 as a table. As written in previous section, PAA with molar volume of 1.25M was used. To prepare this electrolyte, this slurry was agitated from stirring plate for 24 hours with 800 rotation per minute (RPM) before it was used .

Table 4 Composition of Zinc Slurry

Substance	Zn	KOH	ZnO	PAA	H2O
Mass Fraction in wt%	33,8	19,9	4	0,7	41,7

- Membrane and Ionomer

As membrane is very important to operate the battery, both membrane and ionomer were provided by Fumatech GmbH, and they are called FAB-PK-130, and Fumion FAA-Ionomer respectively. They are both anion exchange polymer, and their counter ion is Br^-. Therefore, counter ion for both membrane and ionomer needs to be changed into OH^- form, so they were immersed in 1M of KOH for 24h then they were rinsed with Deionized water then

dried before they were used in the cell. For Fumion FAA Ionomers, it had one more step, which was dissolved in IPA. Ionomer was initially provided as a shredded film, hence after shredded film was rinsed with deionized water, then it was dissolved in IPA with 5wt%/V so it became solution from shredded film.

- Catalyst preparation

In the begging of the experiment, catalyst for oxygen reduction reaction (ORR) was synthesized with platinum on carbon (Pt/C), Fumion FAA Ionomer, DI Water and IPA. First, platinum loading was changed to 1mg cm^{-2} from 2mg cm^{-2}, as this amount of loading is also higher than literature values. This value was chosen to minimize the catalytic and spraying influence. Hence, after weighing Pt/C catalyst, few drops of DI was added to prevent spark of catalyst. Then 23% of ionomer was added followed by 4mg of IPA was added in the end. Then synthesized catalyst was agitated for 24 hours.

- Membrane Electrode Assembly (MEA)

When both membrane and catalyst are prepared, then MEA was synthesized. MEA was first synthesized by using Catalyst Coated Membrane (CCM) method. Hence, synthesized catalysts after agitation were sonicated for 30 minutes followed by ultrasonication for 5 minutes. Then catalyst was sprayed directly onto the membrane which was placed on the hot plate with 85° of temperature. After spraying whole catalyst onto the membrane, it was dried on the hot plate for 1 hour for IPA and water to evaporate. Figure 20 below is finalized MEA by using CCM method.

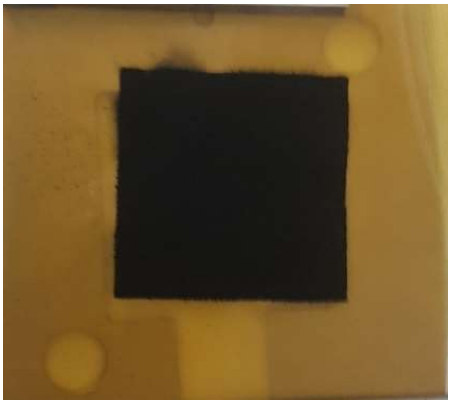

Figure 20 Picture of finalized CCM MEA

- System construction:

Once every equipment is delivered including the single cell, then it can be constructed based on P&ID. As figure 21 shows, all the equipment from P&ID such as synthetic air, tank, pump, humidifier and gas flow meter have installed to make system complete. Additionally, few more devices were used to make system like DC power supply, magnetic stirrer/heater, and potentiostat. DC power supply was used to apply voltages on the slurry pump, and magnetic stirrer/heater was introduced to keep zinc slurry agitated, as zinc slurry is non-homogenous electrolyte, hence agitation makes more zinc particles involves in the reaction. Lastly, potentiostat is used to perform electrochemical performances.

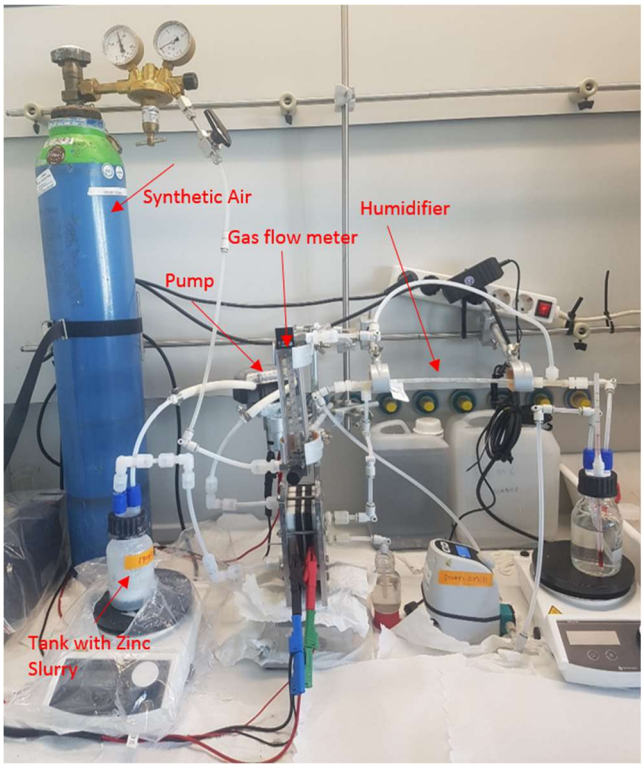

Figure 21 Lab scale Zinc Slurry Air RFB

By designing a lab-scale zinc slurry air RFB system systematically by selecting material appropriately, and drawing P&ID diagram, an optimized parameter for zinc air RFB have achieved. As discussed in previous section, one of the important parameters for lab scale system was pump selection, because flow rate influences RFB performances. Furthermore, all the materials in the system including single cell were chemically resistance against highly alkaline media. This completed system has been used to perform electrochemical result of zinc slurry air RFB and also, all the test conditions used in this system was applied to the simulation studies for further investigation.

2.3.3 Single Cell results

2.3.3.1 Air Catalyst

- **Motivation**

Renewable energy applications have been under enormous attention nowadays due to its environmentally friendly advantage. Therefore, most of renewable energy applications are associated with natural environments such as solar energy, wind energy, and wave energy [67]. Also, oxygen from air can be used to produce electricity. One of the well-known oxygen consumption devices is a fuel cell, but also there are number of metal-air batteries including lithium-air, aluminum-air, zinc-air that requires oxygen to generate power [53]. Hence, among those chief, zinc air battery is promising secondary battery as they have relatively higher energy capacity and also cost advantage as zinc is plenty in the earth [54].

Zinc Slurry Air Redox Flow Battery also have a high potential for renewable energy application. The operating principle of this battery comprises zinc as an active anode material, and air flowing on the cathode. However, as opposed to conventional configurations [49], the anode is formed by zinc particles suspended in the electrolyte forming a slurry which can flow in and out of the stack. When air is flowing during discharge, oxygen reduction reaction (ORR) occurs, and when it is charging, oxygen evolution reaction (OER) occurs [55,56]. Hence, as two opposite reactions are occurring in one electrode, it is extremely important to develop materials that will enhance these reactions and thus charging and discharging the battery. As a subsequent, selection of catalyst for oxygen reduction reaction needs to be worked as well as its electrode needs to be optimized to develop zinc air battery.

- **Experimental procedure**

For oxygen reduction reaction (ORR), selection of catalyst is critical as oxygen reduction reaction is occurring by catalytic reaction. Hence, two commercial ORR catalysts platinum on carbon (Pt/C) and palladium on carbon (Pd/C), which shows good stability in alkaline media were selected and their electrochemical performance was measured by using three electrodes single cell system. [57]. Three electrode system set up of single cell system was achieved by placing extra platinum wires next to electrochemical active area as a reference electrode and counter electrode hence this allows to measure cathodic voltage from overall

cell voltage. Hence, by using three electrode setup, ORR performance of different catalyst can be measured.

Both catalysts pastes were synthesized by mixing catalysts with Ionomer, IPA and deionized water and sonicated for 30 minutes. Synthesized catalyst paste was sprayed onto the electrode, which is gas diffusion layer (GDL) and it was dried at 80ºC for 1hour. Catalyst coated electrode (CCE) was placed right next to porous membrane (commercial cellophane) to make membrane electrode assembly (MEA) in the single cell to perform electrochemical measurement such as current-voltage characteristic curve (I-V Curve) and also electrochemical impedance spectroscopy (EIS).

To find optimized gas diffusion electrode, three different types of MEA were synthesized. Normal CCE was prepared, and also, catalyst coated membrane (CCM) was prepared by using same catalyst but it was sprayed directly on membrane. Lastly, CCE without ionomer in catalyst was prepared to observe the influence of binder. In this test, commercial battery separator was used to prevent swelling for the CCM method.

For the zinc slurry, it was prepared from section 2.3.2 in the zinc slurry part.

- **Result:**

For three electrode system, I-V curve have performed to measure cathodic voltage between Pt/C and Pd/C.

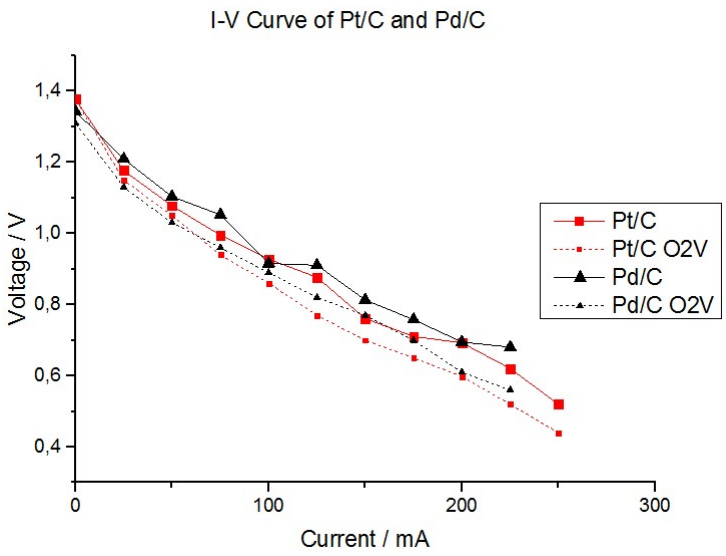

Figure 22 I-V curve of two different catalyst

As shown in figure 22 above, average cathodic voltages (shown in dashed line) between Pt/C and Pd/C does not differ much. In fact, Pd/C shows slightly higher voltage than Pt/C.

However, as zinc air redox flow battery do not have static electrode in the single cell, voltage fluctuation occurs when I-V curve performs. Hence, even Pd/C catalyst shows slightly better performances than Pt/C, voltage fluctuation was much bigger when Pd/C catalyst is used, and this voltage fluctuation get bigger as currents increases. This is why Pt/C could perform at 250mA current whereas Pd/C could not reach 250mA. Moreover, EIS indicates that charge transfer resistance of Pt/C is slightly smaller than when Pd/C is used as shown in fig 23 below.

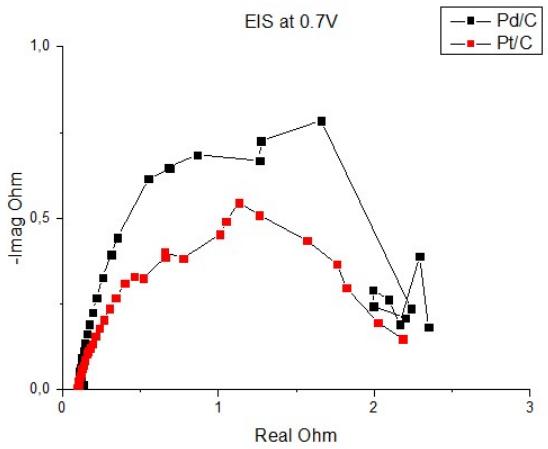

Figure 23 EIS curve of two different catalyst

Consequently, Pt/C catalyst was selected for further experiment. To find an optimized cathode for ORR, three different MEA have been prepared. As porous membrane separator allows water to be diffused through the separator, CCE without ionomer was tested to find out an influence of ionomer, which also can act as a binder. Hence, as separator allows water to diffuse along with OH^- from zinc slurry to oxygen electrode, function of ionomer can be neglected. However, function of binder is still not yet determined. If binder is not required, ionomer can be neglected in the catalyst, in other words it will be economically more advantage for larger scale system. However, water from zinc slurry might damage and tear catalyst apart from electrode. Hence catalyst with and without ionomer was tested with electrochemical impedance spectroscopy to measure resistance, I-V curve to measure performances and discharge curve to measure durability of electrode.

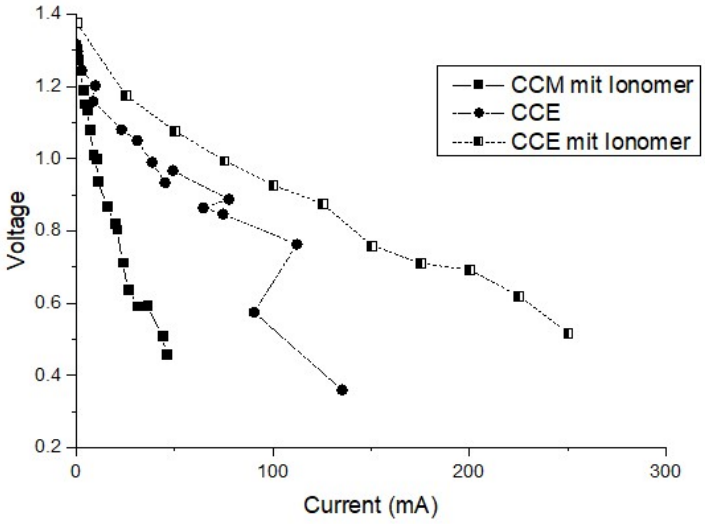

Figure 24 I-V curve of different types of MEA

As figure 24 shows, CCE with ionomer shows the highest electrochemical performances. At the same time, CCM shows the lowest currents output. This can be explained by following picture. Outlet of oxygen side of single was collected after experiment, and result is shown in figure 25 below.

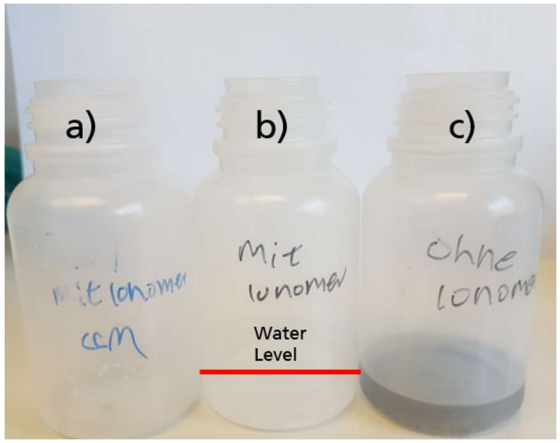

Figure 25 Oxygen side outlet after experiment

As shown in figure 25 above, it can be seen that CCM method (Fig 25 a) did not have any water diffused to the oxygen side from zinc slurry as there was no water collected after experiment. Also, CCE without ionomer (Fig 25 c) much of catalyst got teared away from electrode and collected with water. Whereas CCE with ionomer (Fig 25 b) water was diffused from zinc slurry without damaging catalyst on electrode as water looks more crystal clear than fig 25 c. This can explain a result from I-V curve that CCM shows the least current output as there was not sufficient water for the ORR, and also CCE performance

without ionomer was better than CCM yet still low currents were measured compare to the CCE with ionomer. Furthermore, this can be also explained by EIS which is in shown 26.

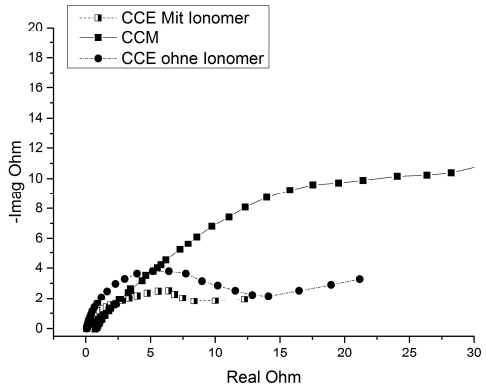

Figure 26 EIS of different MEA

As EIS shows that ohmic resistance of different MEA are very close to 0 Ohm. However, charge transfer resistance of CCM is very high where it continues higher than 30 Ohm. This indicates nearly no ORR reaction occurred with CCM method, hence catalyst sprayed on the membrane was blocking water diffusion from zinc slurry. With CCE without ionomer, charge transfer resistance is smaller than CCM method but still resistance tends to be higher than CCE with ionomer. As charge transfer resistance indicates kinetics of reaction, this result indicates that CCE with ionomer showed the fastest ORR kinetics.

- **Conclusion:**

In conclusion, to optimized GDE cathode for ORR in three electrode zinc air battery, different types of experiments were performed. For the catalytic performances, two different commercial ORR catalysts were performed and Pt/C shows better stability than Pd/C. Also, with Pt/C catalyst, three different types of MEA have been synthesized and CCE with ionomer showed the highest current output among the others as well as showed the smallest charge transfer resistance.

2.3.3.2 Zinc Slurry

- **Motivation**

All the viscosity measurement of the zinc slurry was performed by Diego Milian from University of Grenoble in France. However, interpretation and text are written by Nak Heon, Choi

As redox flow batteries are promising topic for renewable energy sources, variety types of RFBs are investigated to develop RFBs, including vanadium redox flow battery, hydrogen bromine redox flow battery, organic redox flow battery and etc. [58]. Unlikely with other types of batteries, RFB innovating approach requires the flow of the electrolyte throughout the cell. Consequently, it is important to study an electrolyte as it is one of the key roles in RFBs [58].

Zinc Air Batteries are promising secondary battery, which have been researched for many years [59]. However, Zinc Slurry Air RFB have not yet been much investigated as zinc is hardly soluble in alkaline solution. This is important because Zinc Air Batteries requires anionic exchange reaction which can be performed under alkaline media such as sodium hydroxide or potassium hydroxide. Hence, to perform Zinc Air RFB, instead of zinc liquid electrolyte, zinc slurry electrolyte can be prepared by making zinc particles suspended in highly concentrated potassium hydroxide, with gelling agent in it. This is very attractive research topic as zinc is not hard to obtain metal in world, so it is relatively cheaper than other metals used in RFB, and also, zinc has a potential to show higher energy capacities than other RFBs.

When formulating slurries for energy systems, one has to consider that there is a tradeoff between the concentration of active material and the bulk viscosity; [60] in the case of Zinc Slurry Air RFB, energy density can increase by adding more zinc, but at the same time, the viscosity increases adding pump losses and possibly clogging the system.

If any homogenous dispersion is pursued, it is necessary to build a network that will hold a particle taking into account its nature (shape, size, density). The stability of the network plays an important role because if there is a significant aging on it, the starting conditions will be very different that the actual ones. Because of this, rheology has been widely introduced to different application fields, among them RFBs.

Formulation of zinc slurry is not a trivial step because of the complexity of the system and the interactions between each of the components. The slurry composition has to be analyzed from a multidisciplinary approach as in RFBs there are different phenomena affecting the design of the cell. From the point of view of rheology, low viscosity systems and homogeneity are pursued, but this does not mean that the best zinc slurry in rheology terms will also show the best performance in electrochemical means, therefore the importance of both disciplines to formulate an optimum zinc slurry. Zinc particles in the slurry need to be in contact with each other to be able to be discharged properly, reducing the amount of inactive zinc particles in the network. A network behaving like this is known as a percolated network that will result in a homogenous discharge of the slurry [61].

There are different types of rheology modifiers as gelling agents with different features. They play an important role in the formulation because they build the network, and thus the characteristics of the slurry. There are different behaviors that the rheology modifiers can give to a Newtonian solution; changes in viscosity at different deformation rates can be observed as concentration of additive is increased. Generally, the behavior can follow a continuous decrease in viscosity, known as a shear thinning fluid (i.e. latex), on the other hand if the viscosity increases when the deformation rate increases, this will be known as shear thickening fluid (i.e. corn starch) [62].

- **Rhelogy Modifier:**

In the zinc slurry case, a homogenous low viscosity material flowing across the cell is desired, therefore a shear thinning behavior is adequate for this application, where viscosity will drop during pumping with a plug flow profile. Carboxymethyl cellulose (CMC) and xanthan gum (XG) are widely used in industry as shear thinning agents. Stability tests were performed to assess the compatibility of these organic additives with the alkaline media. As seen in figure 35, CMC and XG are not stable over time in an environment of 6M KOH, and this is an example of the limitation of gelling agents and additives that can be used in highly alkaline media [63].

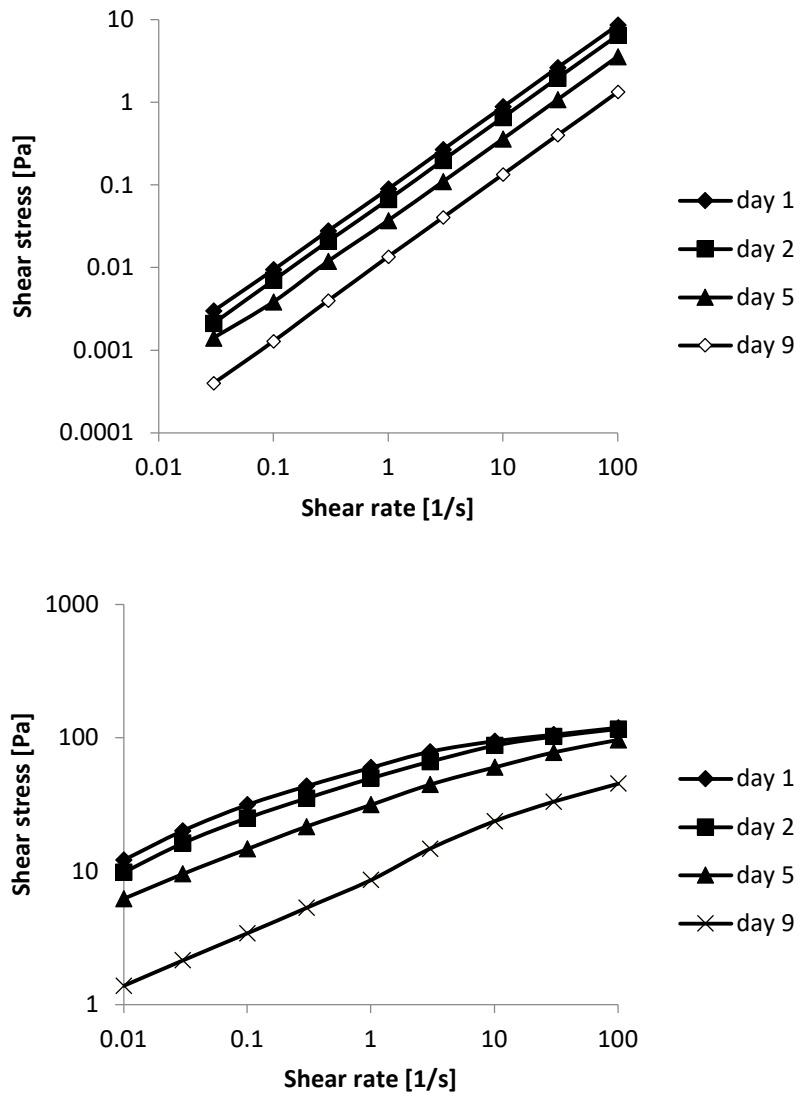

Figure 27 Flow curves over time in 6M KOH of a: top) CMC 2 % wt, b: bottom) XG 2 % wt.

In figure 27, it is possible to see that the shear stress for the same sample is decaying over time, meaning a bulk viscosity drop and therefore a weakening of the network. This would affect directly the performance of the slurry, as there is the risk that during longer times, more zinc will be settled in the bottom.

After assessing the compatibility of different gelling agents, it was found that the more stable ones were Carbopol 940 (PAA) and Attagel type 50 (ATT). Carbopol 940 and Attagel type 50. Carbopol (PAA) is the commercial name of a high molecular weight polyacrylic acid; this polymer is widely used in industry and research as thickener and yield stress fluid because of its stability. Attagel is a thixotropic clay material that acts as a thickener after being activated physically by a high shear homogenizer. Stability tests were performed and shown in figure 28 and 29:

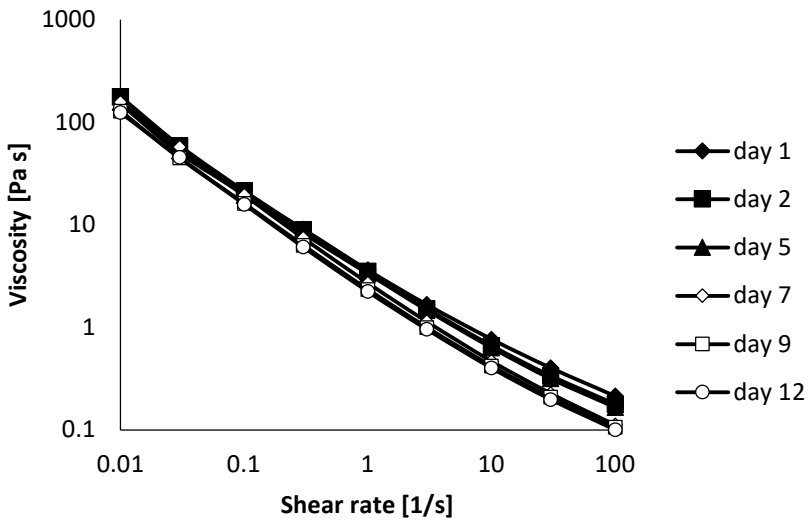

Figure 28 Viscosity curves for 1% wt. Carbopol 940 in 6 M KOH.

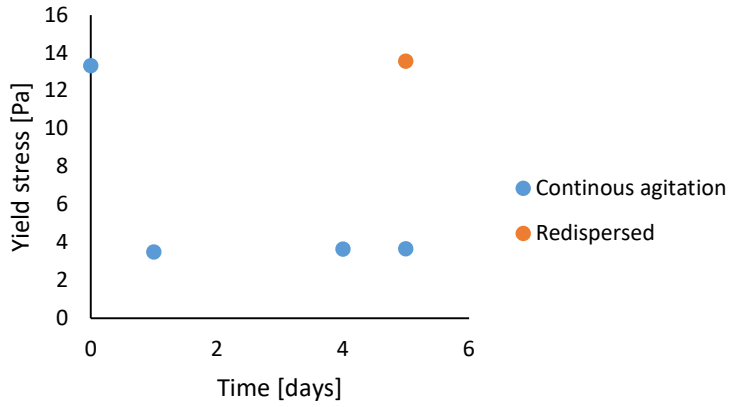

Figure 29 Yield stress values for 5.5% wt. Attagel dispersion.

Viscosity values in figure 28 for Carbopol 940 shows that at low shear rates, viscosity values are constant, and this means that the yield stress of the solution is not changing and the strength of the network remains the same, the shear thinning behaviour is remarked by the viscosity drop from low shear rates to high shear rates.

Attagel dispersant is stable in 6 M KOH but on the other hand this material needs to be re-dispersed when it is used by itself, as seen in figure 29. It is not possible to use carboxymethyl cellulose as water ligand with Attagel because it is not stable (as shown in figure 27a), and it is the same case for several gelling agents. Therefore, Attagel is an attractive rheology modifier by its stability in alkaline media but it has to be pre-homogenized each time prior to its use to activate its initial gelling properties. Finally, slurries were prepared from these two gelling agents.

- **Results:**

Rheological behavior of slurries was studied with both Carbopol and Attagel gelling agents. Two stable formulations where found with viscosity values of interest for RFBs, these were Attagel 5.5 %wt and PAA 1.25 %wt. With these gelled matrixes at 6M KOH, the effect of zinc concentration was studied.

As shown below in figure 30, it is possible to see that the increase of zinc concentration (in %wt) does not affect dramatically the viscosity. For Attagel slurries (figure 38a and 38c), the increase of Zn concentration affects the rheological behavior, becoming less shear thinning as the concentration of particles increase. This same behavior occurs for PAA slurries but at a smaller extent (figure 30b and 30d). This result is important as the concentration of zinc can be increased without affect significantly the viscosity of the system and thus, it is possible to reach higher energy density by having more particles that are active in the network.

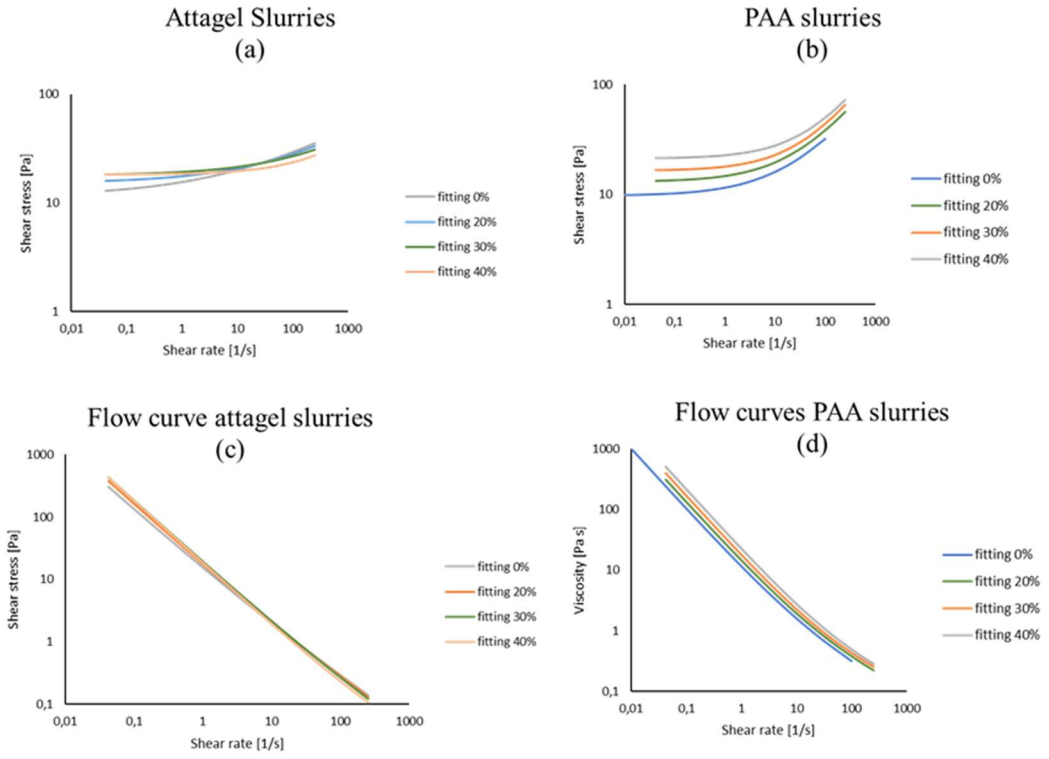

Figure 30 Flow curves and viscosity curves for slurries prepared with different concentrations of zinc ranging from 0% to 40% wt, 6M KOH and Attagel 5.5 %wt (a and c) and PAA 1.25 %wt (b and d).

Attagel slurries tend to preserve low viscosity even at high Zn particle concentration. Zn concentration effect is more visible in PAA slurries. Further experiments on viscoelasticity are needed in order to understand the phenomena behind these types of slurries.

For electrochemical measurement, current-voltage characterized curve (I-V Curve) as well as Electrochemical Impedance Spectroscopy (EIS) have been tested. To do this, positive electrode needs to be prepared. Oxygen reduction reaction will be occurring on air cathode during discharge, hence mixture of platinum on carbon catalyst with a loading of 1mg cm^{-2}, isopropyl alcohol and deionized water mixed with ionomer was sprayed onto the gas diffusion layer and it was dried on the hot plate with 80°C temperature for an hour. After dried for an hour, catalyst coated gas diffusion layer and cellophane as a separator was placed in the single cell.

Furthermore, in order to optimize zinc slurry composition, not only PAA, Carbopol, and Attagel were used, but mixture of Carbopol and Attagel in different ratio was tested. Hence, three types of mixture zinc slurries were prepared, first mixture (mix 1) with 0.6% of Carbopol which makes zinc slurry more viscous, and second one (mix 2) with 0.3% of Carbopol and last one (mix 3) with 0.2% of Carbopol to make less viscous.

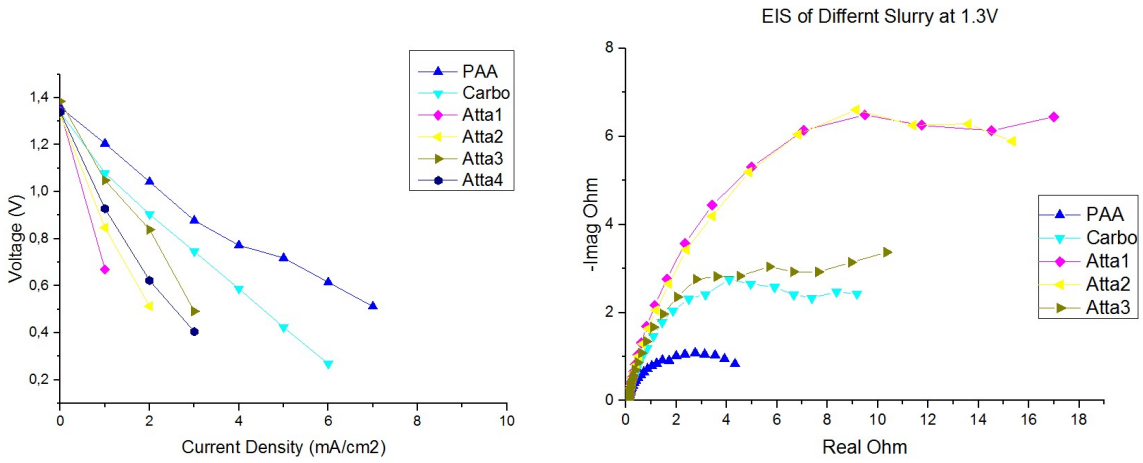

Figure 31 I-V curve and EIS curve of different types of slurry

As figure 31 shown above, it is clear that PAA and Carbopol has smaller charge transfer resistance than any combination of Attagel. Furthermore, it can be observed that when more Attagel is added into the zinc slurry, this increases charge transfer resistance. In case of Attagel 4, which has lowest contents of Attagel in the zinc slurry, is not viscous enough to carry zinc into the cell while it is flowing, hence EIS was not taken.

Furthermore, as I-V curve shown above in fig 31, slurry with PAA gelling agent shows the better performances than others. At 0.6V, current output is approximately 7mA cm^{-2} for slurry using PAA, and 4mA/cm^2 for Carbopol. When only Attagel is used, it can be seen that maximum current output is less than 3mA cm^{-2}.

Hence, to increase the electrochemical performances, mixture of Carbopol and Attagel was performed, and it can be seen from figure 32 below that current output has increased enormously by mixing two different gelling agents.

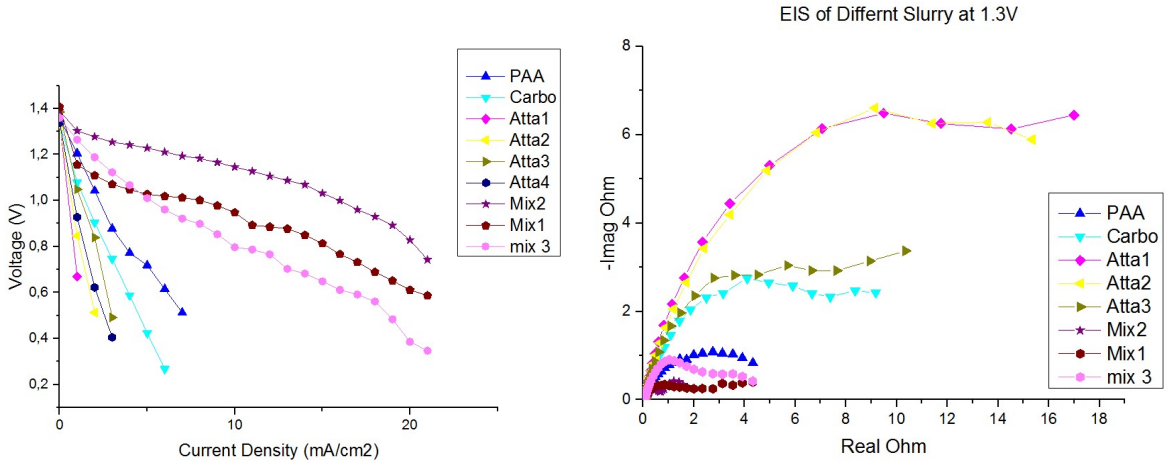

Figure 32 I-V Curve and EIS of different slurries

It can be seen that mixture 1 shows approximately 20mA cm^{-2} current density at 0.6V and approximately 25mA cm^{-2} with mixture 2. Mixture 3 shows the least current density out of three mixtures yet it shows much higher current density than PAA. Also, it can be checked from EIS that two mixture of gelling agent shows much less charge transfer resistance than PAA or other gelling agents when they are not mixed.

- **Conclusion:**

As conclusion, colloidal stability of zinc slurries is closely related to the nature of the gelling agent and to its concentration. Working conditions have to be considered as high pH and salts content can change the nature of rheology modifiers.

When proper gelling agents are selected, it is possible to determine the flow curves of zinc slurries at steady state. From the rheological tests performed, it was concluded that the effect of zinc concentration is not as dominant as the effect of gelling agent concentration, because even if the zinc concentration in wt % is high, its volumetric fraction, when compared to the one of the gelling agents, is smaller. This allows increasing the zinc concentration in the slurry without increasing significantly the viscosity. Hence, when gelling agents are prepared individually, PAA shows the highest current density among others. However, when Carbopol and Attagel are mixed, it actually shows at least twice higher current density than PAA, and also EIS indicates that mixture has got faster kinetics as charge transfer resistance is much smaller than individuals.

- **New method for zinc slurry preparation**

Previously, zinc slurries were made by adding zinc, zinc oxide, and PAA in the KOH and stirring them overnight when Attagel is not added. However, it has been found that by using homogenizer, zinc slurries could be improved even without a mixture with the Attagel with shorter preparation time, which is 10 minutes. New method involves following steps.

1. PAA and KOH were mixed by using homogenizer for 3 minutes.
2. Then ZnO were added and mixed by using homogenizer for 3 minutes.
3. Finally, zinc particles were added and mixed by using homogenizer for 3 minutes.

As mentioned in previous part, flow frame was used in the single cell to perform electrochemical performance, I-V curve as shown in figure 33. New method allowed to increase current density up to 30mA cm^{-2} from 8mA cm^{-2}.

By using homogenizer, slurries could be mixed more powerfully and uniformly as rotation per minute (RPM) used for homogenizer was 11000 whereas, with old method, maximum RPM could be performed was 1200. Hence, higher RPM helps zinc particles and gelling agents to form stronger network, and this led to better performances.

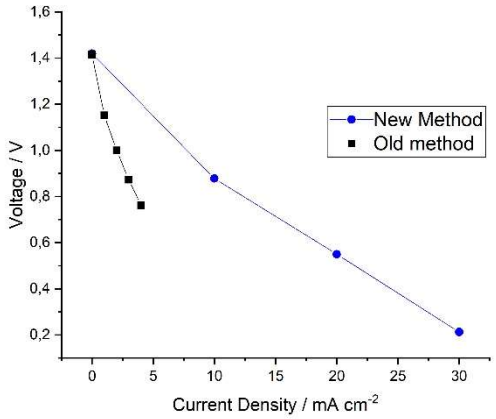

Figure 33 I-V curve of New method vs Old Method

2.3.3.3 Flow Field

- **Motivation**

All the CFD and modelling measurement of the flow field was performed by Diego del Olmo from University of Chemical Technology Praha in Czech Republic. However, interpretation and text are written by Nak Heon, Choi

One of the main considerations in redox flow battery design is the geometry of bipolar plate, which must promote uniform electrolyte flow on the electrode surface for enhanced electrochemical performance [64]. This is very critical as uniform flow distribution of electrolyte will lead to better mass transport leading to lower overpotential losses and, therefore, better electrochemical performances [65]. Furthermore, in stacked systems, uniform flow distribution helps facilitates the dissipation of heat generated by the reactions [66]. Hence, to build a reliable redox flow battery system, uniform electrolyte distribution is key.

For slurry flow batteries as zinc-air RFBs, the electrolyte flow is more important because there is no static electrode to boost the electrolyte distribution. In other words, the carbon felts or gas diffusion layers which are used for electrolyte diffusion in other RFBs will not be part of the negative electrode of zinc-air RFBs. This is because the slurry (zinc particles suspended in a highly alkaline electrolyte) acts as both electrode and electrolyte [67]. Consequently, an optimized design of optimized flow fields is required for the slurry to flow uniformly on the surface of the bipolar plate.

There are many types of flow fields already developed and used for many applications [68]. For example, for RFBs based on soluble species and PEM fuel cells, flow-by can be in parallel, serpentine, interdigitated, pinned or spiral [69]. Nonetheless, for slurry batteries and capacitors in which solid particles are always present (as in our case) most of the investigations were carried out with simple flow-through configurations [70-71]. For zinc air fuel cells with big particle sizes (~1 mm) and KOH overflow (particles are nearly fully dissolved), configurations relying gravity to ensure contact between the particles and the current collector were proposed [72-73] . More recently, some studies also investigated the effect of the current collector surface are in slurry batteries [74-75].

Hence, several types of flow fields, including plastic flow frames have been designed to find an optimized flow geometry for the zinc slurry electrolyte. These flow fields were first

evaluated by computational fluid dynamics (CFD) simulations. Then, experimental measurement was performed to find an optimal flow geometry for zinc-air slurry cells.

- **Experimental**

In the anode, zinc slurry acts as both an electrolyte as well as an electrode. To produce the slurry, 10 M KOH was first prepared. Then polyacrylic acid was added as gelling agent and the mixture was stirred for three minutes by using homogenizer which was introduced in the previous part with new method of preparing zinc slurries. Then, zinc oxide (ZnO) and Attagel were added and homogenized for another three minutes by using homogenizer. Finally, zinc particles (Grillo-Werke AG) were added and again stirred for three minutes with homogenizer. For the cathode, a membrane electrode assembly (MEA) was synthesized by placing a gas diffusion layer GDL (SGL) between the bipolar plate and a membrane. Platinum on carbon (1 mg cm^{-2}) was used as catalyst, it was directly sprayed onto the GDL. Cellophane was used as a porous membrane separator.

In this test, three different types of flow field were designed which are serpentine, parallel and flow frame as introduced in the previous section. For the cathode bipolar plate, a conventional serpentine flow field figure 34 (a) was chosen, whereas for anode bipolar plate, wider width of in figure 34, serpentine (b), parallel (c) and flow frame (d,e) were designed to determine the electrochemical performance of the system. The flow frame consists in placing a plastic frame on the top of the flat bipolar plate, instead of manufacturing flow fields on the graphite bipolar plate. The main difference between flow frames (d) and (e) is the distance between gaps. In flow frame (d) gaps are uniformly distributed whereas (e) has skewed distances between each gap. This was manufactured as the skewed flow frame showed more evenly distributed flow/electrolyte in CFD simulations.

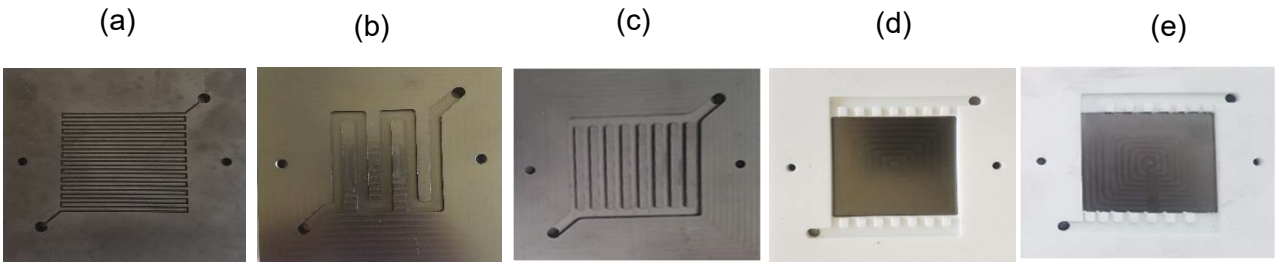

Figure 34 Different types of flow field used in the Zinc Slurry Air RFB

- **Simulation results**

The flow fields and frames proposed were investigated numerically by means of computational fluid dynamics using the software COMSOL Multiphysics. The negative of the original CAD drawings (i.e. the spaces were the slurry flows) were reproduced using the Geometry module of COMSOL. Then, the CFD analysis was carried out with the following assumptions:

- The slurry (electrolyte and particles) was treated all together as a single phase.
- Incompressible and laminar flow.
- 2D model was used.
- The rheology was described with a Herschel-Bulkley model.

The rheological parameters used were those measured by Diego Milian from Univ. Grenoble for a slurry with 40% weight of Zn and 1.25% weight of Carbopol (PAA) in 6 M KOH. It should be noted that the comparative results and trends between designs were the within the range of gelling agent concentrations studied. The summary of the simulation parameters is as follows:

Table 5 Parameters used during the CFD simulations.

Flow rate	114 ml min^{-1}
Fluid density	1500 kg m^{-3}
Flow consistency index	1.529 Pa·s
Flow behaviour index	0.634
Yield shear stress	11.022 Pa

In Figure 35 shows the flow distribution for the different geometries, the left graphs (colored) show the distribution of the velocity (m s^{-1}) in the cell while the right graphs show the velocity streamlines. Comparing, for example, the two-flow frame (FF) designs figure 35 (c & d) the streamlines indicate that the flow distribution is more homogeneous for FF-2. The pressure drop for all the geometries is summarized in Table 6. It can be noted that the

flow frames give the lowest pressure drops whereas the serpentine flow field leads to the highest pressure drop. It must be noted that the pressure drops given by the 2D simulation should be taken as qualitative rather than quantitative comparisons.

Table 6 Pressure drop of the different flow configurations.

	ΔP [Pa]
Flow frame 1 (FF-1)	888.01
Flow frame 2 (FF-2)	1338.8
Parallel	2421.5
Serpentine	6060.1

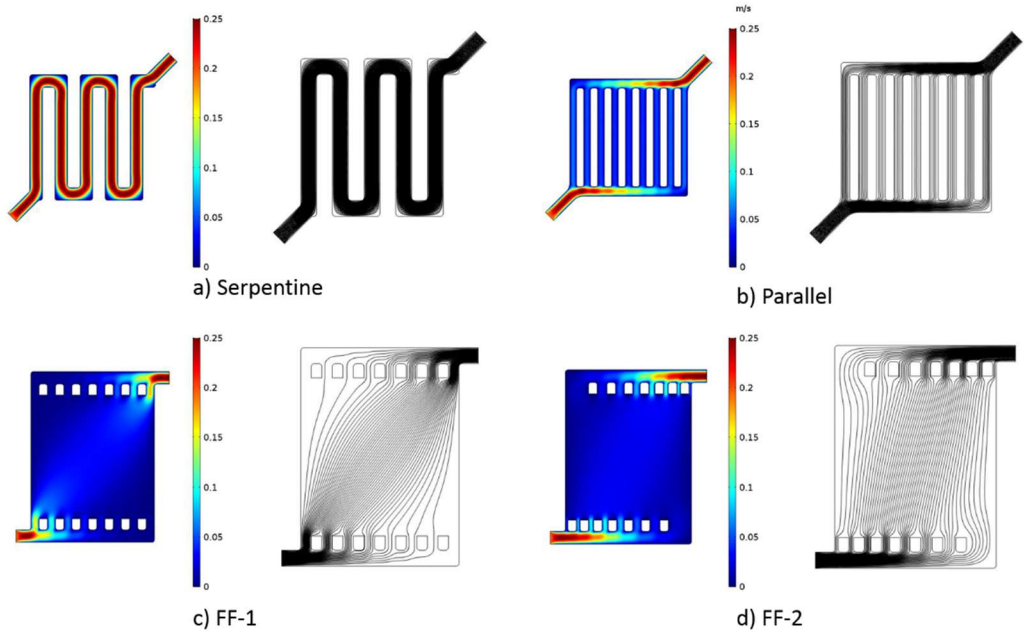

Figure 35 Velocity distribution and velocity streamlines for different flow fields.

Furthermore, some initial 3D simulations were conducted for the serpentine flow channel to assess the validity of the 2D approximation for this geometry. Figure 36 shows the streamlines from the CFD simulation for both a zero-gap serpentine channel (b) and a

serpentine channel with a 0.2 mm gap on top (c), corresponding to the experimental setup. The results indicate that most of the flow goes by the main channel and does not by-pass the serpentine geometry, suggesting that the assumption 2D flow is indeed sensible.

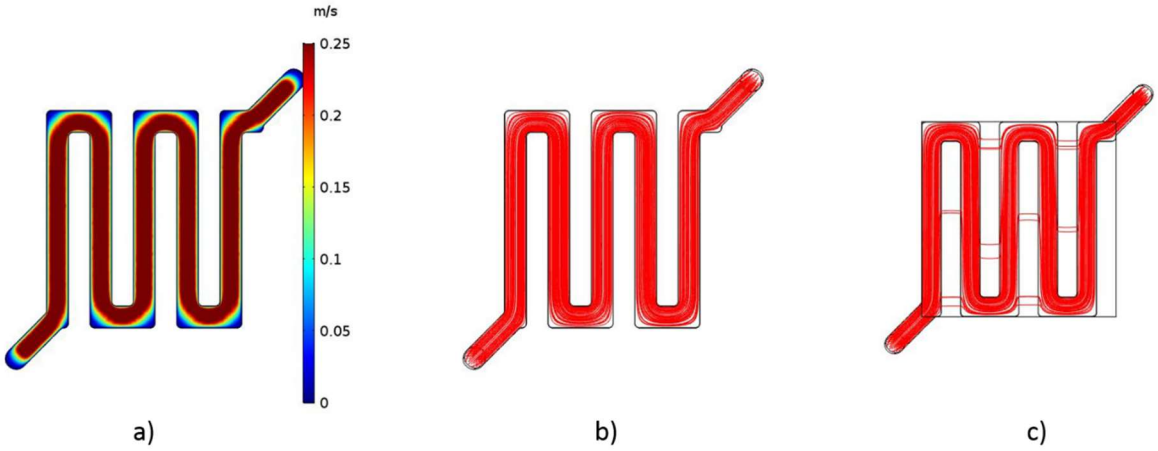

Figure 36 Simulations of the serpentine flow field:
a) 2D simulation, and 3D simulation with b) zero-gap and c) 0.2 mm gap.

- Experimental results

The four anode flow field designs were tested by measuring the polarization curve (I-V). In the previous tests, it was noticed that air pockets were present in the flow fields when flowing the electrolyte from the top of the cell. This led to a lower electrochemical performance and contradictory results when comparing experiments and simulations (as the simulation assumed that liquid was present in the whole flow field). Therefore, to make sure zinc slurries are filling whole flow fields, slurries were thereafter flowed from the lower inlet to the upper outlet. The serpentine flow field is labelled as S, parallel as P, uniformly distributed flow frame as FF-1 and skewed distributed flow frame as FF-2.

As shown in Fig. 37, Serpentine flow field shows the highest current densities, which is up to 80 mA cm^{-2}. Then, parallel shows approximately 70 mA cm^{-2} then FF-2 with 45mA cm^{-2} and FF-1 with 40mA cm^{-2}. Therefore, from simulation result, it has been proved that design of FF-2 shows better performance than FF-1. Also, it has been noticed that electrochemical performance is better in order of higher pressure drop when it is compared with values of pressure drop as shown in table 6. Furthermore, as EIS graph indicates, charge transfer resistance of serpentine and parallel types is much smaller than flow frames. However, not only higher pressure drop influences an electrochemical result but also, it has been discussed

about corrected geometric area which have an effect on the performances. The reason that serpentine and parallel types show better performance than flow frame types where they have larger corrected electrochemical active area than flow frames. For example, as shown in figure 38, based on 25cm^2 of geometric area, serpentine flow field also have walls where zinc particles can react. However, with flow frame, plastic flow frame is placing on the top of flat graphite plate, hence geometric area and corrected electrochemical area is same. Consequently, as serpentine and parallel types have more electrochemical area than flow frames, it shows better results.

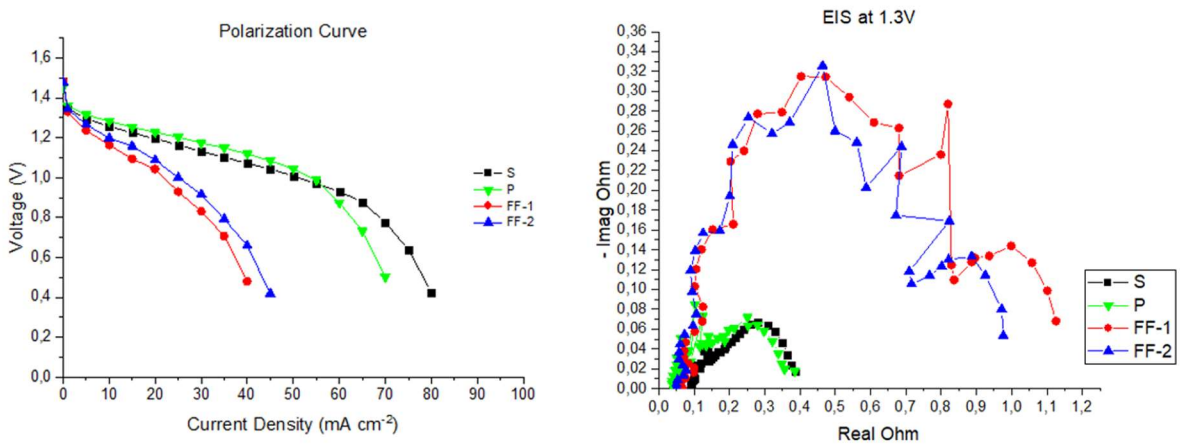

Figure 37 Polarization curves for the different flow configurations.

The higher-pressure drops are directly related with the area of the walls (note that higher pressure drops can lead to higher pump power consumption but this falls outside of the scope of the present study). For electrochemical systems, the electroactive surface area is a key parameter as it influences the cell performance. The electroactive surface area is the area of all the zinc particles electrically connected to the bipolar plate, which in turn will be related to the interfacial area electrolyte-bipolar. The reason that serpentine and parallel types show better performance than flow frames were that they have larger corrected electrochemical active area than flow frames. For example, as shown in Figure 38, based on 25 cm^2 of geometric area, serpentine flow field also have walls where zinc particles can react. However, with flow frame, as the plastic flow frame is placed on the top of flat graphite plate, the initial and corrected geometric areas are same. Consequently, as serpentine and parallel types have more electrochemical area than flow frames, they showed a better electrochemical performance.

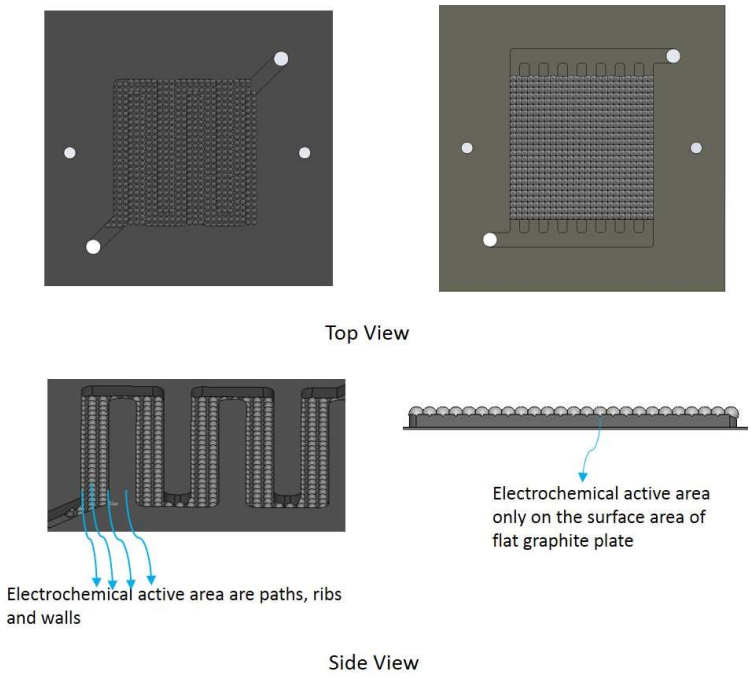

Figure 38 Illustration of the corrected electrochemical area.

- **Conclusion**

In conclusion, different types of flow fields including flow frame were designed to optimize the negative electrode and flow geometry of the zinc air slurry battery. These designs were tested both experimentally and by CFD simulations. In the CFD simulations, the flow frame type 2 (FF-2) showed a better electrolyte/electrode distribution than the flow frame 1 (FF-1). Similarly, experimental results showed that FF-2 has better electrochemical performance than FF-1. However, as serpentine and parallel types have larger corrected geometrical areas, they showed better performance than flow frame types.

2.3.3.4 Membrane

Previously, FAB-PK-130 anion exchange membrane from Fumatech was selected to operate Zinc Air Flow Battery. However, water uptake for this membrane is extremely low, hence humidifier was installed. However, even humidifier was installed, the water uptake from the humidifier is still not enough as this system is operating at room temperature. Also, from the EIS graph above, the ohmic resistance, which is highly influenced by membrane resistance is very high compare to other redox flow batteries. Hence, different types of membrane including porous membrane (separator) and commercial cellophane have been tested. Also, with separators, humidifier was not used as they can exchange water through their pores.

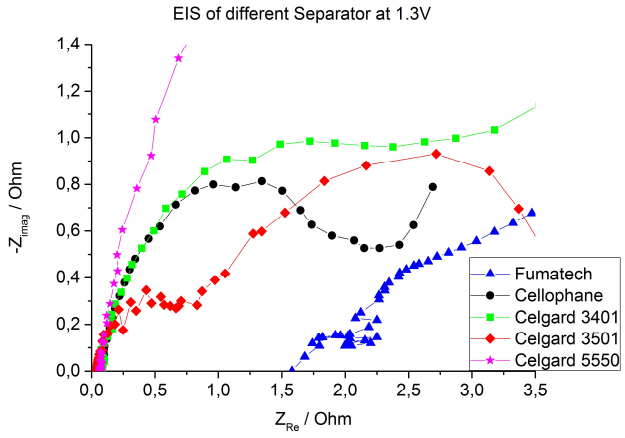

Figure 39 EIS with different membranes at 1.3V

As shown in fig 39 above, separators including cellophane have very low ohmic resistances. Hence, using separator can be helpful to improve the cell performances as well as reduce the system cost as humidifier is not required. However, as water uptake by separators are very high, zincate will also crossover, which will damage cathode electrode. Therefore, this experiment is still progressing to find an optimum membrane (separator) for zinc air flow battery.

Chapter 3

Discharge performance of Zinc Slurry Air Flow Battery

3.1 Improvement of Single Cell discharge performances

By summarizing chapter 2, following conditions have been used in order to determine the discharge performance of each flow fields of zinc slurry air flow battery.

3.1.1 Experiments

3.1.1.1 Positive electrode

The positive electrode was prepared by the catalyst-coated electrode (CCE) method. The composition of catalyst ink was mixing a Pt/C catalyst (40% Pt), with 10 wt% Fumion FAA-3 Ionomer (Fumatech), deionized water, and isopropanol. Catalyst mixture was sonicated in an ultrasonic bath for 15 min. Meanwhile, a gas diffusion layer layer(SGL Carbon, 29BC) was cut with a geometric area of 25 cm^2 and dried on the hot plate with a temperature of 130℃. After 15 minutes, catalysts were sprayed directly onto a prepared gas diffusion layer. After spraying, CCE was further dried on the hot plate. The platinum loading and ionomer content for catalysts were 1 $mg \cdot cm^{-2}$ and 23 wt% respectively.

3.1.1.2 Zinc Slurry Preparation

From previous chapter, using homogenizer showed approximately 3 times higher electrochemical performance than using stirrer. Hence, first, the Carbopol TM 940 (Acros Organics) was added to prepared 10 M KOH. The solution was mixed by using a high shear homogenizer with a 11,000 rpm for 5 min. This makes a strong gel network between Carbopol and KOH. Then, ZnO was added to the mixture and mixed again for 5 min. Zinc oxide was added to prevent self-discharge of the battery. Lastly, zinc powder with an average particle size of 50 μm (GC 7-4/200 Bi/200ln, Grillo) was added to the mixed solution and mixed for another 5 min. The total volume of zinc slurry was 70 mL, and the contents of the zinc slurry are shown in Table 7.

Table 7 Composition of the zinc slurry.

Mass fraction (wt%)			
Zinc	ZnO	Carbopol	KOH + Water
33.8	4	0.7	61.5

3.1.1.3 Flow Field Design

From chapter 2, different types of flow fields were introduced. As shown in Figure 40, two additional flow field have been further tested. For the positive plate, as air is flowing in and out, a conventional serpentine flow field (a) was chosen, whereas, for the negative bipolar plate, as the reactant is viscous zinc slurry, different types of flow fields were designed. As slurry can flow in the serpentine type flow field, wider serpentine (b) was designed, to increase the electrochemical area, parallel (c) was selected. Normal RFB flow frame (d) was also designed to perform the electrochemical performance of the battery. The flow frame is a Polytetrafluoroethylene (PTFE) frame placed on the top of a flat bipolar plate, instead of manufacturing flow fields on the plate. Moreover, to investigate the conductivity effect of the bipolar plate, a metal (copper) paper was positioned on the graphite plate for the flow frame configuration (e). Lastly, a modified serpentine flow field by using a copper–nickel (70:30) plate (f) was manufactured.

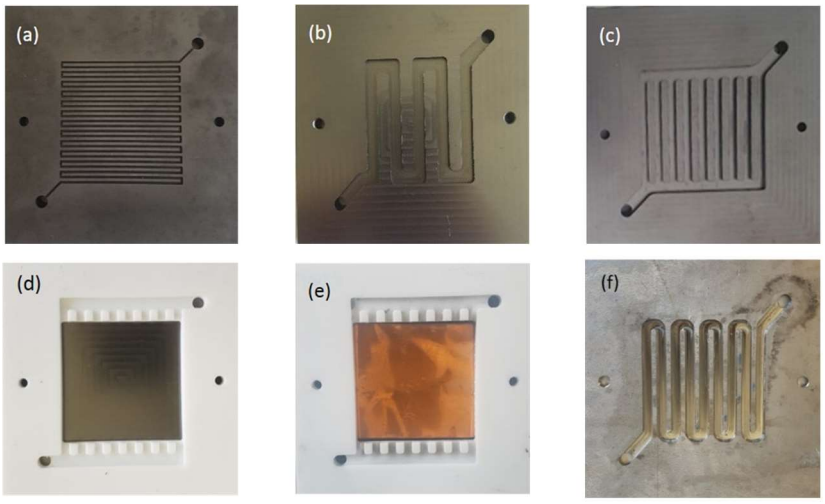

Figure 40 Flow fields used in this study. For the positive electrode: (a) serpentine. For the negative electrode: (b) serpentine, (c) parallel, (d) flow frame, (e) copper-based flow frame, and (f) modified serpentine.

3.1.1.4 Single Cell Assembly and Electrochemical Performance

A house built single cell was designed to determine the electrochemical performance of zinc slurry air flow batteries. As shown in Figure 41, it can be seen that the single cell contains an end plate, a current collector, bipolar plates, gaskets, and a separator. A prepared CCE was located between the separator (Cellophane™ PØØ) and the positive bipolar plate. When flow fields (E.g Serpentine, Parallel) were used, flow frame was not placed in the single cell. After the single cell was assembled, it was used to perform the electrochemical performance of each flow fields by using a technique of current–voltage characteristic curves (polarization curves) and electrochemical impedance spectroscopy (EIS). The condition of EIS measurements were constant voltage mode with a voltage of 1.3 V and 1.0 V to measure the ohmic and charge transfer resistance of flow fields at different polarization. During the measurements, zinc slurry was flowing into the single cell with a flow rate of 160 $mL \cdot min^{-1}$ and synthetic air were also continuously flowed in the positive electrode with a flow rate of 100 $mL \cdot min^{-1}$. As there is no static electrode in the zinc side, voltage fluctuations were occurring during polarization curves. Therefore, at each current density, the voltage was recorded for one minute and averaged.

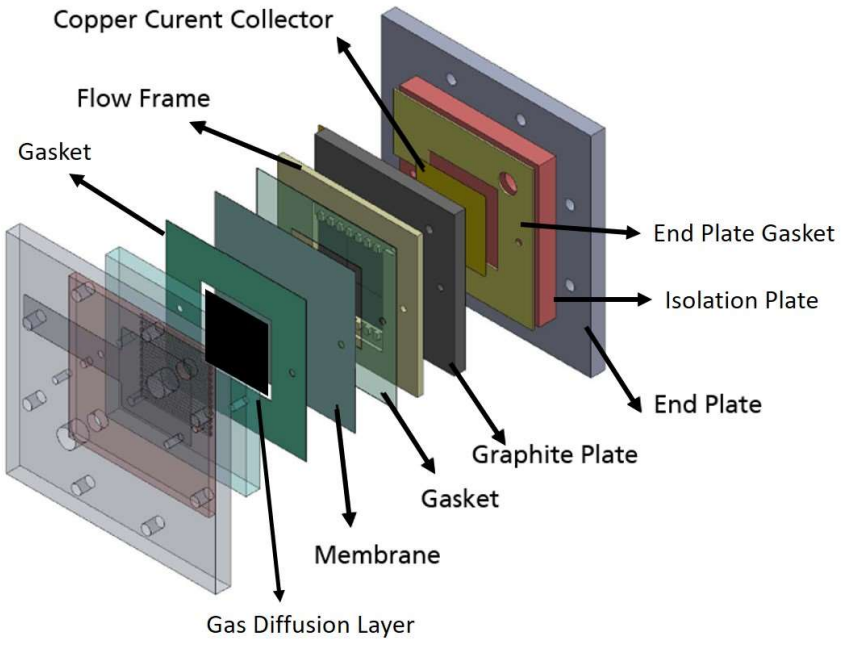

Figure 41 Schematic diagram of a single cell zinc slurry air flow battery with a flow frame.

3.1.2 Results and Discussion

3.1.2.1 Effect of Flow Fields

The polarization curves in Figure 42 show that, when graphite-based bipolar plates are used, the serpentine flow field performed the highest current densities than other types like parallel or flow frame at 0.7 V with 75, 40, and 15 $mA \cdot cm^{-2}$, respectively. This led, the maximum power density of serpentine flow field was 55 $mW \cdot cm^{-2}$ followed by parallel and flow frame 30 and 10 $mW \cdot cm^{-2}$ respectively. Also, figure 43 shows EIS results with a type of Nyquist plots shows, the ohmic resistance of battery (where the semi-circle cuts the real axis at high frequency) was mostly the same for all flow fields apart from the parallel flow field as shown in Figure 43c. The ohmic resistance of parallel flow field at 1.3V was 0.2 Ω and 0.12 Ω at 1.0 V. While the both serpentine flow field and the flow frame exhibited approximately 0.09 and 0.1 Ω at 1.3 V, and 0.07 and 0.10 Ω at 1.0 V. Not only ohmic resistance shows the differences but also charge transfer resistance showed significant differences between each flow fields. As shown in Figure 43 d, charge transfer resistance of flow frame is extremely higher than any other flow fields. Furthermore, different to other Nyquist plots from different RFB, it can be seen that the plots were oscillation and this is because there is no static electrode present in the negative compartment. As a subsequent, a continuous difference conditions were applied on the electrochemically active area, because of the formation and de-formation of percolation networks between the zinc particles in the slurry. Therefore, the EIS figures were fitted to the equivalent circuit which is shown in Figure 43a to calculate the charge transfer resistance. The charge transfer of flow frame showed around 10 times higher than any other types of flow fields which was 2.7 Ω and 0.25 Ω at 1.3 V. Also, results were similar at 1.0 V, where the flow frame showed a charge transfer resistance of 1.75 Ω, whereas the serpentine and parallel type exhibited 0.22 Ω and 0.45 Ω respectively.

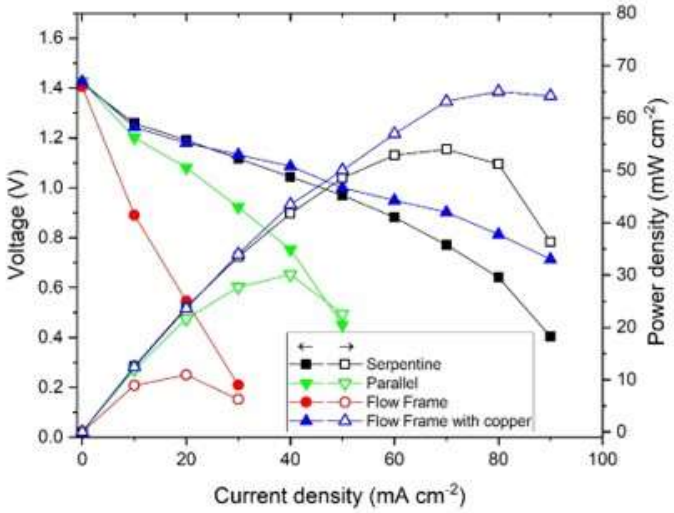

Figure 42 Polarization (solid symbols) and power density (open symbols) curves of the different flow fields.

To analyze the results, the characters of the battery have to be considered. As all the flow fields tested had the identical apparent geometric active area of 25 cm^2 however, the practical geometric active area was different. For instance, for the flow frame, the designed geometric and corrected active areas were identical to 25 cm^2 because it was a flat planar surface. Which means the zinc slurry is electrochemically active on the surface of the flat plate. Conversely, both serpentine and parallel flow fields had paths and walls for the slurry within 25cm^2 active area. Furthermore, as single cell design has a space between the flow field and the separator due to the gasket, it is not a zero-gap configuration for the slurry. Therefore, zinc slurry could flow both via the path and over the walls; within the geometric area of 25 cm^2. As a result, as the zinc particles in the slurry could also get discharged when slurries were touching with the walls of the paths, this led the corrected geometric area of the flow fields are different. Corrected geometric active area is therefore a sum of geometric area and area of walls, Details of the corrected geometric area are shown in Table 8.

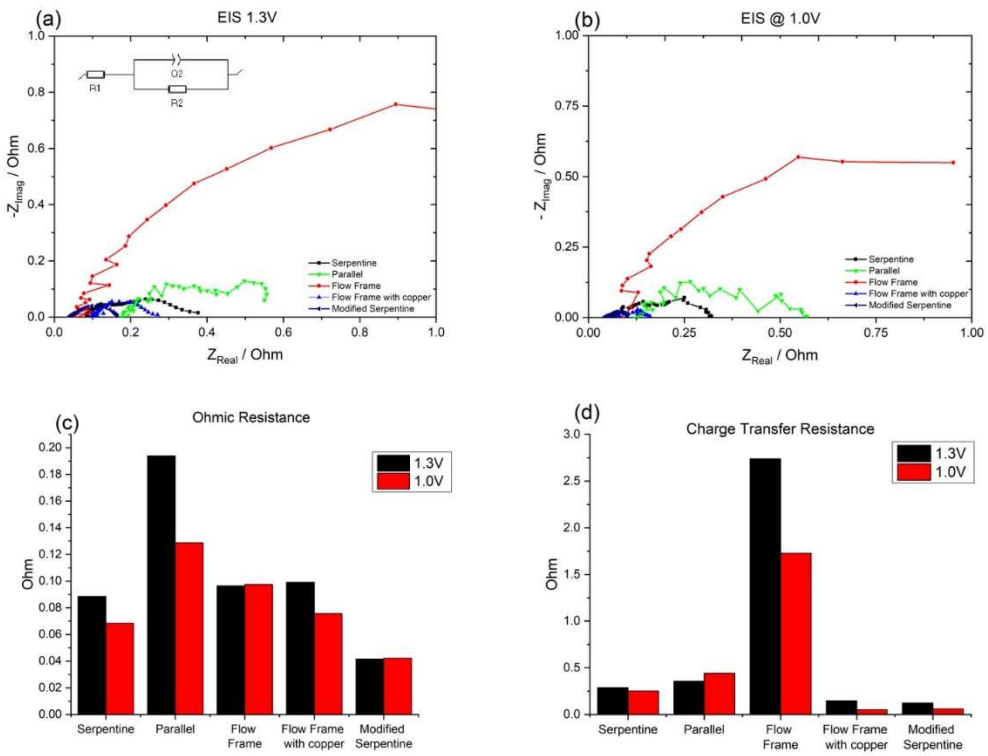

Figure 43 Nyquist plots for the different flow fields at (a) 1.3 V and (b) 1.0 V, and (c) graphs of ohmic and (d) charge transfer resistance.

Table 8 Active area and corrected geometric active area of each flow field.

Flow Field	Geometric Area (cm^2)	Area of Walls (cm^2)	Corrected Geometric Area (cm^2)
Serpentine	25	10.5	35.5
Parallel	25	14.4	39.4
Flow frame	25	0	25
Flow frame with copper base	25	0	25
Modified serpentine	25	17.82	42.9

Moreover, as there is no static electrode in the zinc side, the presence of dead volume in the flow fields are very critical. The zinc particles in the slurry are the electrochemically active material, therefore electrochemical performance can be influenced by the presence of dead volume. Thus, to observe the slurry flow distribution in the serpentine and parallel flow fields, a transparent end plate was placed in the end of the single cell as shown in Figure 44. The zinc slurries were flowing in single cell and observed for 60 seconds. When the parallel flow field is placed, dead volumes could be seen every 5–7 s, as shown in Figure 44b. Dead

volumes can be occurred when the flow distribution is not ideal and stagnant slurry or air is exhibit in the cell, that may direct to a negative influence of electrochemical performance. When serpentine flow field is used, no dead volumes were observed. This is because the serpentine flow fields push the zinc slurry in one direction and also flow is continuously flowing in therefore no dead volumes were observed. Whereas, parallel flow fields do not push the slurry in one way therefore, dead volumes are more expected to be observed. This leads to a harmfully influences to the battery performance as zinc particles are better to react continuously to sustain a good electrochemical performance. The presence of dead volumes is possibly a reason the parallel flow field showed a higher ohmic resistance than the serpentine, which led in worse performances than serpentine flow field.

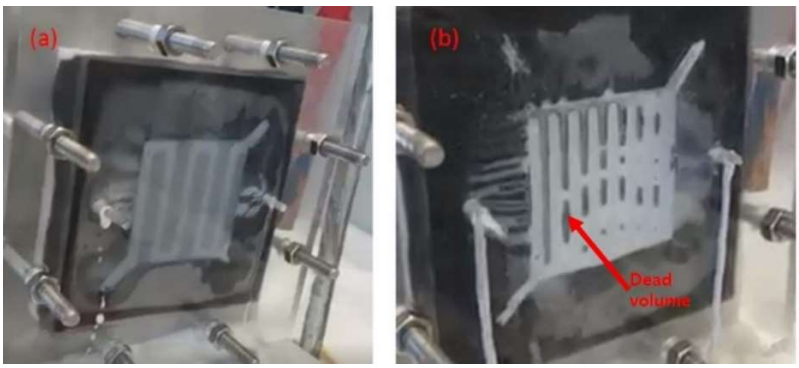

Figure 44 Distribution of the zinc slurry in the serpentine (a) and parallel (b) flow fields.

3.1.2.2 Effect of the Bipolar Plate Material

The material of the bipolar plate additionally acts a critical function as shown in both polarization curve and EIS experiments. Metallic plate copper was used as an alternative material for bipolar plate because copper is around 100 times more electrically conductive than graphite, which has the possibility to enhance the kinetics of zinc oxidation. Consequently, copper plate was placed on the bipolar plate when the PTFE flow frame was used. As a result, the polarization curve in Figure 42 indicates that by just placing a copper foil on the top of the graphite plate, the current density at 0.7 V increased from 20 to 95 $mA \cdot cm^{-2}$. Equally, the maximum power density also increased from 10 to 60 $mW \cdot cm^{-2}$, which was higher than the graphite-based serpentine flow (55 $mW \cdot cm^{-2}$). This indicates that the electrochemical performance of the battery can be enhanced when the metallic material of the bipolar plate is used. Also, the differences in ohmic resistance between copper-based and graphite-based are similar at 1.3 V, 0.09 Ω in both cases, and also at 1.0 V, 0.07 Ω for copper-based and 0.09 Ω for the graphite-based plates were observed, as shown in

Figure 43c. This shows that by changing bipolar plate to metal based from a graphite based, the ohmic resistance was decreased at higher current densities. Intriguingly, the charge transfer resistance of a copper-based flow frame was decreased 2.7 to 0.15 Ω at 1.3 V and also from 1.7 to 0.05 Ω at 1.0 V. As a result, it can be assumed that the zinc oxidation reaction is highly affected by the material of the bipolar plate.

The enhanced electrochemical performance of metallic bipolar plate can be connected to the zinc plating happening on the bipolar plate while discharging; it is well known from the literature that zinc plating occurs onto metals via an electroless process [102]. When the zinc particles touch the copper plate, part of the zinc particles dissolves into zincate, which further zincate plates onto the copper as zinc. The copper is not used throughout this process, as a subsequent in a catalytic effect, as the presence of a copper plate improves the zinc oxidation [103]. This directs to a state where not only the zinc particles touch the bipolar plate will be discharged, but also the material that is constantly plated on top of it. As a result, this allows a higher electrochemical active area and therefore causes a reduce in the charge transfer resistance.

3.1.2.3 Modifying a Flow Field with a New Material

From the results above, higher corrected geometric area with the flow field of the serpentine type based on metallic bipolar plate is required in order to boost the electrochemical performance of the battery. Consequently, a new bipolar plate by uniting the advantages of the previous result was introduced to further enhance the discharge performance. Instead of copper plate, a copper–nickel (70:30) alloy plate was chosen as a bipolar plate material to maintain low ohmic resistance of the battery. Metal alloy keeps its possessions during discharge with a highly alkaline slurry is flowing, therefore an alloy with high mechanical and corrosion resistance was chosen. Furthermore, it was shown that the corrected geometric active area was a critical feature for slurry-based flow batteries, a modified serpentine flow field with higher corrected geometric area with optimum flow distribution was designed (Figure 40f). Subsequently, the new modified serpentine flow field with a copper–nickel-based bipolar plate showed a big enhancement in the zinc slurry air flow battery performance. As shown in Figure 45, the current density at 1.0 V was 140 $mA \cdot cm^{-2}$, which was higher than any other flow fields at 0.7 V. Furthermore, the EIS results also showed that the both ohmic and charge resistance of the battery showed much lower when modified serpentine flow field was used. As shown in Figure 43c, in both EIS conditions, the measured ohmic resistance was 0.04 Ω which is the lowest throughout the whole experiment.

Additionally, the charge transfer resistances, were 0.12 Ω at 1.3 V and 0.05 Ω at 1.0 V, which were lower than the copper-based flow frame. This indicates that, manufacturing the flow fields by designing higher geometric active area and utilizing a copper–nickel alloy plate, not only it shows the highest power density but also it shows both ohmic resistance and charge transfer resistance can be minimized. In future, as the metal bipolar plate may have an issue about the durability of the battery; a durability experiment of each material, with a constant current discharge curve, should be tested.

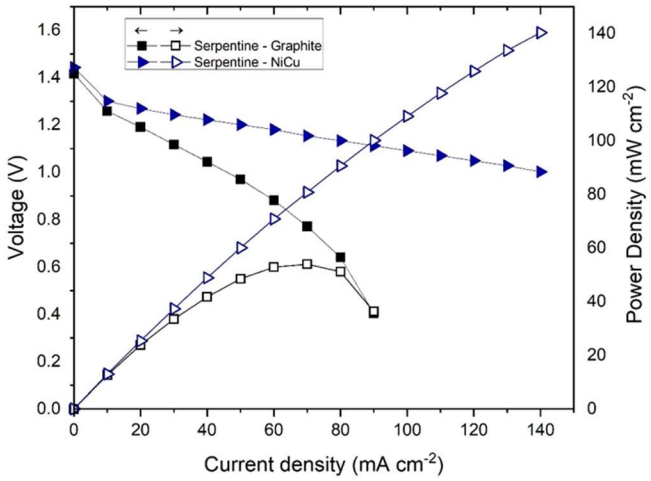

Figure 45 Comparison of the polarization (solid symbols) and power (open symbols) curves of the two serpentine flow fields with different materials.

3.1.3 Conclusions

In conclusion, various types of flow fields with different materials were tested in this chapter to improve the discharge performance of zinc slurry air flow batteries. When graphite-based bipolar plates were used, the serpentine flow field exhibited better performances than the parallel flow field and the flow frame design. This is due to the serpentine flow field showed no dead volume compare to the parallel type flow field, and also it has a higher corrected geometric active area than the flow frame. Moreover, when highly electrically conductive materials like copper or copper-nickel alloys were used, the discharge performance was significantly better. Therefore, for zinc slurry air flow battery, a design of the flow field with high geometric active area is required and also the electrically conductive bipolar plate requires to be used to attain an outstanding battery performance.

3.2 Study on the effect of organic and inorganic additives on discharge behavior

3.2.1 Motivation

The use of additives in zinc air batteries can provide a solution for the technological challenges of the system such as low charging efficiency, electrolyte conductivity or formation of passivating layers [91, 104]. The state of the art and specific challenges to overcome have been presented. It was determined that, although several works have investigated additives for zinc air batteries, specific studies on the effect of additives for zinc-slurry systems are scarce. In the present work, number of additives were selected which was used in the literature and studied their potential for use in zinc-slurry systems. The focus was to improve the discharge performance of the zinc anode, particularly in terms of depth of discharge. The reason following additives were selected is that it has been reported to mitigate hydrogen evolution are organic acids and bismuth-doped silica as particle coating. The use of surfactants to prevented the surface passivation of Zn. It was found that sodium docecyl benzene sulfonate favors the formation of porous ZnO structures rather than compact ones. Calcium oxide has been showed to help the cycling capability of Zn-air battery by providing nucleus for zinc electrodeposition and improving the ion conductivity. An improvement of improve the morphology of electrodeposited zinc at the cost of suppressing kinetics using a branched polyethyleneimine additive was presented. Other additives like carbonates, particularly, K_2CO_3 reduce the CO_2 absorption and the subsequent carbonation of the electrolyte.

3.2.2 Tested additives

In Table 9, we present a list of the additives used in this study together with their reported effect according to the literature. The composition of the slurries was based on the standard formulation presented in previous reports and listed in Table 10. When using additives, we aimed to keep the volume fraction of solids constant except for the tests with conductive additives. The selected amounts of additives used were also chosen according to the literature data. The formulation of all the slurries used in this study is presented in Tables 10.

Table 9 List of additives studied and their reported effects (following [78] and refs. therein unless indicated otherwise

Additive	Reported effect
$Ca(OH)_2$	Reduced zincate solubility and provides sites for ZnO deposition [80]
Tetraethylammonium hydroxide (TEAH)	Improved zinc morphology and energy efficiency [81]
Ethanol	Increased discharge capacity [82].
Bi_2O_3	Increase the electronic conductivity of ZnO and reduce hydrogen evolution.
Na_2SiO_3	Increase zincate solubility, stability and supersaturation [83].
LiOH	Reduced hydrogen evolution
KF	Increase ionic conductivity and lower zincate solubility.

Table 10 Formulation in wt% of the slurries with electrolyte additives.

Additive		Zn	ZnO	PAA	KOH	H_2O
None	-	33.8	4.0	0.7	20.0	41.5
$Ca(OH)_2$	4.8	32.2	3.8	0.7	19.0	39.5
TEAH	0.2	33.7	4.0	0.7	20.0	41.4
Ethanol	1.8	33.2	3.9	0.7	19.6	40.8
Bi_2O_3	0.5	33.8	3.5	0.7	20.0	41.5
Na_2SiO_3	1.0[a]	33.8	3.0	0.7	20.0	41.5
LiOH [7:0.7]	1.8	33.8	4.0	0.7	13.7	46.6
KF [8:2]	6.4	33.8	4.0	0.7	14.3	40.8

Note: in brackets are molar ratios of electrolyte KOH:additive (e.g. [8:2] means 8 M KOH + 2 M KF)

3.2.3 Cell setup

The discharge performance of the slurries under study was tested using our in-house built Zn-slurry/air flow battery. For these experiments, we used a graphite bipolar plate on the air side and NiCu (for electrolyte additives) on the negative side (Figure 46). A Cellophane PØØ (FUTAMURA) porous membrane was placed between the positive and negative electrodes to prevent short-circuiting. The positive electrode consisted of a GDL onto which the catalyst ink (Pt/C, 10wt% Fumion FAA -3 ionomer, deionized water and isopropanol)

was sprayed directly. The platinum loading on the catalyst layer was 1 mg cm^{-2} and the ionomer content 23wt%.

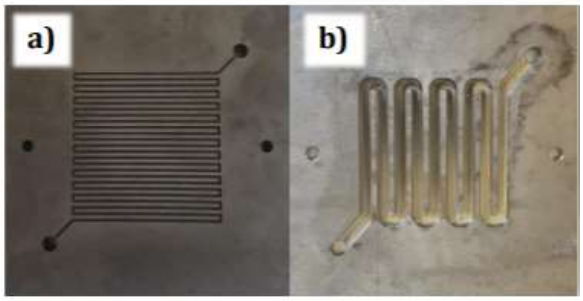

Figure 46 Serpentine flow fields used for the test : a) positive side bipolar plate, b) negative side bipolar plate

The discharge performance of the additives was studied by means of polarization curves followed by single discharge experiments at 50 mA cm^{-2}. During testing, the zinc slurry and compressed air were flown constantly inside the cell negative and positive compartments, respectively

3.2.4 Results

The results of the polarization experiments are presented in Figures 47 and 48, for clarity the slurries have been separated following their performance compared to the standard formulation

Figure 47 shows the additives with worse performance than the standard slurry. The standard slurry showed a maximum power density of around 100 mW cm^{-2} and a current density of 110 mA cm^{-2} and 0.8 V. The slurry with LiOH showed acceptable performance at low current densities but the experiment suddenly terminated at 45 mA cm^{-2}, even if the voltage at 40 mA cm^{-2} was 0.9 V. This effect requires further future investigation as it was the only sample to show such a drastic voltage drop. Therefore, the galvanostatic discharge could not be done for this sample. The slurry with $Ca(OH)_2$ presented a much higher viscosity than the standard, which resulted in a higher ohmic resistance (slope of the curve) and earlier mass transport limitation (sharp decay at higher currents) as shown by the polarization curve.

Furthermore, as it was not able to flow smoothly the galvanostatic discharge experiment was not carried out for this sample. The slurry with KF shows a similar charge transfer polarization as the standard (performance is similar at low currents) but higher ohmic

resistance and mass transfer limitations. This resulted in a peak power density of 75 mW cm^{-2} and a current density of 90 mA cm^{-2} at 0.8 V. The lower polarization performance was an expected behavior due to the lower concentration of OH^- and replacement by less mobile F^- (the additive was aimed to improve discharge capacity).

Finally, the viscosity of the slurry with TEAH was also higher and its polarization performance was overall worse than the standard with peak power density of 73 mW cm^{-2}.

On the other hand, the polarization curves of the slurries with similar or better performance than the standard are shown in Figure 48. The use of ethanol produced a less viscous slurry which could be related to the lower ohmic resistance. However, the charge transfer polarization was worse than the standard, leading to a maximum power density of 83 mW cm^{-2}. Similarly, the slurry with Bi_2O_3 had lower ohmic resistance (in this case attributed to higher solid conductivity promoted by the presence of the additive in the ZnO layers) but worse charge transfer polarization than the standard sample. However, at higher currents, it did not reach the charge transfer limitation which resulted in a similar peak power density as the standard (95 mW cm^{-2}). The best electrochemical performance was presented by the slurry with Na_2SiO_3 which presented a much lower ohmic resistance than the rest of the samples and a similar charge transfer polarization as the standard slurry. The sample reached a peak power density of 185 mW cm^{-2} (nearly double of the standard slurry) and current density of 220 mA cm^{-2} at 0.8 V.

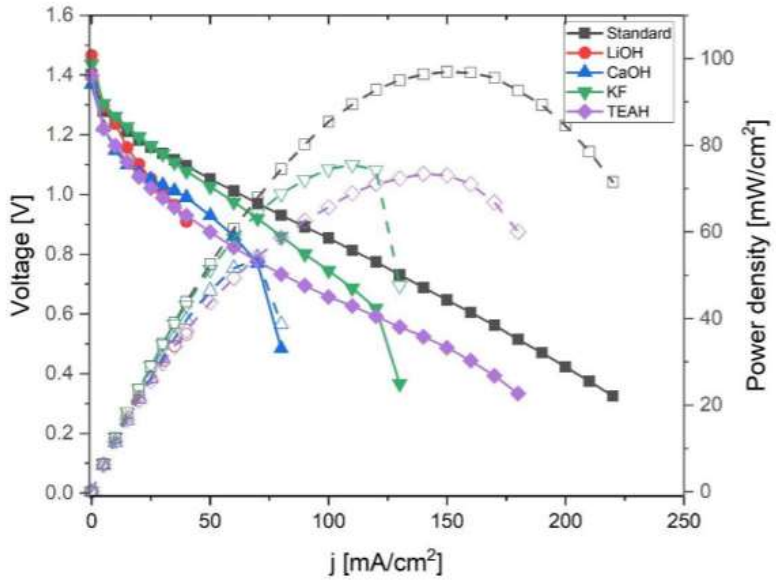

Figure 47 Polarization (solid) and power (dashed) curves for additives with poorer performance than the standard slurry

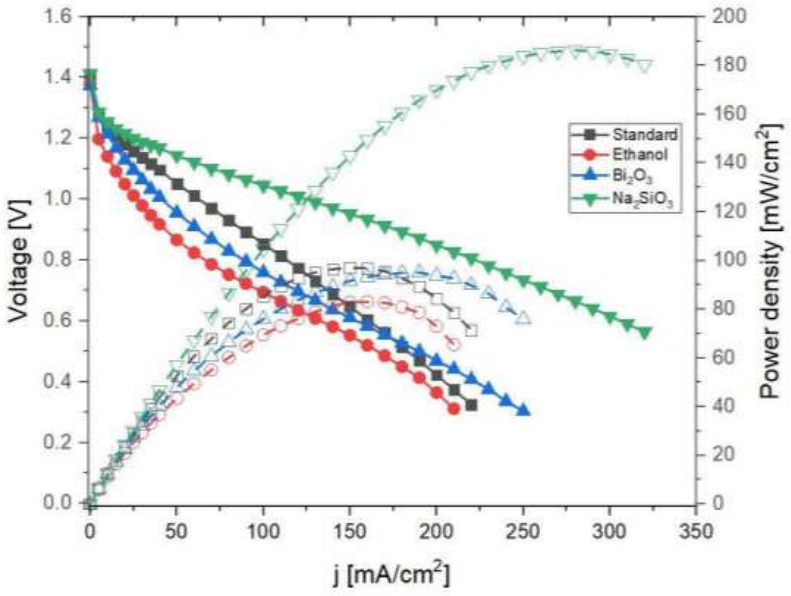

Figure 48 Polarization (solid) and power (dashed) curves for additives with similar or better performance than the standard slurry

The results of the galvanostatic single discharge experiments are shown in Table 11. It should be noted that the discharged capacity and energy from the polarization experiments were also added to the total (as these were carried out just before the single discharge). The volumetric capacity of the slurries with TEAH, KF and ethanol was similar to that of the standard slurry (between 75 and 85 Ah/L_{slurry}). Similarly, the volumetric energy densities were around 75 Wh/L_{slurry} except for ethanol which was only 50 Wh/L_{slurry}. The slurries with Bi2O3 and Na_2SiO_3 had nearly double the volumetric capacity of the standard (close to 150 Ah/L_{slurry}). Particularly, the best volumetric energy density was achieved with Na_2SiO_3 reaching 154.5 Wh/L_{slurry} which is nearly six times higher than commercial all-vanadium redox flow systems [84].

Table 11 Discharge capacity and energy density after polarization and galvanostatic discharge tests

Additive	Capacity		Energy density
	Ah/kg_{Zn}	Ah/L_{slurry}	[Wh/L_{slurry}]
None	136.3	79.4	78.1
TEAH	146.3	85.2	72.0
KF	145.4	84.7	77.7
Ethanol	127.8	74.5	50.9
Bi_2O_3	254.7	148.5	119.2
Na_2SiO_3	250.9	146.2	154.5

4. Conclusion

In this study, it was showed the effect in a Zn-slurry/air flow battery of a few additives reported in the literature for non-flowing Zn-air systems. Two of the additives (Bi_2O_3 and Na_2SiO_3) showed a superior electrochemical performance during discharging in terms of polarization and discharge capacity and energy. The best performance was shown by the slurry with 1wt% Na_2SiO_3 which presented an energy density of 154.5 Wh/L_{slurry} and this is mostly due to the stability and zincate solubility has increased by adding Na_2SiO_3 which leads to the better electrochemical performance especially in the slurry-based flow battery.

Chapter 4

Recharge performance of Zinc Slurry Air Flow Battery

4.1 Preliminary test of recharging

As discharging is no longer a primary problem to operate the zinc slurry air flow battery, now research has been focused on charging and recharging. Hence, by using experimental condition shown in table 12, preliminary charging test have been performed.

Table 12 Experimental Conditions

Single Cell	
Air Side flow field	Serpentine (Graphite and CuNi)
Zinc Side Flow Field	Graphite Serpentine
Cutoff voltage	2.2V and 2.3V
Current density	10mA cm^{-2}
Zinc Slurry	
PAA	0.4%
Carbon black	0-1%
ZnO	4%
Zinc	34%
10M KOH	Rest
MEA	
Catalyst loading	1mg cm^{-2}
Ionomer contents	23%
Membrane	Porous separator

As shown in Table 12, charging has been started with zinc slurry without carbon, which is the basic zinc slurry composition for discharging. Figure 49 shows the only charging graph as 10-minute discharging performances were not varying much. Hence after 10 minute of

discharging, basic zinc slurry can only charge for less than a minute. Furthermore, zinc slurry with 0.2% of carbon, it also shows small improvement but still less than a minute for charging. However, when 0.6% of carbon is added, charging time increased to 2 minutes. Hence, 1% of carbon was added but it decreased the charging time. Hence, 0.6% of carbon was set for charging as it has shown the optimum performance.

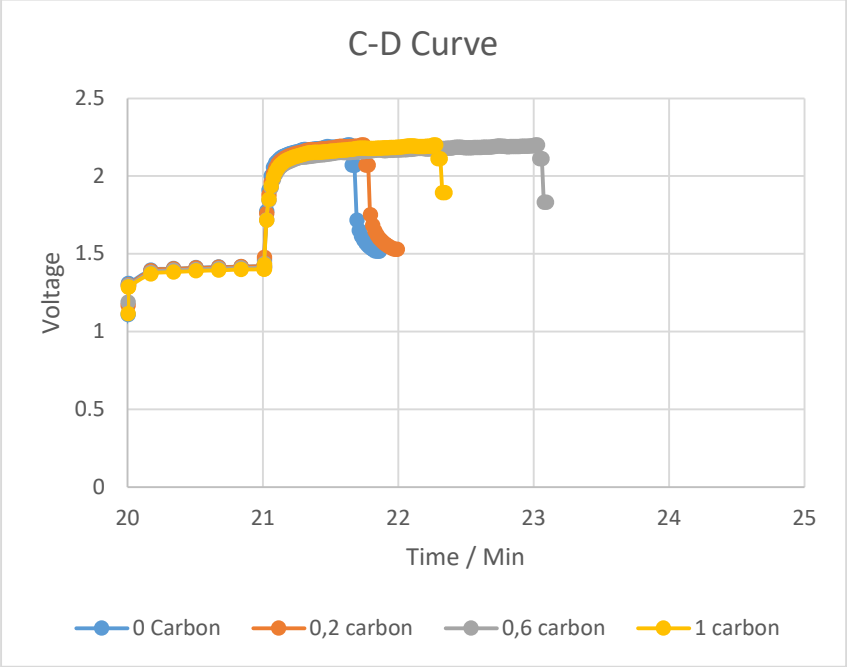

Figure 49 Charge-Discharge curve with different carbon composition

However, even 0.6% shows the better charging performance, 2-minute charging time is too short and it requires improvement. Hence, air catalyst has been changed from platinum carbon to platinum carbon + Iridium Oxide. As charging mechanism is based on oxygen evolution reaction (OER), iridium oxide is added to assist better OER. Furthermore, instead of platinum on carbon, platinum back was also tested as carbon at high voltage may interfere the reaction. Results are shown in figure 50 below. When platinum black + IrO_2 is used, charging time increased to about 6 minutes from 2 minutes.

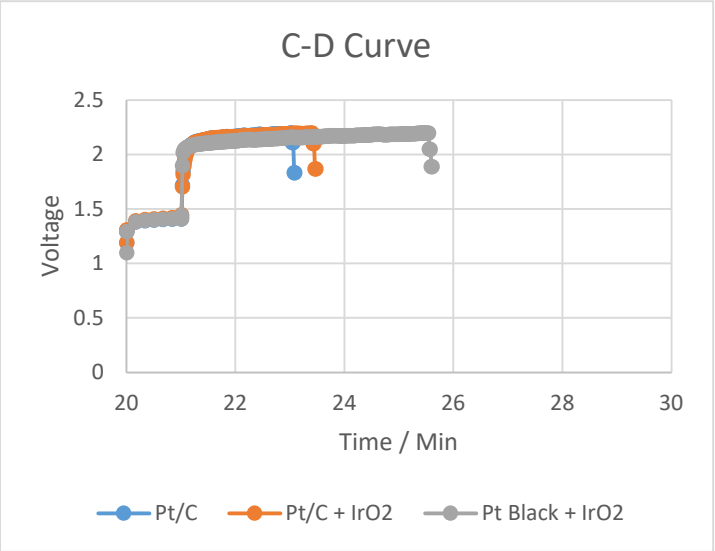

Figure 50 Charge-Discharge curve with different air catalyst composition

Up to this experiment, charging cut-off voltage was set to 2.2V, however, this could be set higher to 2.3V when carbon is not used in air catalyst. Hence, by using 0.6% of carbon in zinc slurry, and using Platinum black+IrO_2 catalyst in air side, I have set the cut-off voltage to 2.3V and also changing air bipolar plate from graphite to copper-nickel alloy metal plate and performed charge-discharge curve and shown in figure 51 below.

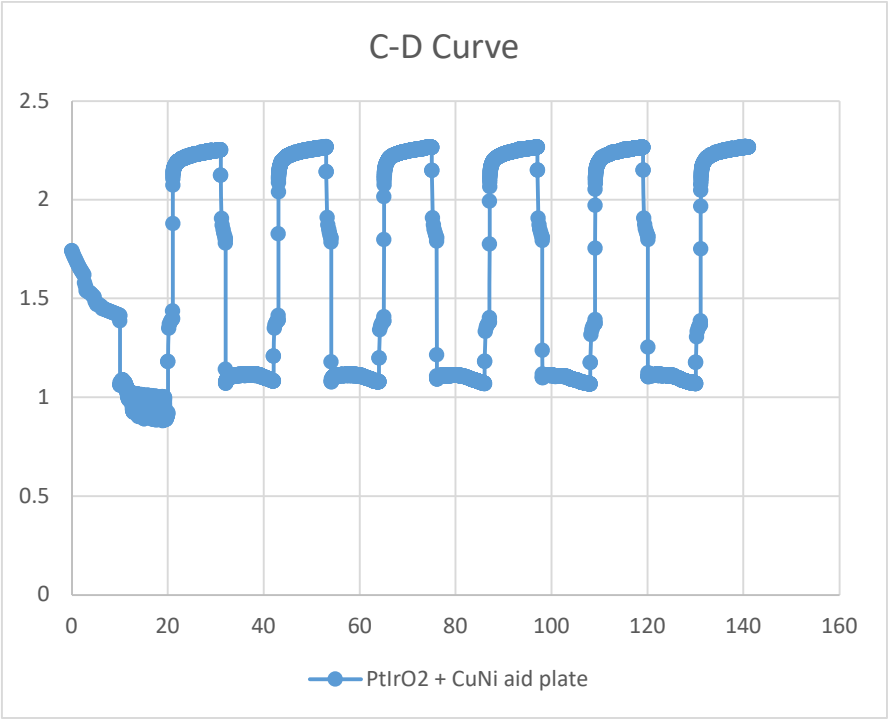

Figure 51 Charge-Discharge curve with new configuration

4.2 Improvement of Single Cell recharge performances

From chapter 4.1, preliminary condition for rechargeable zinc slurry air flow battery was set. Hence test conditions as well as methods are described in following sections.

4.2.1 Experimental

4.2.1.1 Air Electrode

As discharging is ORR, charging is oxygen evolution reaction (OER). Hence, the composition of catalyst should be different to the previous experiments. Again, as separator was used, the MEA was prepared by the catalyst-coated electrode (CCE) method for air electrode. Therefore, the catalyst ink was containing both a Pt black (Platinum black) and IrO_2 with a ratio of 1:1 and also ionomer of Fumion FAA-3 was added with 10 wt.%. Then deionized water, and isopropanol was mixed together. The catalyst was first homogenized by placing it in the ultrasonic bath for 10 min, and then, by using an ultrasonicator, it was further homogenized for another 10 min, to confirm a good dispersion of catalyst mixture. Meanwhile, GDL was cut in the size of $25cm^2$ and it was placed on the hot plate with a temperature of 130°C. After sonication, catalyst ink was sprayed directly on the GDL and after spraying, it was further dried on the hot plate. The catalyst loadings were 0.5 $mg \cdot cm^{-2}$ for both platinum black and iridium oxide with the ionomer content 23 wt.%.

4.2.1.2 Zinc Slurry Preparation

The aim of this chapter is to minimize the zinc plating on the bipolar plate. Therefore, zinc slurry was prepared differently. The base gel polymer electrolyte (GPE) is same as previous condition which contains 10 M KOH by adding Carbopol TM 940 for gelling agent. To make a gel network stronger, the GPE was homogenized by using homogenizer with a rpm of 9.500. Then, the zinc powder (GC 7-4/200 Bi/200ln) with D50 = 55 µm, ZnO and importantly, carbon black (CB, carbon black, acetylene, 50% compressed) with D50 = 0.045 µm were added and the slurry was homogenized in total 9 minutes. As CB is introduced in this slurry, the compositions are shown in Table 13; the sum of the CB and 10 M KOH added to 61.5 wt.%. The total amount of zinc slurry was approximately 70 mL for each experiment.

Table 13 Composition of the zinc slurries.

	Mass Fraction (wt.%)				
	Zinc	ZnO	Carbopol	Carbon Black	KOH + Water
0 Carbon (0%CB)	33.8	4	0.7	0	61.5
0.2 Carbon (0.2%CB)				0.2	61.3
0.6 Carbon (0.6%CB)				0.6	60.9
1 Carbon (1%CB)				1	60.5

4.2.1.3 Cell Design and Electrochemical Characterization

The electrochemical performances of the CB added zinc slurries were tested by using manufactured single cell introduced in previous chapter. It consists of bipolar plates, a porous membrane (separator), gaskets, and current collectors and end plates. This is a single cell configuration, but as this single cell design is aimed on upscaling and also stackable design, the graphite plate on the negative compartment and metallic plate on the air electrode are written as bipolar plates. From chapter 4.1, it was observed that the charging voltage was above 2 V therefore, positive side bipolar plate was manufactured by CuNi alloy with a single serpentine flow field. Despite modified serpentine flow field of CuNi alloy showed outstanding performance for discharge, the negative bipolar plate used in this experiment was graphite with serpentine flow field to minimize zinc plating. The prepared CCE was located between the metallic bipolar plate and the separator (Cellophane™ PØØ).

Every prepared slurry was tested by polarization curves and galvanostatic charge-discharge cycling. The charge-discharge cycling was running for 10 min per half-cycle with the voltage cut-offs conditions were 0.3 V for discharge and 2.3 V for charge. The flow rates of zinc slurries were 160 mL·min^{-1} and 100 mL·min^{-1} for the synthetic air. Like previous chapter, the voltage recorded for each current density during the polarization curves was averaged for 30 seconds and basic schematic diagram of the battery is shown in figure 52.

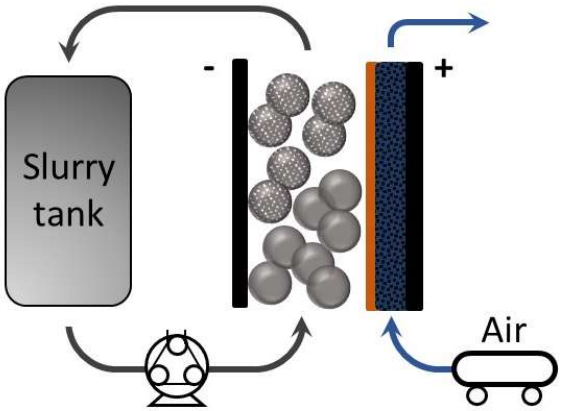

Figure 52 Schematic diagram of a zinc slurry air flow battery.

4.2.1.4 Rheometry

The rheology experiments were performed by Diego Milian from University of Grenoble in France

The rheology of the slurries was tested in terms of steady shear and oscillatory rheometry. A stress-controlled rheometer (AR-G2) was prepared with a four-blade vane-in-cup geometry (L = 45.5 mm, D = 30 mm), which was aimed to decrease the flow-related heterogeneity problems [85-86]. The usage of grill cup was to minimize the influence of slippage [87]. This equipment was calibrated by referring to the following sources : Baravian for large finite gaps [88]. All rheological experiments were tested at room temperature.

The steady-state experiments were attained by operating a constant shear rate range from 100 to 0.01 s^{-1}. It was selected to begin from high shear rates to low shear rates to make sure the viscosity steady-state measurements [89]. To enumerate the rheological variables of the CB slurries, following curves were fitted to Herschel-Bulkley model : shear stress vs. shear rates curves

$$\tau = \tau_y + K\dot{\gamma}^n$$

Where, τ = shear stress

τ_y = yield stress

K = consistency index

$\dot{\gamma}$ = yield stress

n = flow index

Experiments of oscillatory strain amplitude sweep were tested from 0.1 to 1000% at 1 Hz to examine the linear viscoelastic region of both storage and loss moduli.

4.2.2 Results

When 0 CB was tested for charge-discharge cycling, zinc plating on bipolar plate occurred during charging (see Figure 53a). The metal plating on the plate is the well-known results in flow-assisted batteries, like zinc-nickel [90]. However, it is an unwanted result for zinc slurry air flow batteries, as this will be a drawback by restricting the capacity of the battery. Consequently, the highest amount of zinc which can be recharged would be provided by the size of the battery and depth of the flow fields instead of the total amount of slurry. Moreover, the zinc plating on bipolar plate can lead to a dendrite formation that could block the flowing of zinc slurry, finally, dendrite will break the membrane and it will lead to a short circuit of the battery.

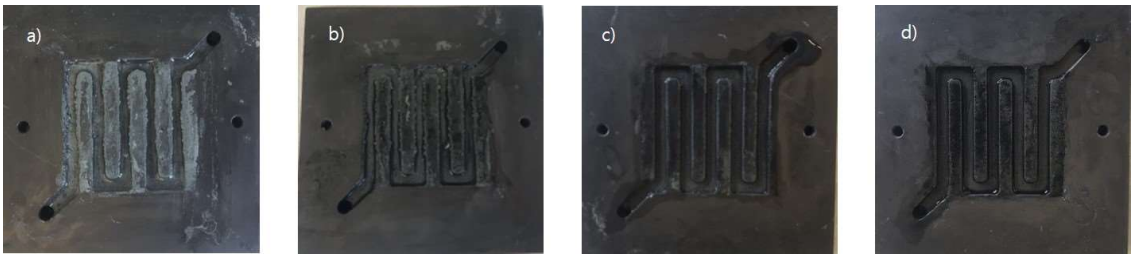

Figure 53 Zinc-side bipolar plate after charging: (a) 0% carbon black (CB), (b) 0.2% CB, (c) 0.6% CB, (d) 1% CB.

Therefore, CB was added in the zinc slurry to minimize this effect, targeting to move the zinc plating from the bipolar to the CB in the slurry. This new zinc slurries would let the recharged zinc slurries flowing in and out of the battery directing to a slurry flow battery system instead of a flow-assisted configuration. The rightness of the idea was visually proved by visible examination of the bipolar plate directly after charging from cycling. It can be observed in figure 53 that the CB in zinc slurry allowed to minimize the zinc plating on the bipolar plate.

4.2.2.1 Oscillatory and Shear Rheometry

Firstly, rheological behavior examination was tested to evaluate their rightness for slurry RFBs. Oscillatory rheometry (Figure 54) showed a linear viscoelastic region (LVR) where G'>>G'', showing that the entire stress was from mainly by the elastic modulus G'. The LVR is examined by a moduli plateau where viscoelastic properties do not rely on strain.

This performance was obtained in all slurries showing that a percolated network occurs within the linear region [91].

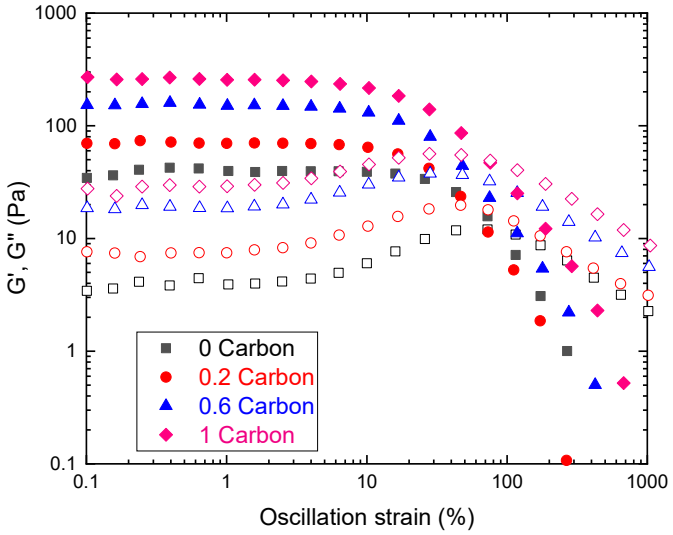

Figure 54 Oscillatory strain amplitude sweep test performed at f = 1 Hz for carbon slurries. Closed symbols represent storage moduli (G') and open symbols loss moduli (G'').

As shown in Figure 54, higher CB slurries produced higher moduli values, showing that the networks be inclined to act more as elastic solids. In other words, an optimal tradeoff from sample structure and viscosity requires to be obtained. Additional critical feature of these curves is that, when a strain is given, the moduli trend was inverted (G''>G'), this indicate a reverse in the performance as the sample breakdowns and flow begins which is a yield stress [92]. There is not yet published to calculate the standardized yield stress by oscillatory methods. Consequently, the yield stress of the slurries was examined using shear rheometry.

The steady-state measurements (Figure 55) indicated that the slurries show a non-Newtonian behavior, to be specific, it is a shear thinning behavior. This behavior verifies advantageous to slurry-based RFBs because it decreases the particle sedimentation and segregation and also viscosity reduces when the slurry is pumped. Generally, the addition of CB directed to a reduce in the flow index (see inset Figure 55b). Newtonian fluids have a flow index n = 1, whereas CB slurries showed in this test showed a shear-thinning behavior (n < 1). When CB is added, this flow index number increased, but when there are too much CB in the slurry, it reduced and showed the values lower than no CB slurry and shear thinning behavior is well established.

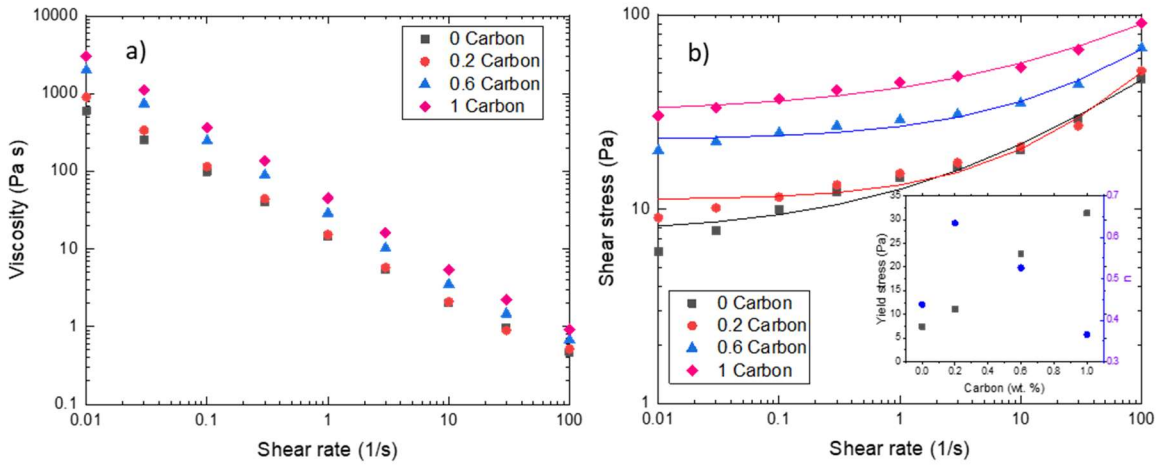

Figure 55 Steady-state rheometry. (a) Viscosity values vs. shear rate for carbon slurries. (b) Shear stress vs. shear rate for carbon slurries. Lines represents Herschel-Bulkley fitting. The inset in the graph shows the values of yield stress and flow index for all carbon slurries obtained from the fit.

In Figure 55a, it can be seen that the values of viscosity reduced by a factor of 104 for 1%CB and a factor of 103 for 0CB in the range of shear rates analyzed. Between the 0CB and 0.2%CB slurries they presented similar values at high shear rates (from 0.1 s−1), showing that the by adding 0.2 wt.% of CB, viscosity was not changed even if it changed its viscoelastic properties (Figure 54). When higher CB zinc slurry is used, it showed in an increase of five-fold viscosity at low shear rates and a two-fold increase at high shear rates. This matches with the examination tested by Gallier et al. [93], showing that the shear stress can be increased when there are contact forces due to its friction and roughness of particles next to each other before entering a lubricational regime at higher shear rates when contacts are reduced.

Figure 55b displays the shear stress with a function of shear rate. As these results showed a yield stress behavior, the values were fitted to a Herschel-Bulkley model. As referred by Smith et al. [63], some rheological variables can be modified to enhance the energy efficiency of the battery. As observed in the Figure 55b, the concentration of CB was completely proportional to yield stress. Wei et al. [91] have confirmed that higher yield stresses direct to higher electronic conductivity, in this case, it is very advantageous for the battery. Whereas, higher pressure drops must be achieved to overcome yield stress that can brutally influence the total efficiency of the battery[94].

4.2.2.2 Polarization Curve Analysis

After analyzing rhelogical behavior, the influence of the CB in the zinc slurry was tested electrochemically. The polarization curves of each zinc slurries are shown in Figure 56. For discharge performance(Figure 56a), it can be seen that, at low current densities, where the kinetic or activation resistance is dominant, the zinc slurries with carbon showed higher current densities than no CB. At 0.6 V, the current density of CB slurry was 24 $mA \cdot cm^{-2}$ for 0CB, 38 $mA \cdot cm^{-2}$ for 0.2%CB, 36 $mA \cdot cm^{-2}$ for 0.6%CB, and 28 $mA \cdot cm^{-2}$ for 1%CB. The better discharge performance is credited to stronger particle network in the zinc slurry which was enhanced by the CB. As a result, CB made a higher electrochemically active area from percolating zinc particles. At higher current densities, where the mass transfer limitation is dominant, a higher carbon content caused to a fall in discharge performance. The carbon black makes OH^- harder to travel within the zinc slurry by blocking them and therefore, higher mass transfer resistance is caused by CB in the slurry. Nevertheless, the 0.2%CB slurry has similar rheological properties with 0%CB and therefore it electrochemically performs better than 0% CB in all current density region. Additionally, the power density obtained showed that zinc slurries with CB was also higher with 23 $mW \cdot cm^{-2}$ for 0.2%CB, followed by 22 $mW \cdot cm^{-2}$ for 0.6%CB, and 17 $mW \cdot cm^{-2}$ for 1%CB, while the 0% CB zinc slurry performed the lowest maximum power density with 16 mW cm^{-2}.

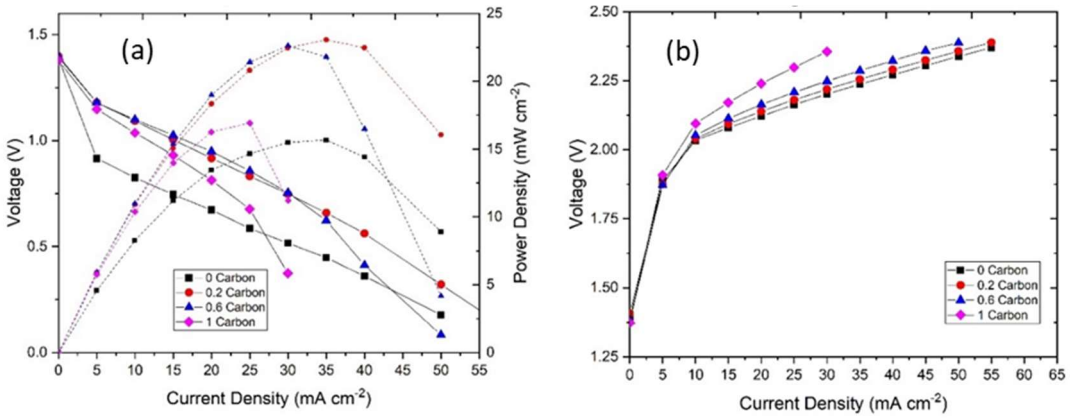

Figure 56 (a) Discharge polarization curves with their power densities and (b) charge polarization of the zinc slurries with different carbon contents.

From polarization curves, slope of the curve can be observed so it can be used to determine the ohmic resistance of each slurries, and it tends to increase with higher carbon content. In this system, ohmic resistance consist of both the ionic and electronic resistance that can be comparable when slurry electrodes are used [95]. Consequently, more powerful particle

network in the zinc slurry which is caused when CB is added gives better network connectivity which leads to lower electronic resistance. At the same time, when the CB contents get higher, it also gives negative effect by increasing the ionic resistance because this led to smaller volume fraction of electrolyte. Likewise, the basic porosity of the carbon particles, which includes the pores of the CB particles which may be filled with electrolyte makes problematic to hydroxyl ions for their travel to the zinc particles. It can be also seen that higher viscosity slurries lead to higher the mass transfer resistance of the battery.

Moreover, the charging performances (Figure 56b) exhibit that an higher CB content makes worse performance. This is again due to the increment of ohmic resistance by the lower ionic conductivity. In charging performance, the charge transfer resistance of the zinc electrode was not a big influence like in discharge, consequently, the higher electroactive area of the slurries with zinc particles does not have an effect on the charge transfer polarization significantly.

4.2.2.3 Cycling Performance

After confirming that charging is possible, the galvanostatic charge-discharge cycling performance of the slurries were performed and is shown in Figure 57 below. As shown in figure, all slurries were well cycled at 10 $mA \cdot cm^{-2}$, however, at 20 $mA \cdot cm^{-2}$ it can be seen that the slurry with 1%CB was unsuccessful to finish the 10-min charge-discharge cycle, due to it hits the charge cutoff voltage. Correspondingly, it can be observed that at 10 $mA \cdot cm^{-2}$ the measured voltage of the 1%CB when charging was higher than other slurries, which was already proved by polarization results. Mainly it is due to the decrease in ionic conductivity. Furthermore, when 1%CB zinc slurry was flowing in to the single cell, it was observed that the slurries could not flow smoothly which made air bubbles in the channel. Air bubbles would decrease the electrochemical performance of the cell and, as a result, 1%CB showed the lowest cycling performance.

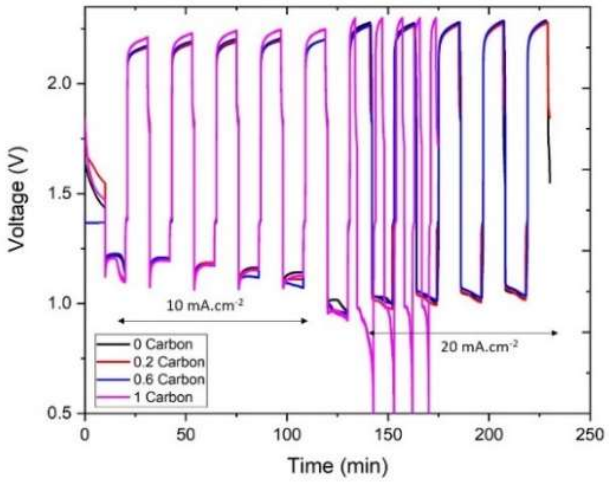

Figure 57 Charge-discharge curves of the different slurries.

Apart from 1%CB zinc slurry, the other slurries showed a similar cycling results at both 10 and 20 mA·cm^{-2}. To evaluate the energy efficiency (EE), the 1st and 4th cycles at each current density is presented in Figure 58. At 10 mA·cm^{-2}, the EE in the 1st cycle was approximately 55% for all zinc slurries, but then it decreased to 50% in the 4th cycle. At 20 mA·cm^{-2}, the 0%CB exhibited a marginally higher EE (46%) than to the CB slurries (43–44%) at the first cycle. After final cycles, the EE of the 0% CB slurry stayed the same, whereas for the CB slurries exhibited different trends, for example with the 0.2%CB, EE fell to 40% while 0.6%CB exhibited a rise to 47%. The main reason the EE was relatively low is because the voltage difference between charge and discharge was big, which can be improved when different catalysts are used, but it was not introduced in this study. Hence, EE was mostly influenced by voltaic efficiency rather than current efficiency.

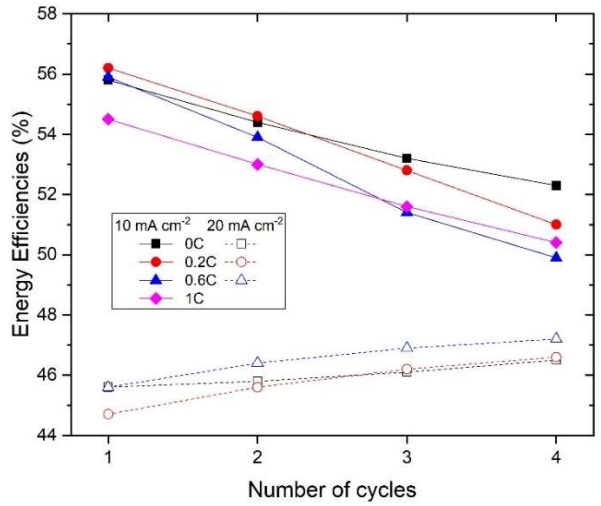

Figure 58 Energy efficiency of the different slurries.

4.2.2.4 Estimation of Charging Efficiency

One of the main purposes of this study is to prove that zinc plating when charging happens on the carbon black in the slurry not on the bipolar plate. Consequently, an additional test was set. Firstly, zinc slurries were charged, then zinc slurries were replaced by 10M KOH. The purpose of this test is to examine the amount of zinc plated on bipolar plate by performing the discharge capacity under KOH circulation. It can be observed in Figure 59 that the duration of discharge was longer than the charge, which made the coulombic efficiencies (CE) higher than 100%. There are two possible reasons which cause this result, first, as the flow field used in this test is not modified serpentine, it has rectangular edges in every corner which may have small dead volumes. This dead volume may still have the zinc slurry which was not flowed out by KOH and discharged. Another possibility is that when charging, the shape of zinc plating on the bipolar plate is not uniform, that could cause to zinc particles from the slurry being stuck into the plated zinc.

CE can be calculated from the discharge curves in Figure 59. As expected, CE of 0%CB exhibited the highest with 159%, followed by 148% for 0.2%CB, then 136% for 0.6%CB, and 132% for 1%CB. Sadly, as restrictions are mentioned above, the test was measured qualitatively. Nevertheless, it showed that the higher CB contents of zinc slurry recorded shorter discharge durations when KOH is flowing into the single cell. This can be related to the more zinc plating occurred on the zinc slurries rather than on bipolar plate (as shown in Figure 53).

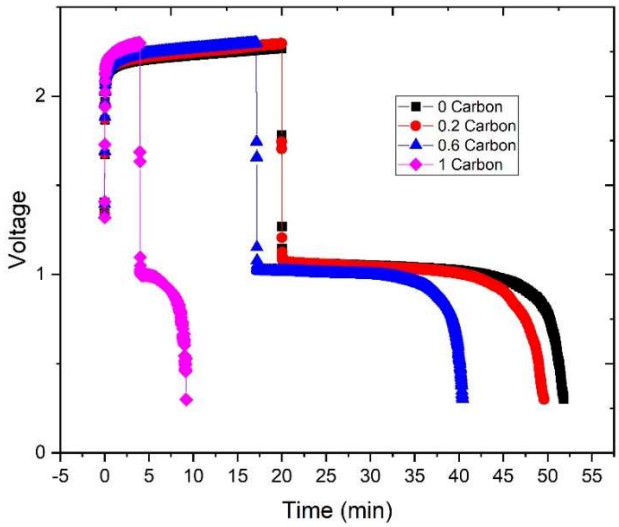

Figure 59 Charge-discharge curves to estimate zinc plating on the bipolar plate: charge with each zinc slurry and discharge after replacing the slurry with 10 M KOH.

To avert the “over-efficient” results, further experiment was tested. Two zinc slurries were prepared differently. This time, theses slurries were prepared without zinc particles in the zinc slurry. In other words, these two slurries had a composition of 10 M KOH, Carbopol and zinc oxide and with 1 wt.% and 2 wt.% of carbon black. When these samples were prepared, the volume fraction of solids is much less than in the zinc slurries. Experiment protocol was also changed as the new slurries did not have zinc, therefore they were charged first. The charge-discharge curve results are shown in Figure 60.

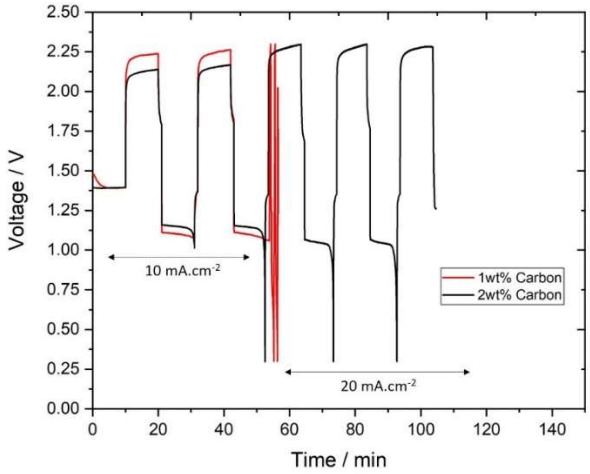

Figure 60 Charge-discharge curves of slurries without zinc particles.

As shown in Figure 60, charge-discharge curve at 10mA cm^{-2} of both slurries was successfully performed. Nevertheless, it can be seen that 2 wt.% of carbon was able to finish charge-discharge curve at 20 $mA \cdot cm^{-2}$, whereas 1 wt.% carbon slurry hit the set charging cut-off voltage which led to the termination of the test. As charge-discharge curve shows, 2 wt.% of carbon showed lower charging voltage than 1wt.% of carbon at current density of 10 $mA \cdot cm^{-2}$, as a subsequent, charging voltage was stable at 20 $mA \cdot cm^{-2}$. The 2wt.% of carbon slurry showed CE of 89% with a current density of 20 $mA \cdot cm^{-2}$ and this can be also interpreted that hydrogen evolution reaction (HER) was happening as a side reaction. HER happens when there is a low voltage on the negative electrode. To verify that the zinc plating was occurred not on bipolar plate but on the carbon particles in the slurry, 10M KOH was again flowed in to the cell and discharged with 2 wt.% carbon sample. As expected, the CE was 4%, which proved that zinc plating on the bipolar hardly occurs when charging.

4.2.3 Conclusions

In this chapter, zinc slurries with different ratios of CB were tested to improve the recharging performance with minimize the zinc plating on the bipolar plate when charging. The rheology of CB slurries showed that, in spite of higher viscosity was measured, higher CB

contents also made a stronger slurry networks which are advantageous to slurry-based RFBs. Even the 0% CB zinc slurry exhibits a stable performance when battery is charging and discharging, too much unwanted zinc plated on the bipolar plate occurred during charging. Whereas, when CB was added to the zinc slurry, not only the discharge performance was improved but also the amount of zinc plating on the bipolar became less and more plating on the carbon additive in the slurry happened. This was further verified by preparing new slurries without zinc, and when they performed charge-discharge cycle tests, it also showed that the zinc plating was more on carbon black in the zinc slurry rather than on the bipolar plate. Which can be very beneficial in future because if plating on CB in slurry can be achieved, a total battery capacity can be much higher for the system.

Chapter 5
Summary of thesis and future work

In the beginning of this thesis, it is shown how to operate the zinc slurry air flow battery as a future energy storage system. This demonstrates how to design a system, including selection of pump, selection of tube and fittings. Furthermore, different types of membranes, air catalyst, zinc slurry and flow fields were also tested for preliminary test. It is shown that better electrochemical performances can be achieved by using a separator (porous membrane) over an anion exchange membrane. This is because the separator lets water diffuse to the air electrode from zinc slurry, which circumvents the need of a humidifier in the air side to keep the positive electrode saturated water for ORR. This led that an anion exchange membrane showing higher membrane resistance compared to separators. Furthermore, by using an ultraturrax, a strong gelling network can be bonded for the zinc slurry, which led higher power density than making zinc slurry with just agitating by magnetic stirrer. Platinum on carbon was chosen as a catalyst over palladium on carbon for ORR, and also when a separator is used, the CCE method has proved more appropriate than CCM as CCM blocks water diffusion from zinc slurry to air, which lead to poor ORR kinetics.

Second part of the thesis, different types of flow field was tried to increase the power density of the battery. As this battery has no static electrode in the zinc side, the flow field is a critical component for the electrochemical performance. When a plastic flow frame is used on the top of the flat bipolar plate, the corrected geometric area is same as the active area as it is just flat electrochemical area. However, when either a serpentine or a parallel flow field is introduced, the power density displayed of those two flow fields is higher than the flow frame. This is because both serpentine and parallel type flow fields have a higher corrected geometric area due to the walls of the flow field. Hence, on the top of the active area, they have additional electrochemically active area that leads to an increase in power density. Furthermore, when the bipolar plate material was changed to metal from graphite, the power density was also boosted up. This is because the electrical conductivity of the metal bipolar plate is higher than that of graphite and zinc plating occurs when discharging. In other words, there is a higher amount of electrochemically active zinc when a metallic bipolar

plate is used. Moreover, different types of inorganic additives were introduced to increase the discharge capacity of the battery. It was shown that by adding different types of additive, there was a nearly a two-fold increase in the discharge capacity which was close to six times that of all-vanadium redox flow battery.

The last part of the thesis shows the rechargeability of the zinc slurry air flow battery. By adding carbon black into the zinc slurry, not only charging was improved but it also helped enhance the kinetics during discharge. Furthermore, it was shown that by adding carbon black in the zinc slurry, the amount of zinc plating on the bipolar plate is smaller than when there is no carbon in the slurry. This was double checked by another experiment consisting in discharging the cell with just KOH after charging with the carbon/zinc slurry. The results showed that when carbon black is present in the slurry, the discharging time with KOH is shorter, which proves that carbon black is minimizing zinc plating during charge.

The zinc slurry air flow battery has a good potential to be selected for future ESS, however, there are still challenges for this battery. For instance, the amount of zinc contents in this thesis was fixed to 33%. To fully utilize the advantages of this battery, higher contents of zinc should also be tested for a higher discharge performance. Furthermore, stacking of the system also requires to be further investigated. The stacking of a slurry flow battery presents several challenges among which the shunt currents, both ionic and electronic, caused by slurry electrolyte/electrode require specific solutions. Hence these problems still need to be studied for future zinc slurry air flow batteries.

References

[1] Yuan Zhang, Tianyang Liang, Zhen Tian, Wenzhong Gao, Ke Yang, A comprehensive parametric, energy and exergy analysis of a novel physical energy storage system based on carbon dioxide Brayton cycle, low-temperature thermal storage, and cold energy storage, Energy Conversion and Management, 10.1016/j.enconman.2020.113563, 226, (113563), (2020).

[2] Boden, T.A., G. Marland, and R.J. Andres. 2010. Global, Regional, and National Fossil-Fuel CO2 Emissions. Carbon Dioxide Information Analysis Center, Oak Ridge National Laboratory, U.S. Department of Energy, Oak Ridge, Tenn., U.S.A. doi 10.3334/CDIAC/00001_V2010

[3] Denholm, P, Ela, E, Kirby, B, and Milligan, M. Role of Energy Storage with Renewable Electricity Generation. United States: N. p., 2010. Web. doi:10.2172/972169.

[4] A.G. Olabi, Renewable energy and energy storage systems, Energy, Volume 136, 2017, Pages 1-6, ISSN 0360-5442, https://doi.org/10.1016/j.energy.2017.07.054.

[5] Eguia, P. (2017) 'Energy Storage Technologies for Electric Applications', (May). doi: 10.24084/repqj09.398.

[6] Wang, W., Luo, Q., Li, B., Wei, X., Li, L. and Yang, Z. (2013), Recent Progress in Redox Flow Battery Research and Development. Adv. Funct. Mater., 23: 970-986. https://doi.org/10.1002/adfm.201200694

[7] Li, L., Kim, S., Wang, W., Vijayakumar, M., Nie, Z., Chen, B., Zhang, J., Xia, G., Hu, J., Graff, G., Liu, J. and Yang, Z. (2011), A Stable Vanadium Redox-Flow Battery with High Energy Density for Large-Scale Energy Storage. Adv. Energy Mater., 1: 394-400. https://doi.org/10.1002/aenm.201100008

[8] Chakrabarti, M.H., Hajimolana, S.A., Mjalli, F.S. et al. Redox Flow Battery for Energy Storage. Arab J Sci Eng 38, 723–739 (2013). https://doi.org/10.1007/s13369-012-0356-5

[9] Redflow, https://redflow.com/, accessed on 11th ,Nov, 2020

[10] JENABATTERIES, https://jenabatteries.de/, accessed on 11th ,Nov, 2020

[11] elestor, https://www.elestor.nl/, accessed on 11th ,Nov, 2020

[12] Lago Clean Energy, https://www.largocleanenergy.com/, accessed on 11th ,Nov, 2020

[13] H_2, http://www.h2aec.com/, accessed on 11th ,Nov, 2020

[14] UniEnergy Technologies, https://uetechnologies.com/, accessed on 11th ,Nov, 2020

[15] Kear, G., Shah, A.A. and Walsh, F.C. (2012), Development of the all-vanadium redox flow battery for energy storage: a review of technological, financial and policy aspects. Int. J. Energy Res., 36: 1105-1120. https://doi.org/10.1002/er.1863

[16] M. Skyllas-Kazacos, L. Cao, M. Kazacos, N. Kausar, A. Mousa, ChemSusChem 2016, 9, 1521

[17] Watt-Smith, M., Ridley, P., Wills, R., Shah, A. and Walsh, F. (2013), The importance of key operational variables and electrolyte monitoring to the performance of an all vanadium

redox flow battery. J. Chem. Technol. Biotechnol., 88: 126-138. https://doi.org/10.1002/jctb.3870

[18] Skyllas-Kazacos, M., Kazacos, G., Poon, G. and Verseema, H. (2010), Recent advances with UNSW vanadium-based redox flow batteries. Int. J. Energy Res., 34: 182-189. https://doi.org/10.1002/er.1658

[19] Selina Weber, Jens F. Peters, Manuel Baumann, and Marcel Weil, Environmental Science & Technology 2018 52 (18), 10864-10873, DOI: 10.1021/acs.est.8b02073

[20] S. Miyake and N. Tokuda, "Vanadium redox-flow battery for a variety of applications," 2001 Power Engineering Society Summer Meeting. Conference Proceedings (Cat. No.01CH37262), Vancouver, BC, Canada, 2001, pp. 450-451 vol.1, doi: 10.1109/PESS.2001.970067.

[21] N H Choi, S-K Kwon, H. Kim, Analysis of the Oxidation of the V(II) by Dissolved Oxygen Using UV-Visible Spectrophotometry in a Vanadium Redox Flow Battery, J. Electrochem. Soc, 160 A973,

[22] A Lucas, S Chondrogiannis, Smart grid energy storage controller for frequency regulation and peak shaving, using a vanadium redox flow battery, Int. J. Electr. Power Energy Syst, Volume 80, September 2016, Pages 26-36

[23] D Reynard, C R Dennison, A Battistel, H Girault, Efficiency improvement of an all-vanadium redox flow battery by harvesting low-grade heat, J. Power Sources, Volume 390, 30 June 2018, Pages 30-37

[24] Kyu Taek Cho et al, High Performance Hydrogen/Bromine Redox Flow Battery for Grid-Scale Energy Storage 2012 J. Electrochem. Soc. 159 A1806

[25] Yujia Bai et al, Hydrogen Bromine Redox Flow Battery Cell Performance Study, 2012 Meet. Abstr. MA2012-02 398

[26] Hugo, Y.A.; Kout, W.; Dalessi, G.; Forner-Cuenca, A.; Borneman, Z.; Nijmeijer, K. Techno-Economic Analysis of a Kilo-Watt Scale Hydrogen-Bromine Flow Battery System for Sustainable Energy Storage. Processes 2020, 8, 1492. https://doi.org/10.3390/pr8111492

[27] Xiaoliang Wei, Wentao Duan, Jinhua Huang, Lu Zhang, Bin Li, David Reed, Wu Xu, Vincent Sprenkle, and Wei Wang, A High-Current, Stable Nonaqueous Organic Redox Flow Battery, ACS Energy Letters 2016 1 (4), 705-711 DOI: 10.1021/acsenergylett.6b00255

[28] Huang, J., Yang, Z., Vijayakumar, M., Duan, W., Hollas, A., Pan, B., Wang, W., Wei, X., Zhang, L., Adv. Sustainable Syst. 2018, 2, 1700131. https://doi.org/10.1002/adsu.201700131

[29] Wei, X., Xu, W., Huang, J., Zhang, L., Walter, E., Lawrence , C., Vijayakumar, M., Henderson, W.A., Liu, T., Cosimbescu, L., Li, B., Sprenkle, V. and Wang, W. (2015), Radical Compatibility with Nonaqueous Electrolytes and Its Impact on an All-Organic Redox Flow Battery. Angew. Chem. Int. Ed., 54: 8684-8687. https://doi.org/10.1002/anie.201501443

[30] M. Pino, D. Herranz, J. Chacón, E. Fatás, P. Ocón, Carbon treated commercial aluminium alloys as anodes for aluminium-air batteries in sodium chloride electrolyte, Journal of Power Sources. 326 (2016) 296–302. doi:10.1016/j.jpowsour.2016.06.118.

[31] X. Zhang, X.-G. Wang, Z. Xie, Z. Zhou, Recent progress in rechargeable alkali metal–air batteries, Green Energy & Environment. 1 (2016) 4–17. doi:10.1016/j.gee.2016.04.004

[32] M.A. Rahman, X. Wang, C. Wen, High Energy Density Metal-Air Batteries: A Review, Journal of the Electrochemical Society. 160 (2013) A1759–A1771. doi:10.1149/2.062310jes

[33] G.E. Gilligan, D. Qu, Zinc-air and other types of metal-air batteries, in: Advances in Batteries for Medium and Large-Scale Energy Storage, Elsevier, 2015: pp. 441–461. doi:10.1016/B978-1-78242-013-2.00012-1

[34] J.-S. Lee, S. Tai Kim, R. Cao, N.-S. Choi, M. Liu, K.T. Lee, J. Cho, Metal-Air Batteries with High Energy Density: Li-Air versus Zn-Air, Advanced Energy Materials. 1 (2011) 34–50. doi:10.1002/aenm.201000010.

[35] J.P. Zheng, R.Y. Liang, M. Hendrickson, E.J. Plichta, Theoretical Energy Density of Li-Air Batteries, Journal of The Electrochemical Society. 155 (2008) A432. doi:10.1149/1.2901961.

[36] J. Adams, M. Karulkar, Bipolar plate cell design for a lithium air battery, Journal of Power Sources. 199 (2012) 247–255. doi:10.1016/j.jpowsour.2011.10.041.

[37] https://researcher.watson.ibm.com/researcher/view_group.php?id=3203

[38] B Balasubramaniam, N Singh, S Verma, R K Gupta, Recycling of Lithium from Li-ion Batteries, Encyclopedia of Renewable and Sustainable Materials, Volume 2, 2020, Pages 546-554

[39] G. Girishkumar, Bryan D. McCloskey, Alan C. Luntz, S. Swanson, and W. Wilcke. Lithium-Air Battery: Promise and Challenges. Journal of Physical Chemistry Letters, 1(14):2193–2203, 2010. doi: 10.1021/jz1005384.

[40] Alan C. Luntz and Bryan D. McCloskey. Nonaqueous Li-Air Batteries : A Status Report. Chemical Reviews, 114:11721–11750, 2014.

[41] James Adams, Mohan Karulkar, and Venkataramani Anandan. Evaluation and electrochemical analyses of cathodes for lithium-air batteries. Journal of Power Sources, 239:132–143, 2013. doi: 10.1016/j.jpowsour.2013.03.140.

[42] M. Eswaran, N. Munichandraiah, and L. G. Scanlon. High Capacity Li-O2 Cell and Electrochemical Impedance Spectroscopy Study. Electrochemical and SolidState Letters, 13(9):A121–A124, 2010. doi: 10.1149/1.3447867.

[43] X.G. Zhang, Fibrous zinc anodes for high power batteries, Journal of Power Sources. 163 (2006) 591–597. doi:10.1016/j.jpowsour.2006.09.034.

[44] Y. Li, H. Dai, Recent advances in zinc–air batteries, Chem. Soc. Rev. 43 (2014) 5257–5275. doi:10.1039/C4CS00015C

[45] Gopalakrishnan, R., Goutam, S., Miguel Oliveira, L., Timmermans, J., Omar, N., Messagie, M., Van den Bossche, P., and van Mierlo, J. (April 11, 2017). "A Comprehensive Study on Rechargeable Energy Storage Technologies." ASME. J. Electrochem. En. Conv. Stor. November 2016; 13(4): 040801. https://doi.org/10.1115/1.4036000

[46] J.-Y. Huot, M. Malservisi, High-rate capability of zinc anodes in alkaline primary cells, Journal of Power Sources. 96 (2001) 133–139. doi:10.1016/S0378-7753(01)00496-7.

[47] H. Arai, M. Hayashi, PRIMARY BATTERIES - AQUEOUS SYSTEMS | Zinc-Air, in: Encyclopedia of Electrochemical Power Sources, Elsevier, 2009: pp. 55–61. doi:10.1016/B978-044452745-5.00101-5.

[48] G.E. Gilligan, D. Qu, Zinc-air and other types of metal-air batteries, in: Advances in Batteries for Medium and Large-Scale Energy Storage, Elsevier, 2015: pp. 441–461. doi:10.1016/B978-1-78242-013-2.00012-1.

[49] Y. Li, H. Dai, Recent advances in zinc–air batteries, Chem. Soc. Rev. 43 (2014) 5257–5275. doi:10.1039/C4CS00015C.

[50] Appleby, A. J., Jacquelin, J., & Pompon, J. P. (1977). Charge-Discharge Behavior of the C.G.E. Circulating Zinc-Air Vehicle Battery. SAE Technical Paper Series. doi:10.4271/770381

[51] Marshall, A., Hampson, N. A., & Drury, J. S. (1975). The discharge behaviour of the zinc/air slurry cell. Journal of Electroanalytical Chemistry and Interfacial Electrochemistry, 59(1), 33–40. doi:10.1016/s0022-0728(75)80043-x

[52] Smedley, S. I., & Zhang, X. G. (2007). A regenerative zinc–air fuel cell. Journal of Power Sources, 165(2), 897–904. doi:10.1016/j.jpowsour.2006.11.076

[53] X. Zhang, X-G. Wang, Z. Xie, Z. Zhou, Recent progress in rechargeable alkali metal–air batteries, Green Energy & Environment, 1, 1, 2016, Pages 4-17

[54] J. Fu, Z-P. Cano, MG Park, A.Yu, M. Fowler, Z.Chen, Electrically Rechargeable Zinc–Air Batteries: Progress, Challenges, and Perspectives, Advanced Materials, 29, 7, 2016, 1604685

[55] D. Yang, L. Zhang, X. Yan, X. Yao, Recent Progress in Oxygen Electrocatalysts for Zinc–Air Batteries, Small Methods,2017, 1, 12, 1700209

[56] DU. Lee, JY. Choi, K. Feng, HW. Park, Z. Chen, Advanced Extremely Durable 3D Bifunctional Air Electrodes for Rechargeable Zinc-Air Batteries, Advanced Energy Materials, 2013, 4, 6, 1301389

[57] S. Zhu, X. Hu, M. Shao, Impacts of anions on the oxygen reduction reaction kinetics on platinum and palladium surfaces in alkaline solutions, Phys. Chem. Chem. Phys., 2017, 19, 7631-7641

[58] M.H.Chakrabarti, R.A.W.Dryfe, E.P.L.Roberts, Evaluation of electrolytes for redox flow battery applications, Electrochimica Acta, 2007,52, 5, Pages 2189-2195

[59] C.Chakkaravarthy, A.K.Abdul Waheed, H.V.K.Udupa, Zinc-air alkaline batteries -A review, Journal of Power Sources, 1981, 6, 3, Pages 203-228

[60] A-Z. Nelson , R-H. Ewoldt, Design of yield-stress fluids: a rheology-tostructure inverse problem, Soft Matter, 2017, 13, 7578-7594

[61] Z. Zhang, C. Zuo, Z. Liu, Y. Yu, Y. Zuo, Y. Song, All-solid-state Al–air batteries with polymer alkaline gel electrolyte, Journal of Power Sources, 251, 2014, Pages 470-475

[62] A. Puapattanakula, S. Therdthianwongb, A. Therdthianwongc, N. Wongyaoc, Improvement of Zinc-Air Fuel Cell Performance by Gelled KOH, Energy Procedia, 2013, 34, 173

[63] K-C. Smith, Y-M Chiang,W-C. Carter, Maximizing Energetic Efficiency in Flow Batteries Utilizing Non-Newtonian Fluids, ECS, 2014,161 (4), A486-A496

[64] X. Ke, J. M. Prahl, J. I. D. Alexander, J. S. Wainright, T. A. Zawodzinski, and R. F. Savinell, "Rechargeable redox flow batteries: flow fields, stacks and design considerations," Chem. Soc. Rev., vol. 47, no. 23, pp. 8721–8743, 2018.

[65] R. M. Darling and M. L. Perry, "The influence of electrode and channel configurations on flow battery performance," J. Electrochem. Soc., vol. 161, no. 9, pp. 1381–1387, 2014.

[66] M. Rychcik and M. Skyllas-Kazacos, "Characteristics of a new all-vanadium redox flow battery," J. Power Sources, vol. 22, no. 1, pp. 59–67, 1988.

[67] P. J. A. N. Sonneveld, "The zinc suspension electrode," 1991.

[68] X. L. Zhou, T. S. Zhao, L. An, Y. K. Zeng, and L. Wei, "Critical transport issues for improving the performance of aqueous redox flow batteries," J. Power Sources, vol. 339, pp. 1–12, 2017.

[69] H. Liu, P. Li, D. Juarez-Robles, K. Wang, and A. Hernandez-Guerrero, "Experimental study and comparison of various designs of gas flow fields to PEM fuel cells and cell stack performance," Front. Energy Res., vol. 2, no. JAN, pp. 1–8, 2014.

[70] T. J. Petek, N. C. Hoyt, R. F. Savinell, and J. S. Wainright, "Slurry electrodes for iron plating in an all-iron flow battery," J. Power Sources, vol. 294, pp. 620–626, 2015.

[71] C. R. Dennison, M. Beidaghi, K. B. Hatzell, J. W. Campos, Y. Gogotsi, and E. C. Kumbur, "Effects of flow cell design on charge percolation and storage in the carbon slurry electrodes of electrochemical flow capacitors," J. Power Sources, vol. 247, pp. 489–496, 2014.

[72] S. I. Smedley and X. G. Zhang, "A regenerative zinc-air fuel cell," J. Power Sources, vol. 165, no. 2, pp. 897–904, 2007.

[73] P. Sapkota and H. Kim, "Zinc-air fuel cell, a potential candidate for alternative energy," J. Ind. Eng. Chem., vol. 15, no. 4, pp. 445–450, 2009.

[74] P. Pei, Z. Ma, K. Wang, X. Wang, M. Song, and H. Xu, "High performance zinc air fuel cell stack," J. Power Sources, vol. 249, pp. 13–20, 2014.

[75] K. Percin, A. Rommerskirchen, R. Sengpiel, Y. Gendel, and M. Wessling, "3D-printed conductive static mixers enable all-vanadium redox flow battery using slurry electrodes," J. Power Sources, vol. 379, no. January, pp. 228–233, 2018.

[76] Brenner, A. Electrodeposition of Alloys: Principles and Practice; Academic Press: Cambridge, MA, USA, 1963; pp. 411–496.

[77] Vijayaratnam, V.; Natter, H.; Grandthyll, S.; Neurohr, J.U.; Jacobs, K.; Müller, F.; Hempelmann, R. Unwanted electroless zinc plating on current collectors in zinc air batteries. arXiv 2017, arXiv:1706.05929.

[78] Mainar, A.; Iruin, E.; Colmenares, L.; Kvasha, A.; Meatza, I.; Bengoechea, M.; Leonet, O.; Boyano, I.; Zhang, Z.; Blazquez, J. An overview of progress in electrolytes for secondary zinc-air batteries and other storage systems based on zinc. J. Energy Storage 2018, 15, 304–328.

[79] A. R. Mainar, L. C. Colmenares, H. J. Grande, and J. A. Blázquez, "Enhancing the cycle life of a Zinc–air battery by means of electrolyte additives and zinc surface protection," Batteries, vol. 4, no. 3, 2018.

[80] K. Wang, P. Pei, Y. Wang, C. Liao, W. Wang, and S. Huang, "Advanced rechargeable zincair battery with parameter optimization," Appl. Energy, vol. 225, no. May, pp. 848–856, 2018.

[81] D. P. Trudgeon et al., "Screening of effective electrolyte additives for zinc-based redox flow battery systems," J. Power Sources, vol. 412, no. November 2018, pp. 44–54, 2019.

[82] S. Hosseini, S. J. Han, A. Arponwichanop, T. Yonezawa, and S. Kheawhom, "Ethanol as an electrolyte additive for alkaline zinc-air flow batteries," Sci. Rep., vol. 8, no. 1, pp. 1– 11, 2018.

[83] P. C. Foller, "Effects of additives on the suspension of products of discharge of zinc in alkaline solution," J. Appl. Electrochem., vol. 17, no. 6, pp. 1296–1303, 1987.

[84] J. Noack, N. Roznyatovskaya, T. Herr, and P. Fischer, "The Chemistry of Redox-Flow Batteries," Angew. Chemie - Int. Ed., vol. 54, no. 34, pp. 9776–9809, 2015.

[85] Hreiz, R.; Adouani, N.; Fünfschilling, D.; Marchal, P.; Pons, M.N. Rheological characterization of raw and anaerobically digested cow slurry. Chem. Eng. Res. Des. 2017, 119,. 47–57.

[86] Hermoso, J.; Jofore, B.D.; Martínez-Boza, F.J.; Gallegos, C. High pressure mixing rheology of drilling fluids. Ind. Eng. Chem. Res. 2012, 51, 14399–14407.

[87] Owens, C.E.; Hart, A.J.; McKinley, G.H. Improved rheometry of yield stress fluids using bespoke fractal 3D printed vanes. J. Rheol. 2020, 64, 643–662.

[88] Baravian, C.; Lalante, A.; Parker, A. Vane rheometry with a large, finite gap. Appl. Rheol. 2002, 12, 81–87.

[89] Helal, A.; Divoux, T.; McKinley, G.H. Simultaneous Rheoelectric Measurements of Strongly Conductive Complex Fluids. Phys. Rev. Appl. 2016, 6, 064004.

[90] Ito, Y.; Nyce, M.; Plivelich, R.; Klein, M.; Steingart, D.; Banerjee, S. Zinc morphology in zinc–nickel flow assisted batteries and impact on performance. J. Power Sources 2011, 196, 2340–2345.

[91] Wei, T.S.; Fan, F.Y.; Helal, A.; Smith, K.C.; McKinley, G.H.; Chiang, Y.M.; Lewis, J.A. Biphasic Electrode Suspensions for Li-Ion Semi-solid Flow Cells with High Energy Density, Fast Charge Transport, and Low-Dissipation Flow. Adv. Energy Mater. 2015, 5, 1500535.

[92] Dinkgreve, M.; Paredes, J.; Denn, M.M.; Bonn, D. On different ways of measuring 'the' yield stress. J. Nonnewton. Fluid Mech. 2016, 238, 233–241.

[93] Gallier, S.; Lemaire, E.; Peters, F.; Lobry, L. Rheology of sheared suspensions of rough frictional particles. J. Fluid Mech. 2014, 757, 514–549.

[94] Tang, A.; Bao, J.; Skyllas-Kazacos, M. Studies on pressure losses and flow rate optimization in vanadium redox flow battery. J. Power Sources 2014, 248, 154–162.

[95] Petek, T.J.; Hoyt, N.C.; Savinell, R.F.; Wainright, J.S. Characterizing Slurry Electrodes Using Electrochemical Impedance Spectroscopy. J. Electrochem. Soc. 2015, 163, A5001–A5009.

ACKNOWLEDGEMENT

First of all, I would like to my supervisors in Fraunhofer ICT, Prof. Dr Jens Tübke, Prof. Dr. Karsten Pinkwart and Dr. Peter Fischer. I could have start and finish my PhD in Fraunhofer ICT because they gave me a chance to do PhD here with helpful advices. Also, I would like to thank Prof. Dr. rer. nat Helmut Ehrenberg from KIT for accepting me as a second reviewer for my thesis. I would like to thank my FlowCamp colleagues and supervisors especially our zinc slurry air group (Diego del Olmo, Diego Milian, Misgina Tilahun TSEHAYE, Ricardo Paz Moldes Duarte) for their discussions and advices about my work during PhD.

I would also give my thanks to the people in Fraunhofer ICT. Brenda Cantu who spent almost full 3 years with me in the same office, I wish all the best for her future. Dr. Tobias Gerber who helped me from the beginning of the project and without his help, my settlement in Germany and Fraunhofer ICT would have been so difficult. Michael Schäffer and David Bähr who helped me very much when I was struggling to setup my system, their technical advices really helped me a lot. Also, I thank to Michael Küttinger also gave me many scientific advices during my time here. Furthermore, I would like thanks to our redox flow battery group members Jens Noack, Dr. Nataliya Roznyatovskaya, Dr. Soheila Chitsaz, and Matthias Fühl for their scientific discussion and advices which was very scientific helpful for my work in Fraunhofer ICT. Also, I would like to thank to Katharina Ahlbrecht, Jan Meier, Dr. Norman Baltes, Peter Rabenecker, Patrik Fanz and Mechthild Berger for their help during my PhD time.

Moreover, I would like to thank my Korean friends in Karlsruhe, Dr. Won Qook Choi, Sangmi Kim, Lea Choi, Dr. Hans Chen, Yoonji Sim, Mariella and Lorenz Chen, Junwoo Chung, Yoonju Park, Hyung Suk Woo, Jui Ok, and my friends from Korean Church.

Last but not least, I would like to thank all my family members in Korea and Indonesia. Especially my wife Eunbit Koh and my daughter Sharon Choi who gave me a power and motivation during my PhD time. Without their support and love, I would not have achieved this work.

"This project has received funding from the European Union's Horizon 2020 research and innovation programme under the Marie Skłodowska-Curie Grant Agreement no. 765289."